Characteristics of Supraglacial Channels and Drainage Networks on Antarctic Ice Shelves

CHEN, JIAO

Jiao Chen

Characteristics of Supraglacial Channels and Drainage Networks on Antarctic Ice Shelves

Abstract. Supraglacial channels that flow on ice shelves can store and transport large volumes of meltwater to various locations (e.g., moulins, lakes, crevasses) during the melt season, so they play an important role in glacial hydrology and ice shelf stability. However, the current understanding of supraglacial channels is limited, especially the underlying processes and the controls on their development and variability. This study uses multiple remotely sensed data including satellite imagery and Digital Elevation Models (DEMs) to measure supraglacial channels in Antarctica. Five contrasting ice shelves around the margin of the Antarctic Ice Sheet are chosen as the study sites – Bach, Nansen, Nivlisen, Riiser-Larsen and Roi Baudouin ice shelves. Supraglacial lakes and channels are mapped by automatic delineation method during the melt season in 2020 and 2022, and key fluvial metrics are calculated, e.g., number, length, width, depth, sinuosity, bifurcation ratio, orientation, slopes and drainage density. Extensive supraglacial lakes and channels were observed on all five Antarctic ice shelves during the peak of the melt season and most were interconnected to form a total of 119 channel networks at different scales. The results demonstrate that: (i) supraglacial channel networks often occurred in areas with low elevations and near grounding lines, (ii) supraglacial channel networks on different ice shelves exhibited different drainage patterns and hydromorphic characteristics, (iii) the surface topography and structural glaciology of ice shelves affected the distribution of the supraglacial channel network. Future work could focus on long-term observation of supraglacial channels and exploring the applicability of terrestrial river-related research methods (e.g., hydrological modelling) to supraglacial channels.

Characteristics of Supraglacial Channels and Drainage Networks on Antarctic Ice Shelves

Jiao Chen

Thesis submitted for the degree of Master of Science

Department of Geography

Durham University

February 2023

Table of Contents

List of Figures

List of Tables

Statement of Copyright

Acknowledgements

Firstly, I would like to thank my supervisors – Prof. Rebecca Hodge, Prof. Stewart Jamieson and Prof. Chris Stokes. They always give me quick responses and sage advice on my questions, and I appreciate their endless help and continued support over the year of my Master's study. I am very fortunate to be continuing my PhD study under their supervision and look forward to working with them over the next few years.

Next, I would also like to thank my fellow MRes students, the Antarctic group and all research staff in the Department of Geography, from whose generous sharing and help I have learned a lot of knowledge and useful skills.

Finally, I would like to express my heartfelt thanks to my family and friends, whose encouragement and support have always been my motivation.

1. Introduction

1.1 Overall aim

Supraglacial channels redistribute meltwater across the surface of ice sheets and ice shelves, but the current understanding of their characteristics is limited. For example, lakes fed by supraglacial channels have been linked to ice-shelf collapse, but channels may also drain lakes and remove meltwater from ice shelves. The aim of this study is to better understand the characteristics and drainage patterns of supraglacial channel networks on Antarctic ice shelves.

1.2 Context and justification

Antarctica is the fifth-largest continent, which has an area of almost 14 million km^2 and contains 30 million km^3 of ice (Campbell and Claridge, 1987; Council, 2011). The Transantarctic Mountains separate the Antarctic Ice Sheet into two main domains (Figure1.1): the East Antarctic Ice Sheet (EAIS) and the West Antarctic Ice Sheet (WAIS) including the Antarctic Peninsula, and there are some different characteristics between them (Liggett et al., 2015). The EAIS is cold and dry, and much of it is grounded above sea level. In contrast, the WAIS lies largely below sea level, and its crust is thinner than that of the EAIS (Fretwell et al., 2013). Antarctica is fringed with floating ice shelves which cover approximately 1.561 million km^2. These ice shelves are extensions of grounded glaciers and are supplemented by accumulating surface snow and freezing of marine ice below (Rignot et al., 2013).

As the most remote continent on Earth, Antarctica seems to be isolated but affects the global climate system profoundly (Rintoul et al., 2018). For instance, the Antarctic Ice Sheet was thought to be the major contributor to the global mean sea level that was approximately 6–9 metres higher around 130,000 to 115,000 years (DeConto and Pollard,

2016). As a result, the response of the Antarctic Ice Sheet to atmospheric and oceanic warming will directly determine the amount and rate of sea level rise over the next few centuries. In fact, the entire Antarctic ice sheet is melting at ever-increasing rates as climate change accelerates (Khazendar et al., 2016; Bell et al., 2018; Shepherd et al., 2018; Dirscherl et al., 2021b). Rignot et al. (2013) estimated the basal melting of 67 ice shelves around the Antarctic continent. Their results indicated that the rapid melting was happening on ice shelves in both East and West Antarctica, and that basal melting represented a larger proportion of ice-shelf attrition in Antarctica than estimated in the past.

Figure 1.1 *Overview Map of Antarctica: the major ice shelves around the margin are marked as grey areas* (Abrahamsen 2012).

In addition to basal melting, one of the most significant phenomena of surface melting in Antarctica is the increasing amount of water on the ice surface (Bell et al., 2018). Liquid meltwater on grounded and floating ice can be stored in impermeable surface depressions, and supraglacial lakes and channels form (Pitcher and Smith, 2019). Sometimes, surface crevasses can also accumulate meltwater and the stored water may drain through ice fractures on ice shelves, termed hydrofracturing (McGrath et al., 2012; MacAyeal et al., 2015). Despite recent progress in studying supraglacial systems in Antarctica (Bell et al., 2018; Arthur et al., 2020a), our understanding of the underlying processes and influences of Antarctic hydrology remains somewhat limited, particularly in terms of supraglacial channels.

It is hypothesized that the accumulation of meltwater on the surface of ice shelves can play a critical role in the stability of an ice shelf (Banwell et al., 2013; Banwell et al., 2014; Pitcher and Smith 2019). There are several possible mechanisms connecting surface melting to ice shelf collapse, including ice shelf flexure resulting from meltwater loading and drainage (Weertman, 1973; MacAyeal et al., 2015). DeConto and Pollard (2016) added the effects of widespread meltwater on Antarctic ice shelves to their predictive ice sheet model and found that surface meltwater could induce widespread hydrofracture on ice shelves during this century, which may significantly increase the contribution of the Antarctic ice sheet to sea-level rise. Therefore, it is urgent to better understand the fundamental processes of supraglacial hydrology and the factors that impact the production of surface meltwater. Current studies have typically focused on supraglacial lakes and the controls on surface melting in specific locations during specific times of the year (Langley et al.,2016; Stokes et al.,2019; Bell et al.,2018; Arthur et al.,2020,2022; Kingslake et al.,2017). More recently, the drainage through supraglacial rivers and streams has been observed in some locations in Antarctica, delivering meltwater across the ice shelves (Kingslake et al., 2015; Bell et al., 2017; Banwell et al., 2021). Furthermore, their termination points reveal the locations of moulins that may

indicate connections from the surface to the bed (Smith et al., 2015; Yang and Smith, 2016; Tuckett et al., 2019). However, there is still little known about their spatial distribution and transport capacity of supraglacial channels. Although field studies are difficult to conduct due to the lack of human and financial resources, advances in remote sensing technology have made it possible to monitor dynamics without the limitation of space and time (Arthur et al., 2020a).

1.3 Objectives

Given this context, this study was conducted around three specific research questions: (i) What do the channels on the surface of the Antarctic ice shelves look like? (ii) Are there any differences between supraglacial channels on different ice shelves? (iii) What factors control the development of the drainage patterns of the supraglacial channel networks on the Antarctic ice shelves?

According to the above research questions, the objectives of this study are to:

(1) Use multiple remotely sensed data to map supraglacial hydrology features (i.e., channels and lakes) in Antarctica over five different ice shelves;

(2) Quantify the morphology and drainage patterns of supraglacial channel networks over the five different Antarctic ice shelves;

(3) Discuss the controlling factors on the formation of supraglacial channel networks on the five ice shelves.

1.4 Thesis structure

This thesis will first give a background to the current understanding of supraglacial hydrology (Chapter 2) including the basic conception of channel and channel networks on ice surfaces (Sections 2.1 and 2.2). A brief introduction of commonly used data sources (i.e., satellite imagery and digital elevation data) used in studying supraglacial hydrology follows (Section 2.3), along with some background on the supraglacial hydrology in

Antarctica (Section 2.4). A general description of the study sites is then given (Chapter 3) followed by details of the ice shelves selected in East Antarctica (Section 3.2) and West Antarctica (Section 3.3). In the methods section (Chapter 4), the optical remotely sensed image processing and supraglacial channel network delineation method are presented (Sections 4.1 to 4.2), together with how the fluvial metrics and measurements were quantified (Section 4.3). The supraglacial channel networks delineated using this method are presented in the results section (Chapter 5), along with the analysis of the metrics including the spatial distribution of channels, channel length, width, sinuosity, etc. The impacts of surface topography and structural glaciology on supraglacial channel networks are discussed in Chapter 6 together with limitations and future work. Key conclusions of this study are given in Chapter 7.

2. Literature review

2.1 Supraglacial channels

2.1.1. Definition of supraglacial channels

The term ‘supraglacial rivers or streams’ has been used to describe channels that transport water on glaciers and ice sheets (Pitcher and Smith, 2019). Supraglacial rivers are trunk and perennial channels (Yang and Smith, 2016; Gleason et al., 2021) occupying the higher stream orders in the channel network (Strahler, 1957; Yang et al., 2016), while supraglacial streams are usually transient on multiyear timescales and rank in the lower orders. Supraglacial rivers and streams can be collectively referred to as channels (as in this thesis), and they play an important role in glacial hydrology and have potential impacts on ice shelf stability (Pitcher and Smith, 2019). As shown in Figure 2.1, supraglacial channels exhibit complex drainage patterns. Drainage through supraglacial channels occurs in various locations and they can route surface meltwater into lakes, crevasses, and moulins, and even into terrestrial hydrologic systems or the ocean (Yang et al., 2021).

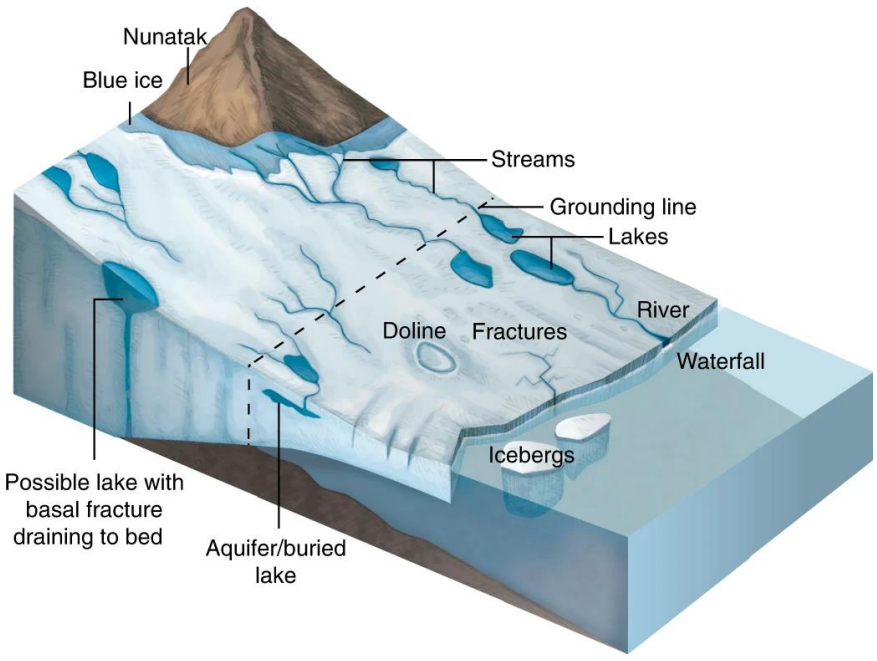

Figure 2.1 *Supraglacial channels across bare ice and ice shelves* (Bell et al., 2018).

2.1.2. Formation and evolution of supraglacial channels

Previous studies have provided important information on the formation of supraglacial channels (Cuffey and Paterson, 2010; Jarosch and Gudmundsson, 2012; Pitcher and Smith, 2019). This process can be summarized in three stages: firstly, meltwater is produced due to the increasing solar insolation early in the melt season. Secondly, meltwater can percolate into the underlying snow and ice. Sometimes, an impermeable layer of superimposed ice forms because of refrozen snow and ice. As the volume of meltwater increases, the snow and firn saturation increase and surface drainage is impeded. Thirdly, surface drainage begins to mobilize snow and firn which can result in slush-flow activity and eventually supraglacial channel formation that follows the ice surface slope or exploits structural weaknesses in the surface (e.g., crevasses, fractures, etc.). It has commonly been assumed that supraglacial channelization is similar to the formation of terrestrial rivers (Yang et al., 2016). However, limited knowledge is available about the physical process of supraglacial channel development or routing.

Ice sheet surfaces with very little debris provide a more homogeneous environment for channel development, but channels can still adjust rapidly and often show meandering characteristics (Knighton 1985). Existing evidence shows that thermal erosion and glacier flow generate a dynamic topographic control on the shape and size of supraglacial channels (e.g., Knighton, 1985; Karlstrom and Yang, 2016). According to Kostrzewski and Zwolinski (1995), channel evolution can be summarised as follows: first, large changes take place in channel depth which is caused by thermal incision. Second, ablation of the side walls leads to channel widening. Third, meandering begins to occur as flow velocity varies with variable channel roughness. The main weakness of this simple model is the failure to address the influence of external forcings, such as ice flow and associated structural glaciology (fractures, rifts, crevasses, flow-stripes, etc.), which could alter many properties including drainage patterns, gradients and length. More recently, several authors have noted that the topography of supraglacial channels may be controlled by internal thermal adjustments at length scales smaller than ice thickness, but that at greater

scales, subglacial topography determines channel morphology (Ewing, 1972; Karlstrom and Yang, 2016; Pitcher and Smith, 2019). This view is supported by the basal-to-surface roughness transfer functions (Figure 2.2), which indicates that when the basal wavelengths are greater than ice thickness, the bedrock has significant influences on the surface topography so supraglacial drainage basins are fixed in space. In contrast, fluvial erosion dominates the topography when at smaller wavelengths (Budd, 1970; Gudmundsson, 2003; Lampkin and VanderBerg, 2011).

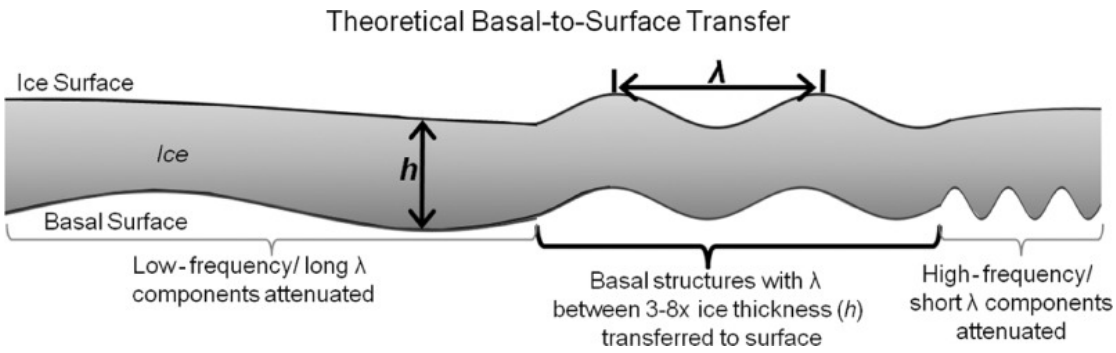

Figure 2.2 *Schematic of the basal-to-surface roughness transfer function, where (h) is for ice thickness and (λ) is for the surface and basal wavelength (not to scale). Components with basal wavelengths (λ) between 3 and 8 times the ice thickness (h) are most readily transferred through the ice, while those longer or shorter than this range are highly weakened* (Lampkin and VanderBerg, 2011).

2.1.3. Spatial distribution of supraglacial channels

Supraglacial channels are widespread in different glacial surroundings during the melt season and exhibit a diversity of drainage patterns (Figure 2.3). Most previous work on supraglacial channels has concentrated on the Greenland Ice Sheet, which has well-developed hydrological systems in the relatively large ablation zone compared to Antarctica (Germain and Moorman, 2016; Smith et al., 2017; Yang et al., 2016a). In addition, investigations of supraglacial channels have been carried out elsewhere, such as in Antarctic Peninsula (Bell et al., 2018), Nepal (Benn et al., 2017), Switzerland (Willis

et al., 2002), and Alaska (Scott et al., 2010). Due to the high cost of fieldwork and the difficulty of observing channels across a large scale, most studies of channels on ice in Antarctica have only ever been conducted on small areas in the field, and often close to Antarctic bases. Therefore, how supraglacial channels and drainage evolve and behave remains poorly understood in Antarctica.

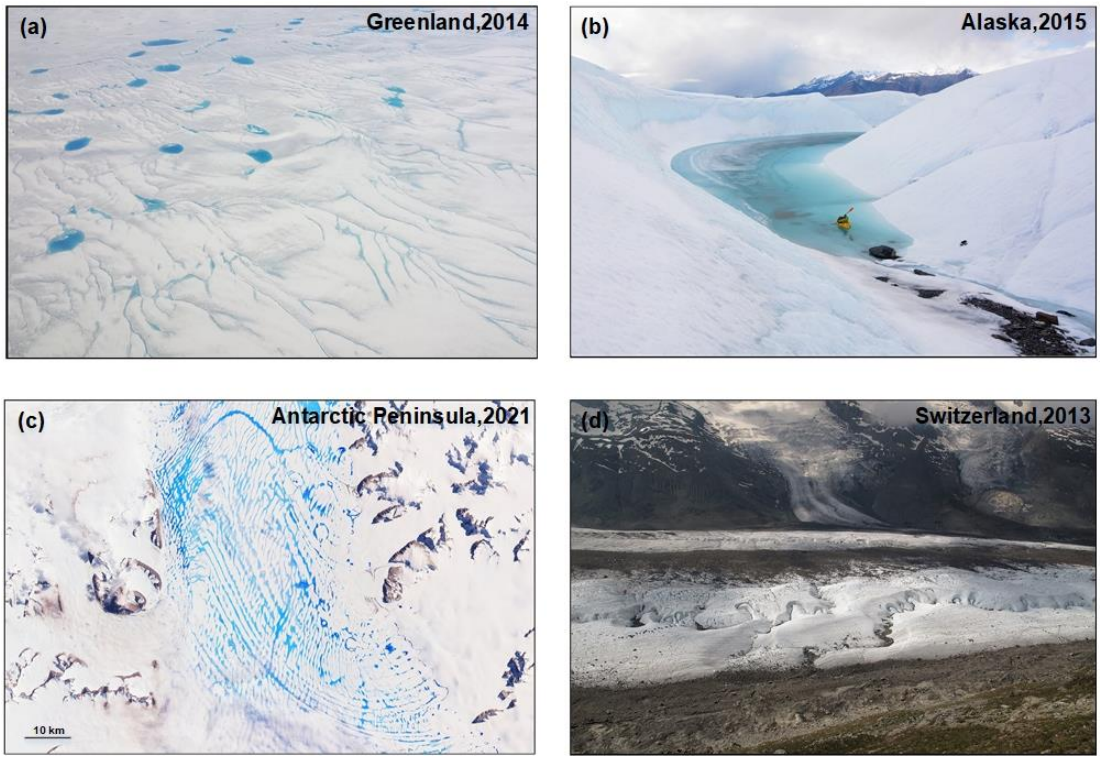

Figure 2.3 *Examples of supraglacial channels: (a) supraglacial rivers are flowing across the Greenland Ice Sheet. (Photo by Bernt Rostad). (b) an anchorage paddler in a supraglacial river on Matanuska Glacier in Alaska (photo by Paxson Woelber). (c) meltwater channels on George VI Ice Shelf, Antarctic Peninsula (Sentinel-2 imagery processed by Julien Seguinot). (d) supraglacial channels meandering on Gornergletscher glacier, Switzerland (photo by Tadeáš Gregor)*. All images used here are distributed under a CC-BY 2.0 license.

2.2 Supraglacial channel networks

2.2.1 Appearance and evolution of drainage network patterns

The drainage pattern is a fundamental concept in channel network analysis because it represents the spatial relationships between stem channels and tributaries in the drainage basin. Terrestrial rivers transport water and sediment from hillslopes to the catchment outlet and form a unique drainage network due to the differences in underlying geology and other natural factors (e.g., topography, climate and tectonic history) (Charlton 2007). Drainage patterns can be classified based on their form and texture. The most commonly occurring drainage patterns are dendritic, parallel, rectangular, and centripetal (Figure 2.4). The dendritic drainage pattern develops like a tree, which means the contributing tributaries (i.e., branches of the tree) in this system usually confluence together to form the stem channels (i.e., trunk of the tree). Compared with the dendritic pattern, tributary streams of parallel pattern tend to join together at acute angles and extend more parallel to the stem channel following the regional surface slope. For the rectangular drainage pattern, channels form a perpendicular net in two directions and converge to the stem channel almost at right angles. A centripetal drainage pattern is generated when channels drain the water into a lake or depression from all directions. The rose diagrams of the flow direction of channel segments also reflect the differences in angles when tributaries join the stem channel in different drainage patterns. The orientations of flowing channels in dendritic and parallel drainage patterns are more concentrated than that of rectangular and centripetal patterns, which indicates there might be strong regional controls that dominate the angle of channel junctions.

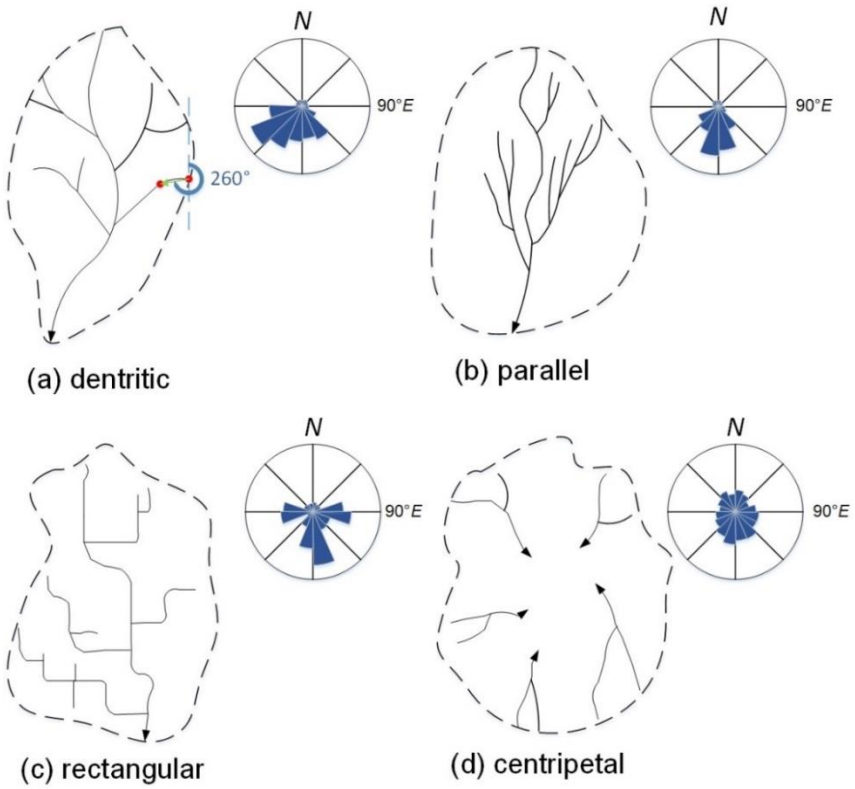

Figure 2.4 *Schematic drawing of typical drainage patterns: the black arrow indicates the flow direction of stem channels, the rose diagram on the right-top corners shows the orientation of channel segments and the length of the radius indicates the quantity.*

The drainage pattern of a terrestrial catchment is dominated by the underlying geological structure, topography, slope, climatic variables, etc. Among all these factors, the geological structure is thought to have the most significant influence on the formation of drainage patterns (Magesh et al., 2012). Channel networks with a dendritic appearance are the most common and basic of all the drainage patterns, which typically suggest homogeneous substrate and no strong geological controls. Where there are steep slopes with some relief or parallel, elongate landforms, parallel drainage patterns develop.

Supraglacial channel networks consist of interconnected supraglacial channels and lakes. Previous studies have reported that supraglacial channel networks also exhibit complex drainage patterns and high drainage densities which are similar to terrestrial rivers (Smith et al., 2015; Yang et al., 2016; Pitcher and Smith, 2019; Yang et al., 2019b; Lu et al.,

2020a). These studies also indicate that the topography of the ice surface is the dominant factor in determining the type of supraglacial drainage pattern, with other potential factors including ice surface albedo, roughness and longitudinal surface flow structures (e.g., flow stripes) (Rippin et al., 2015; Yang et al., 2016; Holt et al., 2013). Although operating as interlinked hydrological networks, supraglacial lakes and channels are often investigated as independent features, and most studies of supraglacial drainage patterns have only focused on the Greenland Ice Sheet. However, despite recent observations of supraglacial melting and the formation of lakes and channels (Langley et al.,2016; Stokes et al.,2019; Bell et al.,2018; Arthur et al.,2020,2022; Kingslake et al.,2017), little is known about drainage patterns of supraglacial channel networks in Antarctica and how lakes and channels differ in their ability to store meltwater during network formation.

2.2.2 Stream order

Stream order is an important characteristic which helps to measure the relative size, and therefore potential discharge, of channels (Figure 2.5). Moving up in size and volume, streams are classified from first-order streams to high order streams, as devised by Strahler (1957). The outermost tributaries are first-order streams, which flow into the larger streams and normally have no sub-tributaries (Charlton 2007). A few fundamental studies on supraglacial stream orders have been carried out. Smith et al. (2015) analyzed supraglacial drainage patterns via mapping from remote sensing and field measurements on the west Greenland Ice Sheet. The findings of this study suggest that Strahler stream orders of supraglacial channels in the study area ranged from 1 to 5 and all the mapped channels terminated in moulins, which means surface water drained efficiently via a well-integrated surface drainage pattern. Stream order has also been used to delineate supraglacial channels in geographic information systems (GIS). King et al. (2016) tested a flow routing algorithm for delineating supraglacial channels from high-resolution (2 m) ice surface DEMs on the Greenland Ice Sheet. They used the Strahler stream order as a proxy for relative stream size and found the performance of the flow routing algorithm

getting worse as stream order decreases. However, few studies have drawn on stream ordering to quantify supraglacial channel networks.

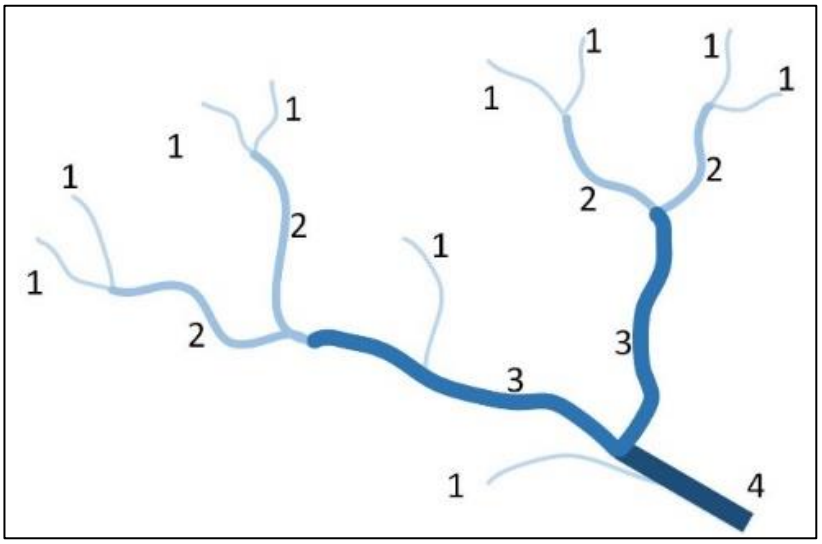

Figure 2.5 *Strahler stream order (black numbers indicate the order)*

2.2.3 Channel meandering

Most supraglacial channels exhibit meandering patterns which are superficially similar to terrestrial rivers, although they are mechanistically distinct from each other (Karlstrom et al., 2013). The formation and development of meandering channels are mainly affected by the erosion and deposition of sediment (Song et al., 2016). Bank erosion and deposition in terrestrial settings usually occur when variations in boundary shear stresses exceed the threshold for sediment movement. However, current understanding indicates that supraglacial channels lack a similar mechanism for the deposition of bank material (refreezing of channel bank is ineffective during the melt season because of the long duration of daily solar radiation) (Karlstrom et al., 2013). Moreover, very little sediment (i.e., ice crystals or rocks) is transported in most supraglacial meltwater channels, which suggests that sediment transport is not necessary for their meandering (Parker, 1975). This led to the question: how do meanders form and evolve in channels on ice with the absence of bank deposition?

There are several possible explanations. Parker (1975) used a model based on linear stability analysis and found that thermal erosion due to differential frictional heating is the main factor contributing to meandering and that meander wavelength is determined by the channel properties (i.e., width, depth). Marston (1983) challenged some of Parker's conclusions, suggesting that meanders do not migrate downstream. Karlstrom et al. (2013) developed depth-averaged conservation equations based on Parker's modelling and their work validates the notion that meandering can form in supraglacial channels when the Froude number (i.e., a ratio of inertial and gravitational forces on the fluid) is higher than 0.4 and channel width-to-depth ratios range from 2.5 to 5. They also indicated that the meandering of channels on ice is driven by channel curvature itself, which results in a flow instability leading the non-uniform melting rates along channel walls. In a more recent study, Fernández and Parker (2021) presented several laboratory measurements on meltwater meandering over ice. Their results demonstrated that the sinuosity growth of supraglacial channels results in interaction between vertical (i.e., depth of channel) and lateral (i.e., displacement of channel wall) incisions, which means that the faster the channel cuts vertically, the less time it takes to migrate laterally and the slower the sinuosity grows. This study also points out that future research on supraglacial channel meandering should focus on how meanders affect channel and planform morphologies.

2.2.4 Seasonal and interannual evolution of channel networks

Supraglacial channels are characterized by pronounced seasonal evolution with fluctuations in air temperature and meltwater production, and their morphology can change rapidly over short timescales (i.e., weeks to months) (Tedesco et al., 2013; Bell et al., 2017; St Germain and Moorman, 2019; Spergel et al., 2021; Yang et al., 2021). Antarctic supraglacial channels generally exist in the melt season during the austral summer (i.e., November to March). During this period, surface ice, snowpack and firn in the ablation zone can produce high volumes of meltwater because of the high temperatures. When there is sufficient meltwater on the surface, the supraglacial channels become gradually active and deliver the water to other places such as moulins, lakes and

crevasses. As mentioned in Section 2.1.2, supraglacial channels evolve through incising vertically, so they can only persist when the channel is cutting down faster than the surrounding ice is melting. However, surface ice, firn and snow will be frozen by low temperatures in the winter months. That means supraglacial channels in cold winters may be refrozen or even removed from the ice surface, or a portion may remain to be re-used in the next melt season despite there being no active flow in them (Yang et al., 2018; St Germain and Moorman, 2019; Hill and Dow, 2021). Consequently, channel discharge and termination (e.g., moulin, lake) inputs will form a temporal pattern as well which is likely to impact the basal sliding and subglacial effective pressure (Hill and Dow 2021).

Recent research has investigated seasonal changes of supraglacial channels and there has been a number of studies that aim to develop "dynamic" models to simulate the drainage system on ice (Kingslake et al., 2015; Koziol et al., 2017; Gleason et al., 2021; Hill and Dow, 2021). These models represent the flow in supraglacial channels (i.e., spillway models) across ice sheets, but also have more complex mathematical calculations. Koziol et al. (2017) applied a supraglacial hydrology model that combined surface water routing with supraglacial lake drainage through channels on the west Greenland Ice Sheet. Their results indicated that the partitioning of meltwater (i.e., water stored in lakes, channels, moulins, crevasses etc.) can vary with the intensity of the melt season, and interannual variations mainly depend on the nature of the supraglacial drainage system (i.e., the initial channel depth and heat transfer function) and the sensitivity of the subglacial system (i.e., fracture area and crevasses extent).

2.3 Methodological approaches used in studies of supraglacial channels

2.3.1 Mapping supraglacial channels using satellite remote sensing

Most studies of supraglacial channels have been conducted by employing various remote sensing methods. Optical imagery produced by satellite or Uncrewed Aerial Vehicle (UAV) platforms has been widely utilized to extract supraglacial channel networks on the

Greenland Ice Sheet (Yang and Smith, 2012; Smith et al., 2015; King et al., 2016; Yang et al., 2019a; Yang et al., 2019b; Lu et al., 2020a). Multispectral methods usually apply the Normalized Difference Water Index (NDWI), especially the NDWI adapted for ice (NDWIice) to discriminate between surface meltwater features and background snow/ice, followed by additional processing techniques (e.g., gabor filter, morphological operations) to highlight the contrast between supraglacial channels and other features (Yang et al., 2015a).

In general, channels with a large width (e.g., >15 m) can be visible in coarse- or moderate-resolution imagery, but narrower channels cannot be identified easily (Yang and Smith 2012). Landsat-7/8 images with 30 m resolution are usually used to map large supraglacial channels on the Greenland and Antarctic ice sheets (Poinar et al., 2015; Kingslake et al., 2017). Yang et al. (2019b) used both Sentinel-2 and Landsat-8 imagery to map supraglacial rivers in Greenland, and their results showed that Sentinel-2 images perform better than Landsat-8 images in delineating narrow (less than 15 m wide) and continuous channels. The growing availability of high-resolution imagery (e.g., IKONOS, WorldView-1/2) provides new opportunities to study supraglacial channels.

2.3.2 Modelling supraglacial flow routing

In addition to optical satellite imagery, elevation data have also increasingly been used in supraglacial hydrology research (Crozier et al., 2018; Yang et al., 2019a). Most channel networks on ice can be modelled from Digital Elevation Models (DEMs) by using flow routing algorithms and velocity parameterizations to calculate flow paths and travel times, respectively (Clason et al., 2012; Banwell et al., 2012; Yang et al., 2018; King et al., 2016; Lu et al., 2020a). Clason et al. (2015) employed a spatially distributed model for prediction of moulins formation and lake drainages on the Leverett Glacier in Southwest Greenland during the 2009 and 2010 ablation seasons. Their results indicate that the model performs effectively in simulating the spatial variability of mechanisms for transferring meltwater from the surface to the bed. Both the model and previous

observations suggest that in the lower part of the catchment (< 1000 m a.s.l.), the primary mechanism for transferring surface meltwater to the bed is through the development of moulins. Koziol et al. (2017) applied the Surface Routing and Lake Filling (SRLF) model to simulate surface drainage in west Greenland for three melt seasons, and they found more than 95% of available melt in the model may enter the englacial drainage system mainly by moulins, crevasses and hydrofracturing events. Hill and Dow (2021) presented the Subaerial Drainage System (SaDS) model that combines distributed runoff across the glacier surface in the bare-ice ablation zone with discrete flow in supraglacial channels. Their SaDS model was successfully applied to a partial region in Greenland and the results match well with the drainage system derived from a satellite-derived map.

Ideally, all the depressions in DEMs can be regarded as potential meltwater sinks. However, some of these depressions are DEM errors which will affect the accuracy of results produced by meltwater routing models (Lindsay and Creed, 2006). Yang et al. (2015b) noted that although DEMs are useful for extracting large-scale fluvial networks on the Greenland Ice Sheet, it is greatly affected by the depression-filling thresholds and not suitable for identifying the location of moulins. Xing et al. (2020) compared the accuracy of channels extracted using four different Greenland DEMs (i.e., the Greenland Ice Map Project (GIMP)1/2 DEM, TanDEM-X, and ArcticDEM). Their results showed that TanDEM-X performs best while GIMP1 performs the worst, and that medium to high-resolution DEMs have great potential for application in supraglacial hydrology. Recently, the Reference Elevation Model of Antarctica (REMA) which provides a high resolution (8 m) terrain map has been released by Howat et al. (2019). With typical elevation errors of less than 1 m, the REMA is a powerful tool for Antarctic research on supraglacial lakes and channels.

2.4 Antarctic supraglacial hydrology and its impacts

Surface melting in Antarctica is primarily influenced by weather and climate variability and is the primary source of nearly all surface water with minor contributions from rain

and condensation (Bell et al., 2018). Recent work shows that surface meltwater is observed to be more widespread in Antarctica than previously thought (Kingslake et al., 2017; Stokes et al., 2019; Corr et al., 2022; Figure 2.6), and it represents a potentially important component of ice sheet mass balance (Bell et al., 2018). For example, Corr et al. (2022) recently mapped all observable supraglacial lakes and channels in West Antarctica using Sentinel-2 imagery, and they found 10,223 lakes and 255 channels on the West Antarctic Ice Sheet and Antarctic Peninsula, with a total area of 119.4 km^2. Stokes et al. (2019) mapped the supraglacial lakes on the margins of East Antarctica during the melt season in January 2017 and found that there were over 65,000 lakes (about 1,300 km^2). These lakes primarily occur on ice shelves, where the most intense surface melting in Antarctica is observed (Cook and Vaughan, 2010; DeConto and Pollard, 2016). Recent studies have shown that Antarctic hydrological systems mainly occur in the following forms: (i) meltwater flowing along the steep slopes and forming supraglacial channels (Bell et al., 2017); (ii) accumulation in depressions and developing a lake/pond, sometimes also fed by channels (Stokes et al., 2019); and (iii) forming a lake after percolating into the sub-surface (Bevan et al., 2017).

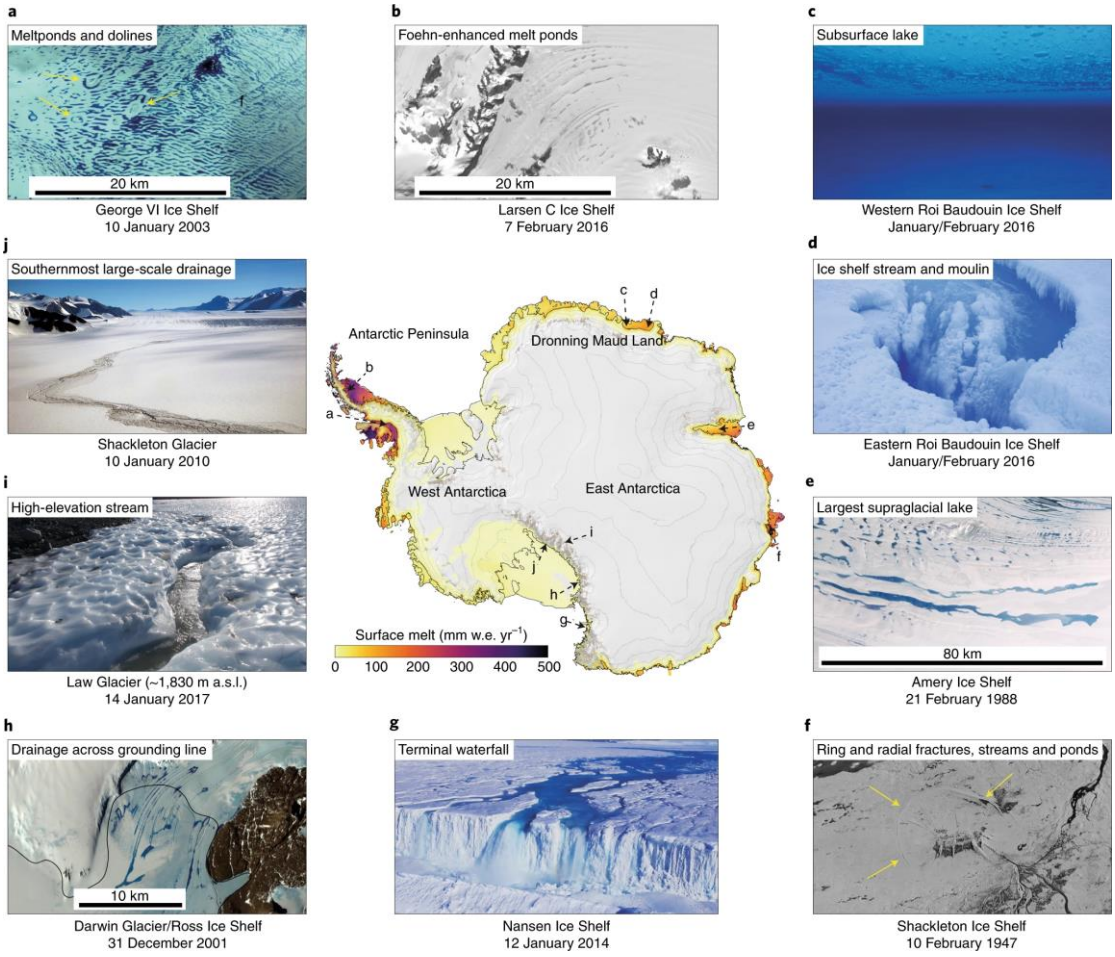

Figure 2.6 *Examples of supraglacial channels and lakes on Antarctic surface melt map* (Bell et al., 2018).

Meltwater on grounded and floating ice can be stored in impermeable surface depressions, and supraglacial lakes and channels form (Pitcher and Smith, 2019). The influences from supraglacial channels go beyond water transport, and there are four ways that they potentially affect the melt rate, ice stability, and ice dynamics (Figure 2.7). Firstly, surface meltwater may decrease the albedo of surrounding ice and accelerate the surface melting (Pitcher and Smith, 2019). Secondly, surface crevasses can also accumulate meltwater and the stored water can initiate or enlarge the ice fractures on ice shelves, termed hydrofracturing (Vieli et al., 2007; Banwell et al., 2014; MacAyeal et al., 2015; Bell et al., 2018; Leeson et al., 2020). Thirdly, when meltwater penetrates through moulins or crevasses and reaches the base of the ice sheet, it can act as a lubricant, making it easier for the ice to slide (Stevens et al., 2015; Tuckett et al., 2019; Smith et al., 2021). Last but

not least, if the channels take the water directly off the ice sheet (rather than percolating into the snow-firn and refreezing), they carry mass off the ice sheet (Smith et al., 2015; Pitcher and Smith, 2019) contributing runoff to sea-level rise and potentially mitigating hydrofracturing (Bell et al., 2017). Therefore, mapping supraglacial channels and understanding how they redistribute meltwater is increasingly important in predicting future mass loss (Bell et al., 2018; Pitcher and Smith, 2019).

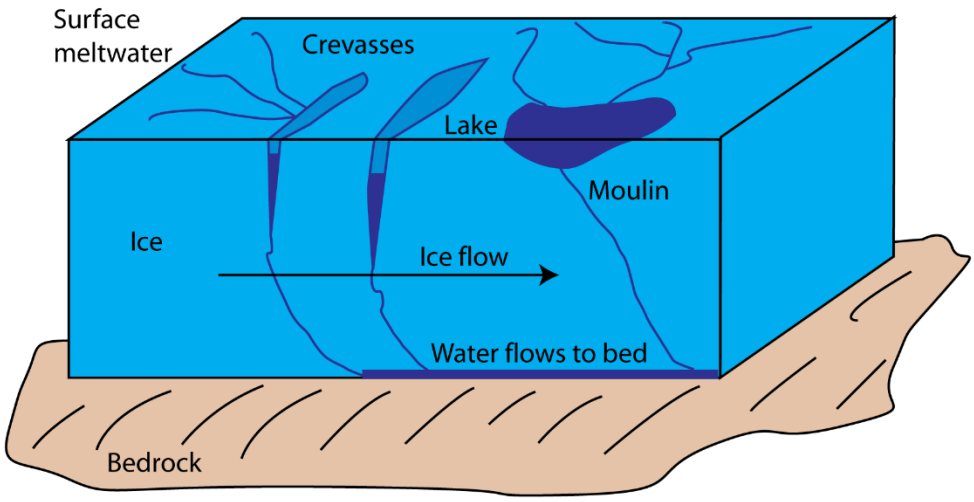

Figure 2.7 *Meltwater propagates to the glacier bed through crevasses and moulins. (Source: www.AntarcticGlaciers.com)*

Satellite observations (Arthur et al. 2020a, Dirscherl et al., 2021b; Spergel et al., 2021; Dell et al., 2022) and climate modelling (Lenaerts et al., 2017; Agosta et al., 2019; Arthur et al., 2022) are the two main approaches corresponding well with *in situ* observations to investigate the surface melting in Antarctica. Much of the current literature on Antarctic ice shelves (e.g., Nivlisen, Roi Baudouin, Riiser-Larsen, Bach and Nansen) pays particular attention to the widespread meltwater on ice shelves given that ice shelves help to hold back the ice flow from ice sheet and so any structural disruption to them may have consequences for inland glacier flow (Kingslake et al., 2015, 2017; Dell et al., 2020, 2022; Dirscherl et al., 2021b; Lenaerts et al., 2017; Bell et al., 2017, 2018; Arthur et al., 2022; Moussavi et al., 2020; Dirscherl et al., 2021b). Kingslake et al. (2015) modelled the drainage of supraglacial lakes across Nivlisen Ice Shelf and which extended for ~ 70 km.

They indicated that the surface drainage from some large lakes located near the grounding line is the most rapid, and the discharge from lake to channel is controlled by whether the drainage is stable or unstable. Kingslake et al. (2017) found aerial photographs from 1947 showing that supraglacial lakes and streams on Roi Baudouin Ice Shelf were present 68 years ago. Dirscherl et al. (2021b) investigated the dynamics of surface hydrological features on Riiser-Larsen Ice Shelf during the melt season from 2015 to 2021. Their results showed that the highest extent of supraglacial lakes on Riiser-Larsen reached ~85 km^2 and lakes expanded further across the ice shelf in years with the highest lake occurrence, while lakes cluster closer to grounding lines, blue ice or nunataks in years with lower lake coverage. According to Bell et al. (2017), active drainage networks including lakes and channels on the surface of Nansen Ice Shelf exported a large fraction (~ 259 to 806 m^3) of meltwater into the ocean between 2006 and 2015. The terminus of these supraglacial channels is a 130 m-wide waterfall that had the potential to export a whole year's worth of surface meltwater in seven days. It is worth noting that Bell et al. (2017) proposed a new discovery of Nansen Ice Shelf hydrology. They found that water has been exported by drainage systems through dolines and waterfalls during the last 100 years and this pattern may help to reduce the impact of warming temperatures on ice shelf.

Generally, supraglacial channels and lakes form an interconnected hydrologic network which will deliver and store surface meltwater, but the nature of the drainage system is often unclear, with most studies focusing solely on the detection of meltwater and, in particular, lakes (Banwell et al., 2014; Stokes et al.,2019; Arthur et al.,2020b; Dirscherl et al., 2021b). Kingslake et al. (2017) conducted the first continent-scale observation of Antarctic surface drainage systems by optical satellite imagery between 1947 and 2015. They found widespread supraglacial lakes and channels across the ice sheet and some of them have persisted for decades. The surface drainage systems consisting of channels and lakes on Amery Ice Shelf are able to deliver meltwater from grounded ice onto and across ice shelves up to 120 km. Arthur et al.(2020b) observed extensive supraglacial lakes on Shackleton Ice Shelf from 2000 to 2020 by applying optical satellite imagery. Their

results indicated that supraglacial lakes presented obvious seasonal variations in area and depth. Moreover, Leeson et al. (2020) found most supraglacial lakes on Larsen B Ice Shelf between 1979 and 2002 refreeze but a few still drain water in winter. Notably, their results also showed there are no significant changes in lake characteristics including lake number and area during this period, which means water has been drained off the shelf by an active supraglacial drainage network. Considering the intrinsic connection between supraglacial channels and lakes, it is critical to understand the evolution processes and morphometric characteristics of supraglacial channels in Antarctica and particularly on ice shelves (Bell et al. 2018, Rintoul et al. 2018, Stokes et al. 2019).

3.Study sites

Surface meltwater in Antarctica is becoming increasingly extensive during the short melt seasons of November to February. Although there is a growing interest in Antarctic hydrological processes, most studies have focused on the extensive supraglacial lakes. Little attention has been paid to supraglacial channels that have an important role in delivering meltwater across the ice surface, often connecting lakes. This chapter will first give an overview of the five Antarctic ice shelves selected for this study and then introduce the detail of previous studies conducted at these sites.

3.1 Overview of the investigated Antarctic ice shelves

As noted above (Section 2.4), supraglacial channels are an important component in the Antarctic hydrology system and play a key role in ice dynamics. On the one hand, meltwater transported by the channels can flow into the moulins or surface crevasses which may modulate subglacial water pressure and basal sliding (Pitcher and Smith, 2019). On the other hand, large volumes of water from the ablation zone can directly drain off the margin of ice shelves, which may affect ice-sheet mass balance and runoff, which contributes to sea level rise (Corr et.al, 2022). However, little attention has been paid to the evolution and characteristics of supraglacial channels. In this study, five ice shelves located in the EAIS (i.e., Riiser-Larsen, Nivlisen and Roi Baudouin ice shelves) and the WAIS (i.e., Bach and Nansen) were selected to provide an important opportunity to advance the understanding of Antarctic supraglacial channels (Figure 3.1).

The ice shelves investigated in this study are displayed in Figure 3.1 and have been chosen for four main reasons: firstly, these ice shelves are characterised by a range of surface melt conditions and features, such as atmospheric temperature and ice velocity (Table 3.1), resulting in a wide variety of surface meltwater distribution; secondly, recent evidence suggests that supraglacial lakes and channels are widespread and well-developed based on previous observations from optical satellite imagery, and these

channels display a range of different drainage characteristics, which would potentially provide new insights regarding the controls on supraglacial channel networks (Bell et al., 2017; Arthur et al., 2020a; Dirscherl et al., 2021b; Arthur et al., 2022; Corr et al., 2022; Dell et al., 2022); thirdly, five ice shelves were chosen from across the Antarctic Peninsula and both East and West Antarctica, which allow investigation of different geographical location and allow comparison between settings; fourthly, increasing quantities of remotely sensed data including satellite imagery and high-resolution DEM data are available for all the sites.

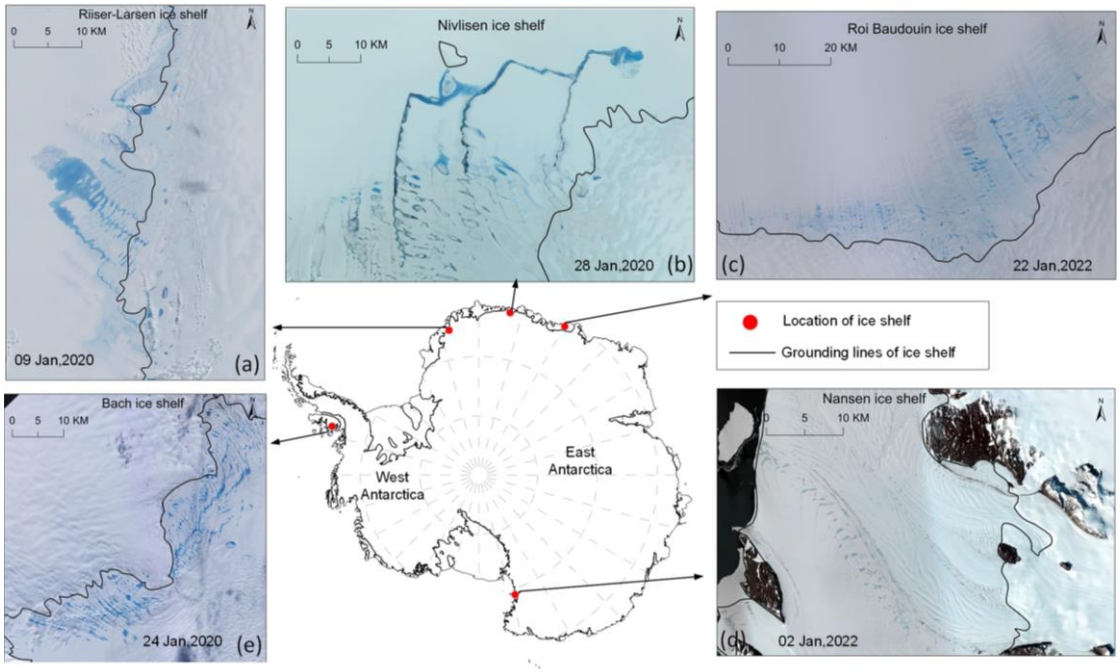

Figure 3.1 *Supraglacial channels on selected Antarctic ice shelves: (a) Riiser-Larsen, (b) Nivlisen, (c) Roi Baudouin, (d) Nansen, I Bach using Landsat-8 true colour composites*.

Table 3.1 Overview of the studied Antarctic ice shelves.

Attributes	Area (km^2)	Location	Mean annual temperature (°C)	Mean ice velocity ($m\ yr^{-1}$)
Bach	4,540	72°S,72°W	-1.8	76
Nansen	2,000	75°S,163°E	-8.2	110
Nivlisen	7,600	70°S,11°E	-10.0	100

Riiser-Larsen	48,180	72°S, 15°W	-15.6	200
Roi Baudouin	33,000	70° S, 24°E	-9.9	220

* Mean annual temperature datasets were obtained from the British Antarctic Survey (https://legacy.bas.ac.uk/met/READER/), and the Mean ice velocity data were produced by Shen et al (2020).

3.2 Ice shelves in East Antarctica

Three ice shelves (Riiser-Larsen, Nivlisen and Roi Baudouin) in Dronning Maud Land, East Antarctica, with well-known supraglacial meltwater dynamics are used as study sites. The Nivlisen Ice Shelf (70°S, 11°E: Figure 3.1b) lies in central Dronning Maud Land and is mainly fed by the Potsdam Glacier. It is 123 km wide and 92 km long, occupying a total area of about 7,600 km^2. The ice thickness of Nivlisen Ice Shelf ranges between 150 m to 700 m from the calving front to the grounding line (i.e., where the ice shelf begins to float) in the southeast, and it has an average ice shelf flow speed of nearly 100 m yr^{-1}. The Roi Baudouin Ice Shelf (70° S, 24°E: Figure 3.1c) in eastern Dronning Maud Land has an area of approximately 33,000 km^2 and is separated by the Derwael Ice Rise into its western and eastern parts (Eisermann et al., 2021). It extends along the coastline in a southwest-northeast direction for about 350 km, with a width of about 50 to 100 km. The Riiser-Larsen Ice Shelf (72°S, 15°W: Figure 3.1a) extends ~400 km between Cape Norvegia and Lyddan Island, in western Dronning Maud Land. It covers ~48,180 km^2 and has an ice velocity generally below 1 m d^{-1} (Dirscherl et al., 2021b). The grounding line of Riiser-Larsen Ice Shelf is developing parallel to the calving front for hundreds of kilometres.

3.3 Ice shelves in West Antarctica

The two ice shelves investigated in West Antarctica are Bach Ice Shelf (72°S,72°W: Figure 3.1e) and Nansen Ice Shelf (75°S,163°′E). The Bach Ice Shelf has an area of ~4540 km^2 and is located in the southwest Antarctic Peninsula region, and ice flows at an average

speed of 76 m y^{-1}. The Bach Ice Shelf has a maximum thickness of 821 m. The Nansen Ice Shelf (70°S,11°E: Figure 3.1d) is located along the edge of the Ross Sea, covering an area of 1,800 km^2 in Victoria Land. The Priestley and Reeves Glaciers are two primary glaciers that feed Nansen Ice Shelf, and the ice shelf thickness of Nansen ranges from 1000 m at the grounding line of Priestley Glacier to 120 m at the ice shelf terminus.

4. Methods

This chapter introduces the data and methods used in this study. The overarching approach taken in this project is to use remotely sensed data to map supraglacial channels on the five selected ice shelves in Antarctica (Section 3), and to conduct a quantitative analysis of the characteristics of the supraglacial channel networks. The first section of the methods (Section 4.1) demonstrates the data sources and general approaches to extracting hydrological features using satellite imagery. Processes for delineating the supraglacial river networks are presented in Section 4.2. The final Section 4.3 illustrates the procedures for calculating fluvial properties of supraglacial channels.

4.1 Water detection using remote sensing approaches

Remotely sensed data, particularly satellite imagery, is nowadays the most prevalent data source in polar studies. Numerous new approaches for surface water detection using remote sensing data have been proposed, which can be divided into two main categories: threshold-based methods (Yang et al., 2019b; Lu et al., 2020a; Moussavi et al., 2020; Lu et al., 2021; Yang et al., 2021) and machine learning methods (Acharya et al., 2019; Dirscherl et al., 2020; Yuan et al., 2020; Dirscherl et al., 2021a). In this study, supraglacial water bodies were extracted by a water index threshold-based method that is simple to implement and widely used.

4.1.1 Overview of remotely sensed data

The remotely sensed data used in this study consist of Landsat-8 Operational Land Imager (OLI) imagery and the Reference Elevation Model of Antarctica (REMA) data (Table 4.1). Landsat-8 Level 2 datasets were obtained from Earth Explorer (http://earthexplorer.Usgs.gov/). The surface reflectance and land surface temperature of Level 2 products have been atmospherically corrected, removing the need to do processing steps for alleviating the atmospheric effects. REMA mosaic data were downloaded from the U.S. Polar Geospatial Centre (https://www.pgc.umn.edu/data/rema/) (Howat et al., 2019),

which provides the elevation information of each ice shelf at 8 m spatial resolution.

Table 4.1 Landsat-8 OLI images information

Ice Shelf	Landsat-8 OLI			REMA DEM
	Row	Path	Date	Scene ID (8 m)
Bach	111	219	24 Jan, 2020	36-11/12, 37-11/12
Nansen	113	61	02 Jan, 2022	15-35/36
Nivlisen	109	167	28 Jan, 2020	50-34/35
	110	167		
Roi Baudouin	109	154	22 Jan, 2022	49-42/43
Riiser-Larsen	111	178	09 Jan, 2020	49-27, 50-27

4.1.2 Landsat-8 OLI imagery

Landsat-8 was launched by NASA on February 11 in 2013 and carries two instruments – the Operational Land Imager (OLI) and the Thermal Infrared Sensor (TIRS). It has provided multispectral imagery since 30 May 2013, including 30-meter visible, near-infrared, and shortwave infrared bands (15-meter panchromatic) by the OLI and land surface temperature bands by TIRS. The Landsat-8 satellite has a large swath (185 km) and seasonal coverage of the global landmass of a 16-day repeat cycle. Due to the limitation of data availability and quality (e.g., limited satellite image acquisition time and cloud cover), it is difficult to obtain imagery of different ice shelves in the same year. The acquisition timing of satellite imagery in the year is of great importance. In this study, Landsat-8 OLI level 2 images were collected on one date in January 2020 and 2022 (Table 4.1), because meltwater is considered to be their peak volume during this time of year, and channel networks are at the near-maximum extent which would be easier to compare their characteristics on different ice shelves (Nicolas et al., 2017; Stokes et al., 2019; Arthur et al., 2022). The focus of the study was not to investigate temporal evolution, which future work could address.

4.1.3 REMA DEM data

REMA is a digital elevation data of Antarctica with 8 m spatial resolution, which is generated from high-resolution optical satellite imagery acquired between 2011 and 2017 (Howat et al. 2019). The REMA mosaic data covers nearly 95% of the entire continent, and it is the highest spatial resolution DEM available for Antarctica. REMA has been widely used in Antarctic studies (Dunmire et al., 2020; Alley et al., 2021; Dong et al., 2021; Spergel et al., 2021; Pratap et al., 2022). The elevation errors of REMA are less than 1 m when comparing with airborne laser altimetry which provides more accurate topographic information. REMA DEM data captures the elevation from a large time span of images (9 May 2015 with a standard deviation of 432 days), which does not exactly correspond to the timings of satellite imagery used in this study. Given that the elevations are unlikely to change significantly in selected sites during the period of study, temporal non-coincidence would not have a great influence on the results.

4.2 Delineation of supraglacial channel networks

4.2.1 Data pre-processing

Landsat-8 level 2 images have been officially corrected to eliminate the atmospheric effects, and its projection system is Polar Stereographic which corresponds with REMA. All satellite imagery was captured in low cloud cover (below the ≤ 30% threshold) conditions. Therefore, some pre-processing steps (i.e., atmospheric calibration and reprojection) are not necessary. The first step in this study was to determine the scope of the study area (or part of the ice shelf) to be analysed on the images. All the Landsat-8 imagery were acquired in January as the supraglacial meltwater features are easily identified. First, the areas of the images with supraglacial lakes/channels could be approximately defined by visual interpretation. Second, images including Landsat-8 and REMA were cropped visually to the same area in ArcGIS 10.3 to a smaller area which includes as much visible surface water as possible for the following analysis.

4.2.2 Automatically delineation of surface water

This study employed automated mapping to obtain supraglacial channels on Antarctic ice shelves for two main reasons: firstly, the automatic classification method (Yang et al., 2015) adopted in this study is widely used to extract supraglacial channels on Greenland Ice Sheet, and here this study applied it to the mapping of channels on Antarctic Ice Sheet to confirm its feasibility and enrich the scope of the research. Secondly, although a limited number of satellite images were used in this study, the selection of the study sites encompasses ice shelves with varying area scales ranging from 2,000 to 48,180 km^2, and the size of the channel networks on their surfaces varies considerably. Therefore, the use of automatic mapping allows for more efficient and consistently objective results in the classification map of surface meltwater. In this section, the process of automatically detecting surface water was divided into three parts (Figure 4.1): preliminary extraction, refined extraction and then combine water features from the previous two steps, and finally map the centrelines of supraglacial channel networks. The details of the method are described in Sections 4.2.2.1 to 4.2.2.3 and are summarised in Figure 4.1.

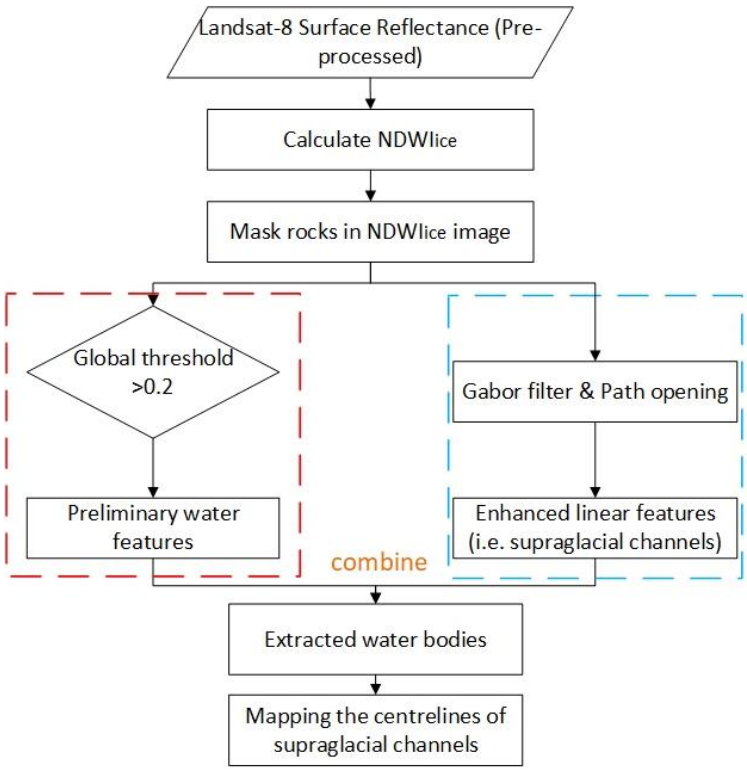

Figure 4.1 *Supraglacial channel networks delineation scheme: the red box represents the preliminary extraction based on a global threshold of normalized difference water index for ice (NDWIice); the blue box illustrates the process of refined detection of supraglacial channels following Yang et al. (2015).*

4.2.2.1 Preliminary extraction based on a water index method

This study adopted an automated mapping method to delineate the channels on ice. After clipping the pre-processed Landsat-8 imagery into the areal extent, the next step was to obtain all open water features present on the ice shelf. The normalized difference water index (NDWI) is commonly used in terrestrial environments to extract water bodies from satellite imagery (Yang et al., 2015a; Moussavi et al., 2016; Stokes et al., 2019; Yang et al., 2019b; Arthur et al., 2020b; Moussavi et al., 2020; Corr et al., 2022). The NDWI result can be computed with the normalized ratio of the Near-Infrared (NIR) and Green Bands, Eq. (1) (McFeeters, 1996), and surface water in the NDWI image shows brightly which is sharply contrasted with the dark background. The reflectance in NIR wavelengths of surrounding terrestrial vegetation and soil (generally not relevant in Antarctica) is higher than water, while the snow, bare ice and firn also have low reflectivity in NIR Band which is easily confused with water in glaciological environments. Consequently, NDWI for the combination of NIR and Green bands works best in terrestrial environments (Yang and Smith, 2012).

For better discriminating water in supraglacial surroundings, the modified NDWI has been proposed and termed the NDWI adapted for ice (NDWIice) (Yang and Smith, 2012). NDWIice uses the Blue and Red Bands, Eq. (2), instead of the NIR and Green Bands, because there is an apparent difference between the reflectance of water and ice in the Red Band and the high reflectance of water in the Blue Band. Compared with other versions of the NDWI, NDWIice is found to detect surface water more accurately, especially for areas containing slush and blue ice (Arthur et al., 2020b; Dell et al., 2022). Bell et al. (2017) applied the NDWIice to Landsat-8 imagery and precisely distinguished

the ice surface water and slush by setting the shallow (0.12 < NDWIice < 0.14), medium (0.14 < NDWIice < 0.25) and deep (NDWIice > 0.25) thresholds. As a result, this study adopted NDWIice as the basis for all further water delineations.

$$NDWI = \frac{Green-NIR}{Green+NIR} \quad \text{Eq. (1)}$$

$$NDWI_{ice} = \frac{Blue-Red}{Blue+Red} \quad \text{Eq. (2)}$$

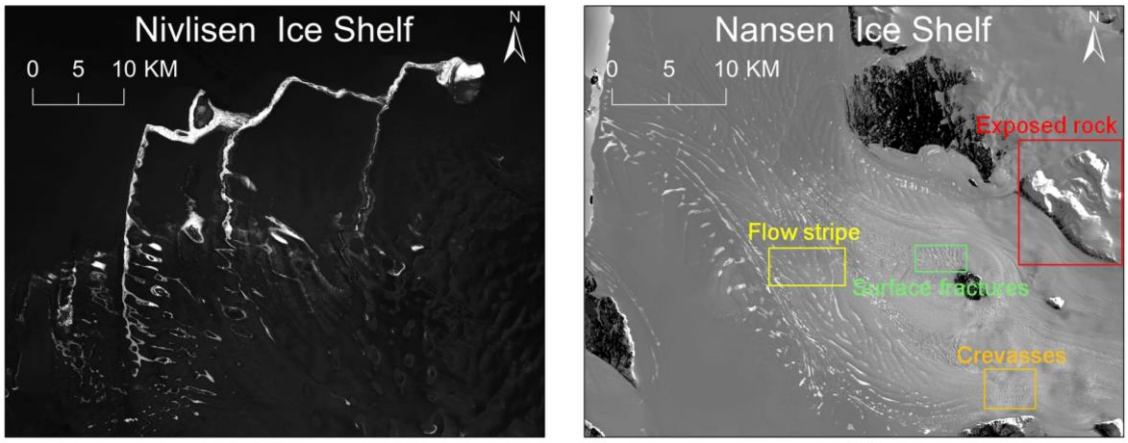

Figure 4.2 *NDWIice images for (a) Nivlisen Ice Shelf and (b) Nansen Ice Shelf.*

As shown in Figure 4.2(a), there are some obvious supraglacial channels and lakes displayed as brighter pixels in the NDWIice image for Nivlisen Ice Shelf. Ideally, all pixels of open water should be brighter than other objects in the NDWIice image. However, the NDWIice image for Nansen Ice Shelf (see Figure 4.2 b) has generated some confusion between water and exposed rocks, shades of flow stripes and surface fractures. NDWIice values of rocks are even greater than those of water and appear brighter in the image, which is due to the similarity of spectrum in the Red Band between bedrock and water (Burton-Johnson et al., 2016; Arthur et al., 2020b). To avoid the misclassification resulting from exposed bedrock, all rocks were masked by manually inspecting each NDWIice image. In detail, the bare rocks showing as bright pixels (i.e., misclassified as

water) on the NDWIice image have been manually digitized and removed using the ArcGIS tools. The processed NDWIice images were used to conduct further analysis.

Next, appropriate thresholds were set for each NDWIice image of all study ice shelves to discriminate between the water and non-water. Across Antarctic ice shelves, there is commonly observed “ice slush” along supraglacial channels (Dell et al., 2022). Ice slush is a transitional material formed when the pores of firn become saturated, and it usually occurs in the ablation zone particularly around refrozen lakes and blue ice areas causing it to have an albedo between water and snow (Figure 4.3) (Yang and Smith, 2012; Zatko and Warren, 2015; Dell et al., 2022). As a result, it is necessary to determine the threshold to classify water and slush. An NDWIice threshold of 0.25 was the most widely used in previous studies (Bell et al., 2017; Williamson et al., 2017; Banwell et al., 2019; Arthur et al., 2020b; Dell et al., 2020) which can better classify liquid water from slush and other non-water features. However, the threshold of 0.25 was found to underestimate the liquid surface water in this study (Figure 4.4b). Although most slush was not classified in the result, many pixels of shallow streams that visually appears to be light blue and narrow on the Landsat-8 imagery have been excluded. This phenomenon is also consistent with the findings of Bell et al. (2017) which demonstrates that the NDWIice was sensitive to the amount of surface melt during the melt season. To identify as many fine channels as possible, this study decreased the threshold value starting at 0.25 at 0.01 intervals and observed the resulting binary water mask to determine the threshold that would detect more meltwater (Figure 4.4c, d). As shown in Figure 4.4, a lower 0.2 NDWIice threshold was deemed satisfactory to provide a conservative estimate of the surface water for further analysis.

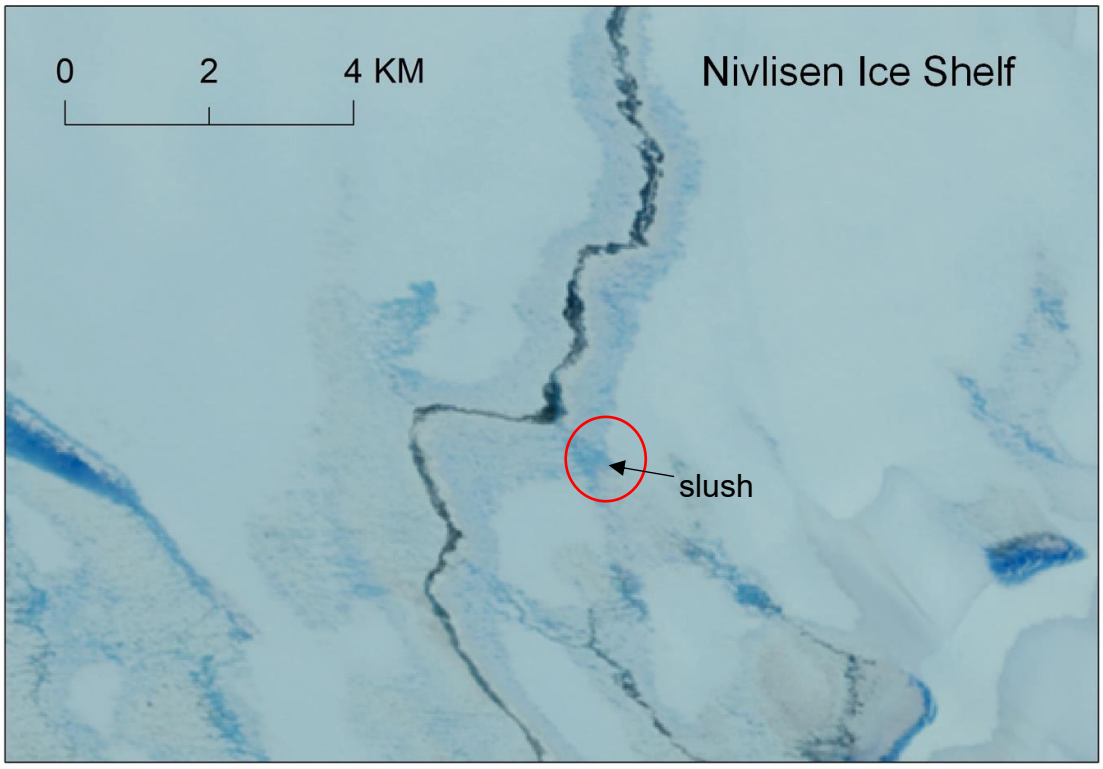

Figure 4.3 *Ice slush along the supraglacial channels on Nivlisen Ice Shelf (Landsat-8 OLI 30 m imagery in true colour).*

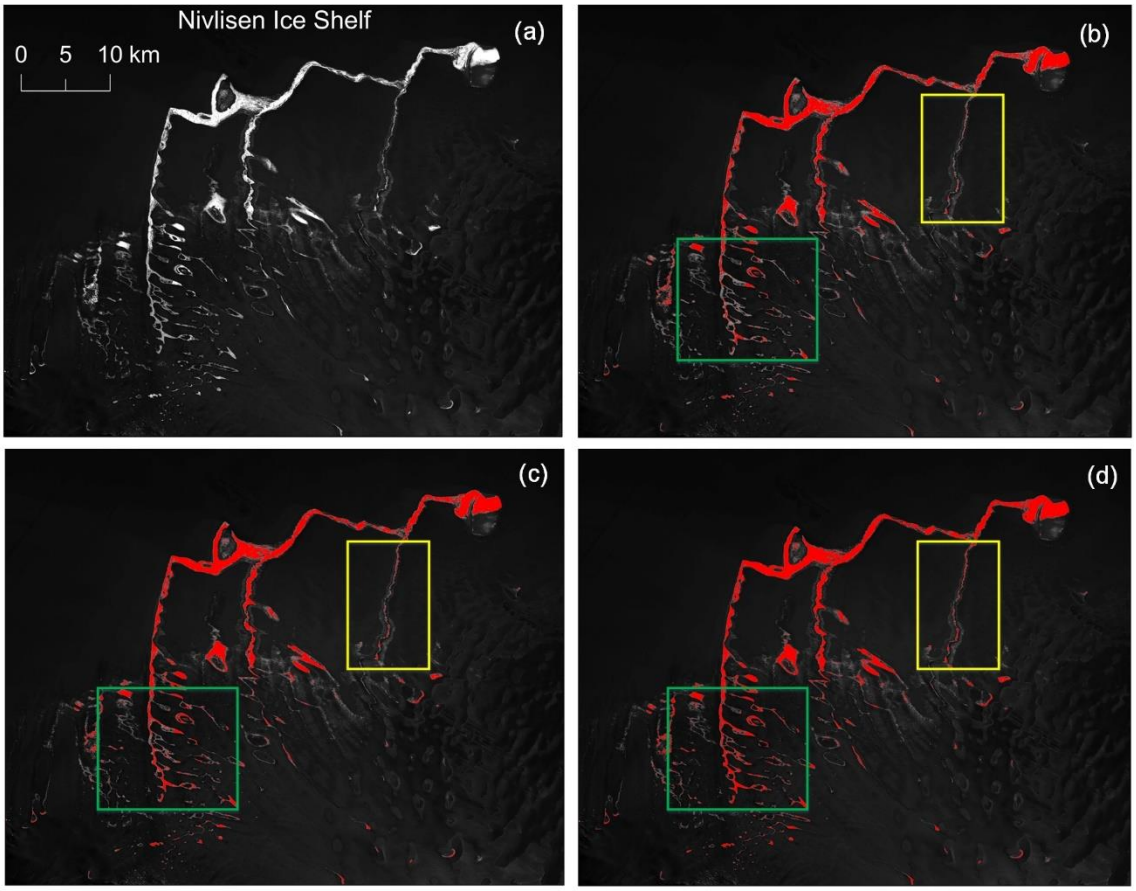

Figure 4.4 *Binary water mask from different NDWIice thresholds: (a) NDWIice image generated from Landsat-8 imagery; (b) 0.25 threshold value; (c) 0.23 threshold value; (d) 0.2 threshold value. The red polygons are the detected surface meltwater. The areas corresponding to the green and yellow boxes in the graph are able to detect more surface water as the threshold is reduced to 0.2.*

4.2.2.2 Refined extraction of linear features by image enhancement

In the previous step, a NDWIice threshold of 0.2 was set to separate water from the snow and ice, but some pixels belonging to water were still ignored because of the low contrast between shallow or narrow flowing streams and surrounding land (Cooley et al., 2017; Feng et al., 2019; Lu et al., 2020a). As a result, using a single global threshold of NDWIice is unable to fully delineate the supraglacial channels. To address this problem, the Gabor-PPO method proposed by Yang et al. (2015) was employed here to improve the detection of supraglacial channels. This method aims to increase the contrast between linear or curvilinear features and the image background in three steps.

Firstly, a band-pass filter (BPF) was applied to denoise the NDWIice image (Yang et al., 2015). Secondly, a Gabor filter (3 × 3 moving window) was applied to highlight the cross sections of channels. A two-dimensional Gabor filter is a sinusoidally modulated Gaussian kernel function often applied to texture separation in image processing, and it also helps enhance the detection of supraglacial channels whose cross-sections appear Gaussian in imagery as they increase from low values at the edge of the channel (shallower water), to the higher values (deeper water) in the centre (Yang et al., 2015a; Yang and Smith, 2016). Thirdly, a morphological operator called Parsimonious Path Opening (PPO) was matched to enhance the connectivity of supraglacial channels longer than 20 pixels (600 m). After this enhancement process, channels on the ice surface are better identified from the image background. Finally, a global threshold (i.e., out of 255 in a grey level image) was automatically determined based on the resulting image histogram to generate a binary stream mask (Yang et al., 2015a) (Figure 4.5). The adopted

Gabor-PPO method was implemented using MATLAB2017b. This enhancement processing helps to delineate those curvilinear supraglacial channels, particularly improving the completeness of the extracted channel networks (Figure 4.5).

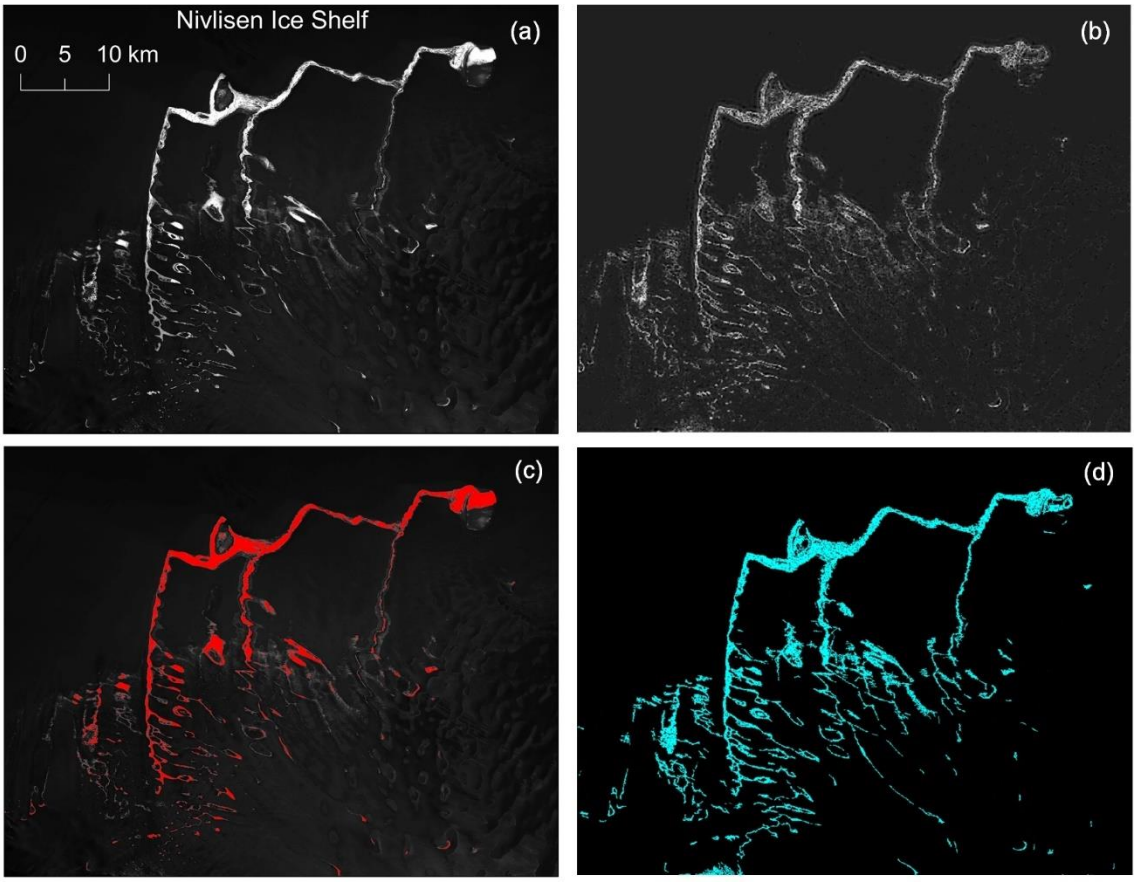

Figure 4.5 *Extracted surface water on Nivlisen Ice Shelf: (a) original NDWIice image;(b) enhanced NDWIice image;(c) preliminary water mask (red) extracted by 0.2 NDWIice threshold;(d) refined water mask (blue) extracted by enhanced NDWIice image.*

4.2.2.3 Combining surface water masks

After the refined extraction of surface water (including supraglacial channels and lakes), there were two binary open water masks: a preliminary result including lakes and deeper channels, and a refined result containing continuous and shallow channels. An additional processing step is needed to combine these two masks to produce the final water delineation result. This scheme used the Merge tool in ArcGIS 10.3 to create the extracted

water map for each selected ice shelf (Figure 4.6), and it is clear to see that supraglacial channels are better delineated when integrating the cross-sectional and longitudinal information.

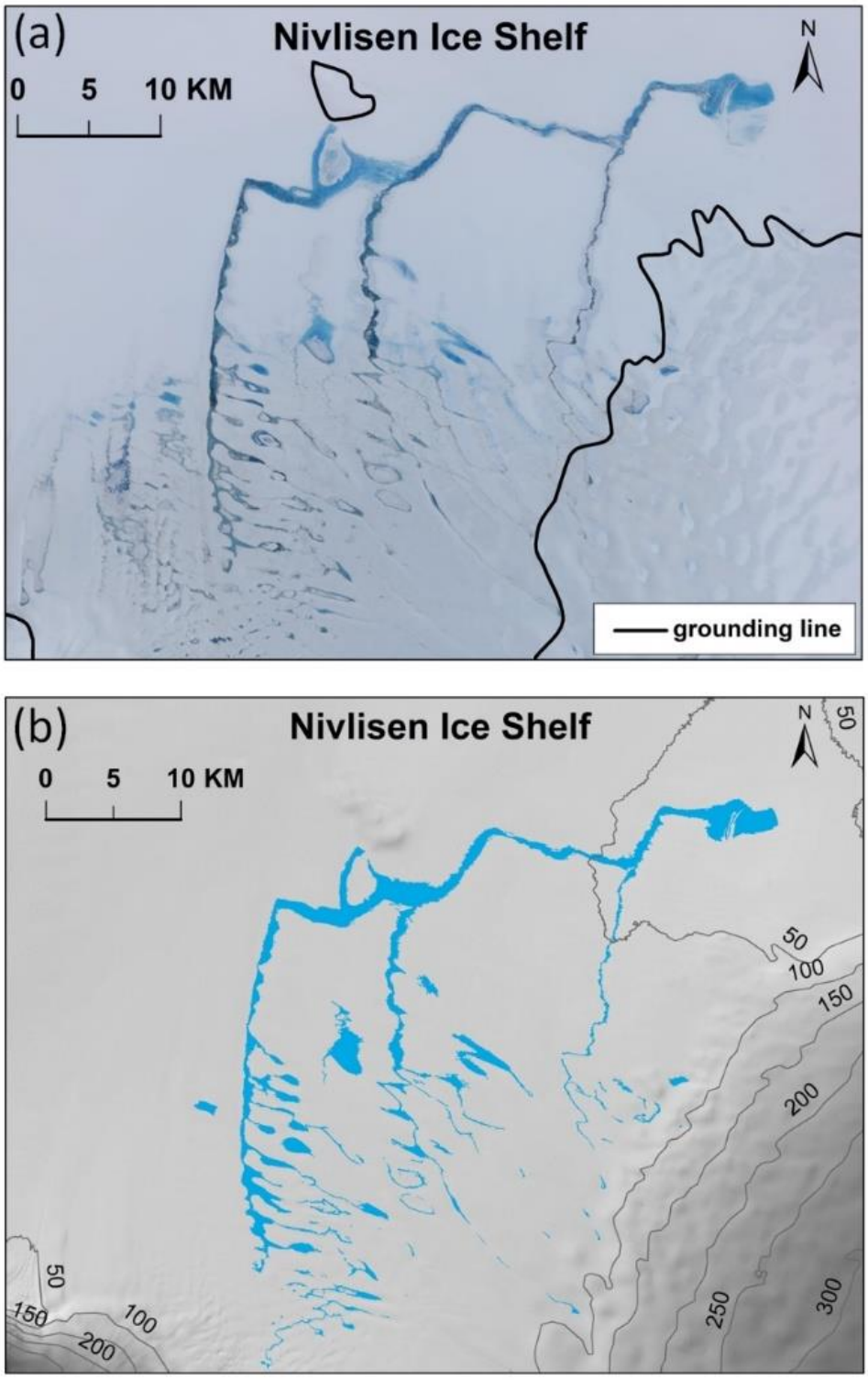

Figure 4.6 *Supraglacial channels and lakes extracted by combining preliminary and*

refined water masks (a)Landsat-8 OLI imagery in true colour for the Nivlisen Ice Shelf, (b)blue polygons indicate the surface water overlaying the REMA DEM image (8 m spatial resolution) with contours.

4.2.3 Mapping the centreline of supraglacial channel networks

To understand the fluvial geometry and connectivity of supraglacial channels, the extracted water mask should be transformed into polylines to represent the river networks. In this study, three popular automatic methods, the ArcScan tool (Bajjali, 2017; Lu et al., 2020a), RivGraph (Schwenk and Hariharan, 2021) and Natural-Rule-Based-Connection (NRBC) (Zeng et al., 2015), were tested to map the centrelines of supraglacial channels including those that flow through lakes from the polygons of extracted water (see Figure 4.7).

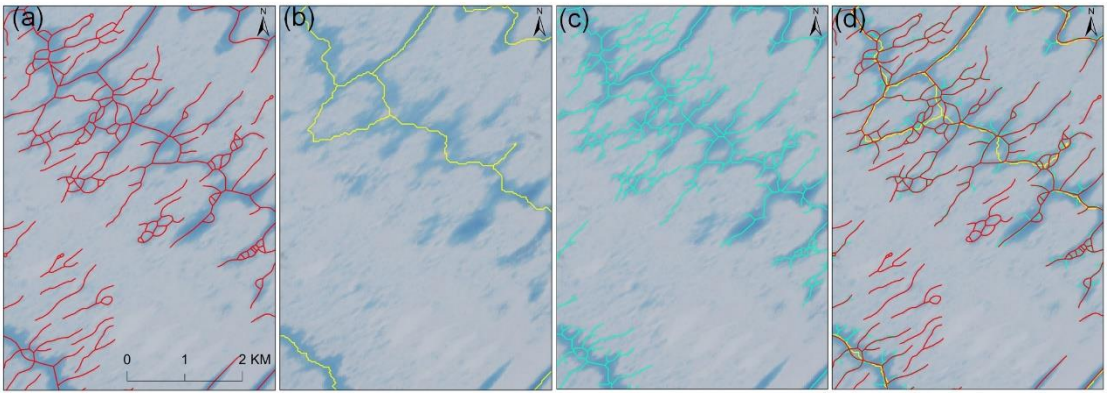

Figure 4.7 *Centrelines for partial supraglacial channel networks on the Bach Ice Shelf mapped by different methods: (a) ArcScan tool;(b) NRBC;(c) RivGraph. Figure (d) shows the result of the superimposition of the centrelines drawn by the above three methods.*

Figure 4.7 shows the centrelines for some supraglacial channels on Bach Ice Shelf mapped by different approaches. For comparison purposes, all methods are tested with default parameters. Each method exhibits different characteristics, but almost all of them incorrectly drew some circular centrelines at channel junctions, especially where multiple channels occur. The result of the ArcScan tool retains a good level of detail in the

centrelines of supraglacial channels, although some tributaries appear disconnected. However, the NRBC method only mapped the centrelines of the trunk channels and did not plot most of the tributaries. For RivGraph's result, there are a lot of unnecessary spurs as the channel crosses the lake. As shown in Figure 4.7(d), when the centrelines drawn by the above three methods are superimposed on each other, their respective advantages and disadvantages become more apparent. It was decided that the most appropriate method to adopt for this investigation was the ArcScan tool in ArcGIS software, because centrelines generated by the ArcScan tool retain more detail, have better continuity and make fewer errors at channel crossings.

4.3 Hydromorphology of supraglacial channels

4.3.1 Supraglacial channel network ordering

The motivation for this study lies in exploring the characteristics of supraglacial channels and their drainage networks. Thus, it is key to quantify the morphometric statistics of channel networks on ice and their connectivity with lakes. Here the Strahler ordering system was used to classify types of channels based on their number of stream junctions (Strahler, 1957; Yang et al., 2016; Lu et al., 2020a). As shown in Figure 4.8(a), a channel without any tributaries will be assigned as first-order, and a channel assigned second-order has two first-order streams flowing into it. If two streams with different orders join the same stream, it would be labelled as the same order as the higher order of these two tributaries. Some studies used the automatic algorithm to label the numeric Strahler order for vector channel networks (Maidment and Morehouse, 2002; Gleyzer et al., 2004; Omran et al., 2016; Lu et al., 2020a). However, these methods were found to be unsuitable for this study. This is because there are numerous multichannel segments in supraglacial channel networks (see Figure 4.8(b)), and the automatic methods cannot classify the order accurately. Given that the following analysis is all based on the order of river networks, this study assigned the Strahler stream order manually in ArcMap 10.3 software to avoid classification errors.

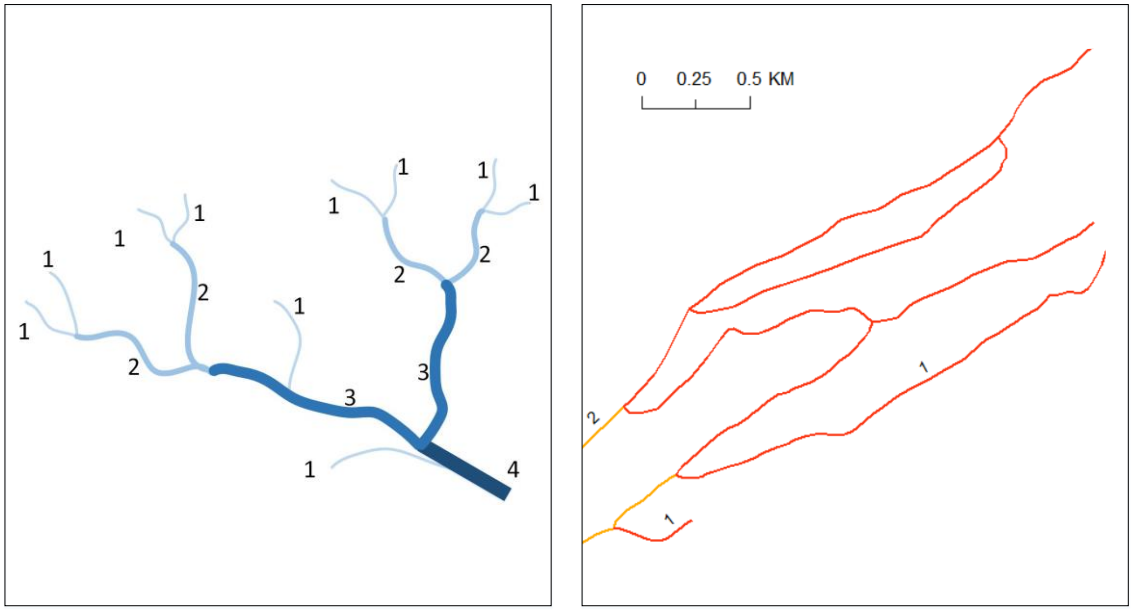

Figure 4.8 *Examples showing multichannel of supraglacial channel network and manually labelled Strahler stream order (black numbers): (a) Strahler ordering system; (b) multiple channels on Riiser-Larsen ice shelf, there are nine first-order (red) and three second-order (yellow) channel segments in the example network.*

4.3.2 Fluvial morphology

To calculate some fluvial metrics, the supraglacial channel networks with assigned stream orders were further analysed at different scales (i.e., channel segments of fixed interval or different orders, and whole river networks). Channel length, width, depth, slope, bifurcation ratio and orientation were computed for all segments; drainage area and drainage density were calculated for each supraglacial channel network.

Table 4.2. Fluvial metrics of supraglacial channels calculated in this study

Morphometry metrics	Scales	Definition	Reference
Strahler stream order	Channel segments	a n^{th} order stream is always located downstream of the confluence of two $(n-1)^{th}$ order streams	(Strahler, 1957 ; Yang et al., 2016 ;

Width (m)	30 m channel segment	width between banks on both sides	Gordon et al., 1992 ; Gioia et al., 2018 ; Frasson et al., 2019)
Depth (m)		depth from surface to bottom of flowing water	
Surface slope	100 m channel segment	the surface elevation difference divided by horizontal distance	
Bed slope		the bed elevation difference divided by horizontal distance	
Sinuosity	2000 m channel segment	the ratio of the length between two points on a channel to the straight-line distance	
Length (m)	Channel segments of different orders	the path distance and area between segment endpoints (Confluences)	
Bifurcation ratio		the ratio of the number of channels for a given order N_u to the number of channels in the next higher order N_{u+1}	
Orientation		The compass direction that that section of channel flows along	
Drainage/catchment area	Downstream end of channel segments	The area of the ice sheet that drains into that point in the channel	

Drainage density (km/km^2)	Channel network	the total length of channels in a drainage catchment divided by the area of the ice watershed	

4.3.2.1 Width and depth of supraglacial channel

Widths and depths of all supraglacial channels were sampled at 30 m intervals along each river segment using the FluvialCorridor toolbox (Roux et al., 2015). The measurement interval was set to 30 m as the Landsat-8 OLI image has a spatial resolution of 30 m, thus ensuring that all variations in width and depth are captured. The width was derived from the polygons extracted from the water delineation maps. Depths of all supraglacial channels and lakes were retrieved by using spectral band ratios that are widely used in the literature (Smith et al., 2015; Moussavi et al., 2016; Pope et al., 2016; Yang et al., 2021). This spectral band-ratio approach relies on the relative reflectance in two different wavelengths, and the Band-1 (coastal) and Band-3 (green) bands of Landsat-8 OLI imagery have been validated to be one of the best combinations to derive water depth based on the dual-channel model (Eq.3) (Moussavi et al., 2016; Pope et al., 2016). The empirical derivation of calibrated coefficients is as follows (Pope et al., 2016):

$$z = a + bX + cX^2 \quad \text{Eq.(3)}$$

$$X = \ln(Band_1/Band_3) \quad \text{Eq.(4)}$$

where $a = 0.1488$, $b = 5.0370$ and $c = 5.0473$, $Band_1/Band_3$ is the ratio of the reflectance of Landsat-8 OLI Band-1(coastal) and Band-3 (green), and z stands for the derived water depth.

To evaluate and compare with other studies in the literature with the results of this study, the depths of supraglacial lake from Arthur et al. (2022) were sampled in the same melt

season (i.e., 2020) and the same locations (i.e., Nivlisen and Riiser-Larsen Ice Shelf) as the reference. Arthur et al. (2022) estimated the depth of supraglacial lakes across the EAIS by using a physically-based model which is also commonly used for deriving water depth (Sneed and Hamilton 2011, Banwell et al. 2014). Some earlier studies suggested that the spectral band-ratio method is expected to be more robust than a physically-based model (Stumpf et al. 2003, Legleiter et al. 2009). Pope et al. (2016) compared several approaches to estimate the depth of supraglacial lakes based on Landsat-8 OLI data. They found that the empirical method (i.e., spectral band-ratio) with the ratio of coastal and green bands of Landsat-8 performs well because the derived depth result has the high correlation coefficients and lowest RMSE with field sample result (r = 0.9228, RMSE=0.38). Figure 4.8 shows the comparison between depths derived from this study (Depth_Br) and the reference study (Depth_Re). As can be seen from Figure 4.9 (a) and (b), a positive correlation is found between the Water depth_Br estimated in this study and the Water depth_Rf, and the results are significant at the p = 0.05 level. Given the differences in the timing of data collection, such water depths estimated by the spectral band ratio method are considered reliable in this study.

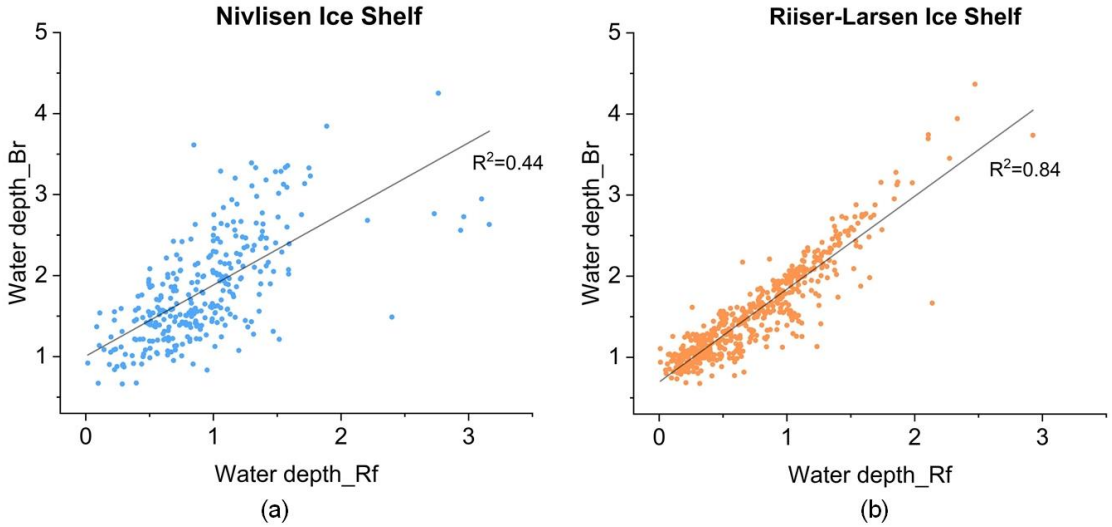

Figure 4.9 *Correlation analysis of the depths derived from the reference study (Water depth_Rf)* (Arthur et al., 2022) and *this study (Water depth_Br).*

4.3.2.2 Channel sinuosity

The channel sinuosity index (*Si*) is the ratio of the along-channel length and the straight-line distance between segment endpoints (Lu et al. 2021). It is worth noting that the *Si* depends on the length of the channel being measured, so the lengths of channel segments should be used. According to Leopold et al. (1964), 20 times the width of the bankfull contains at least one meandering wavelength, which means the segment length should be measured at least 20 times the channel width (Gordon et.al, 1992). In this study, the sinuosity of individual channel segments was computed at 2,000 m intervals by the Stream Sinuosity Toolbox in ArcMap 10.3 (Frasson et al. 2019).

4.3.2.3 Bifurcation ratio

As an important metric of one stream ordering system, the bifurcation ratio demonstrates the branching patterns of river networks. It was obtained by arithmetically averaging the ratios by order. For example, B_{12} means the number of first-order channels divided by the number of second-order channels.

4.3.2.4 Channel orientation

Channel orientation is a particularly useful metric to study the topographic influence on the geometry of the channel network. After calculating the sinuosity and bifurcation ratio of each supraglacial channel network, a channel orientation analysis was conducted by an automatic procedure in ArcMap 10.3. The channels were subdivided into 100 m equal-length segments and then the orientation of each segment was measured. Finally, a rose diagram based on a statistical analysis of channel orientation of different orders was drawn to show the overall trend of each supraglacial channel network (Whipple et al., 2000; Ortega et al., 2014; Resmi et al., 2019; Banwell et al., 2021).

4.3.2.5 Channel slope and bed slope

In this study, REMA DEM data with 8 m resolution was used to obtain the surface elevation profiles of supraglacial channels at finer spatial scales. To minimize slope errors,

the surface slope was calculated for each 100 m segment (nearly 13 times the DEM pixel size) from the elevation difference of its start and end points. The bed slope was computed by subtracting the water depth from the DEM elevations to get the bed elevation and then calculated for 100 m channel segments.

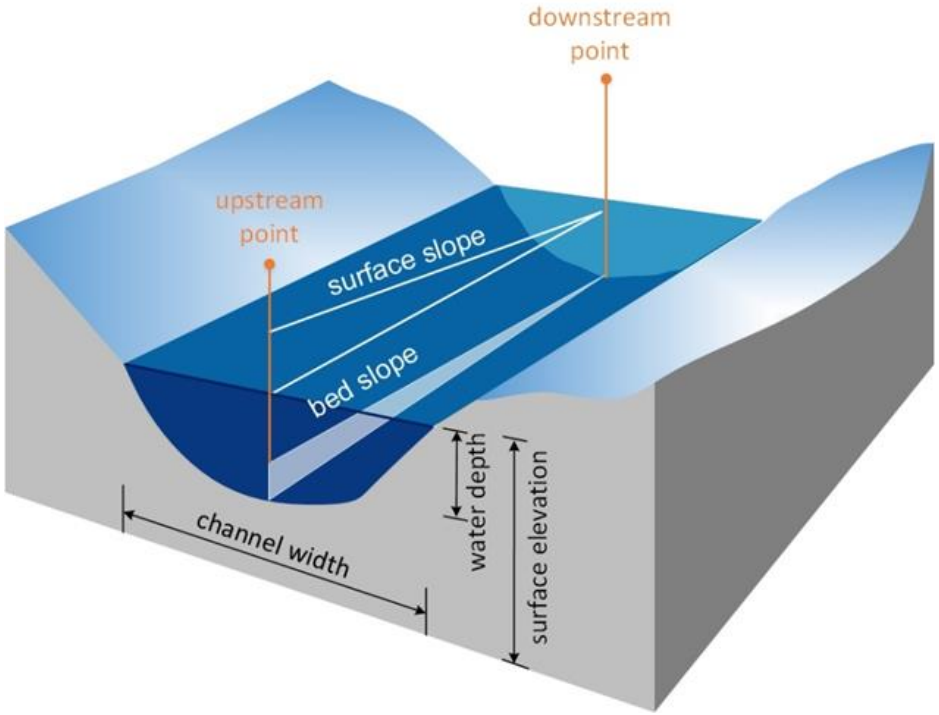

Figure 4.10 *Schematic diagram of channel surface slope and bed slope*

4.3.2.6 Drainage basin and drainage density

Drainage density (D_d) was defined as the ratio of total stream length within a network and its catchment area, which illustrates the overall abundance of channel networks (Horton 1945, Yang et al., 2016). To calculate D_d, the convex hull method and DEM-based method that have been most frequently used in generating drainage basins were both applied by ArcGIS 10.3 for comparison (Tay et al., 2006; Smith et al., 2015; Yang et al., 2018; Yang et al., 2019a; Lu et al., 2020a). DEMs are widely used to model supraglacial drainage patterns by GIS tools following the procedure for hydrologic analysis of terrestrial river networks. However, the accuracy of derived drainage basins from DEM-based methods relies on the quality of data. Further, DEMs are sometimes insensitive to the locations of moulins that also affect the whole supraglacial drainage

pattern. The term “convex hull” of a non-convex set refers to the area within the boundary of the route that a tight rubber ring follows as it warps around a non-convex object (Turcotte et al., 1998). As noted by Tay et al. (2006), the channel network is a non-convex set, while its drainage basin is convex (Figure 4.11).

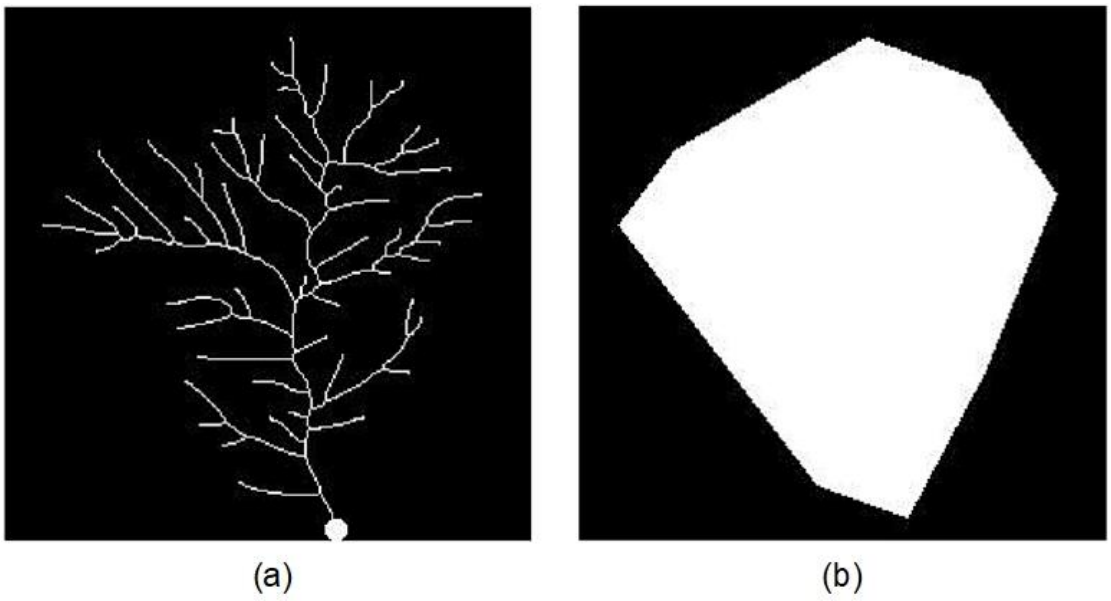

Figure 4.11 *Schematic diagram of convex hull method: (a) An example of a fourth-order channel network (nonconvex set), the white dot indicates an outlet; (b) the convex hull of channel network in Figure(a).* (Tay et al., 2006)

Figure 4.12 displays the derived drainage basin of supraglacial channel network on the Roi Baudouin Ice Shelf. It is obvious that the result from the DEM-based method has generated some false subbasins in the middle of the area. The REMA DEM-based method used here also failed to produce an accurate drainage area for other chosen ice shelves. According to Yang et al. (2015b), there are certain limitations in modelling supraglacial hydrology based on DEM methods. The causes of such errors can be attributed to three aspects: first, the DEM data itself can have some inaccuracies and voids which may influence the quality of results; second, filling depressions (e.g., moulins, crevasses) is usually required during processing and the optimal thresholds can be hard to determine; third, the supraglacial channel networks are complex and fragmented, and their seasonal

changes in morphology impair the assessment of DEM accuracy. Moreover, REMA DEM acquisition is not simultaneous with the Landsat-8 imagery used in this study. These problems lead to the inaccurate delineation of drainage basins and thus affect the calculation of D_d. Therefore, the supraglacial drainage basins obtained by the convex hull method are deemed to be more appropriate and reproducible for the overall analysis.

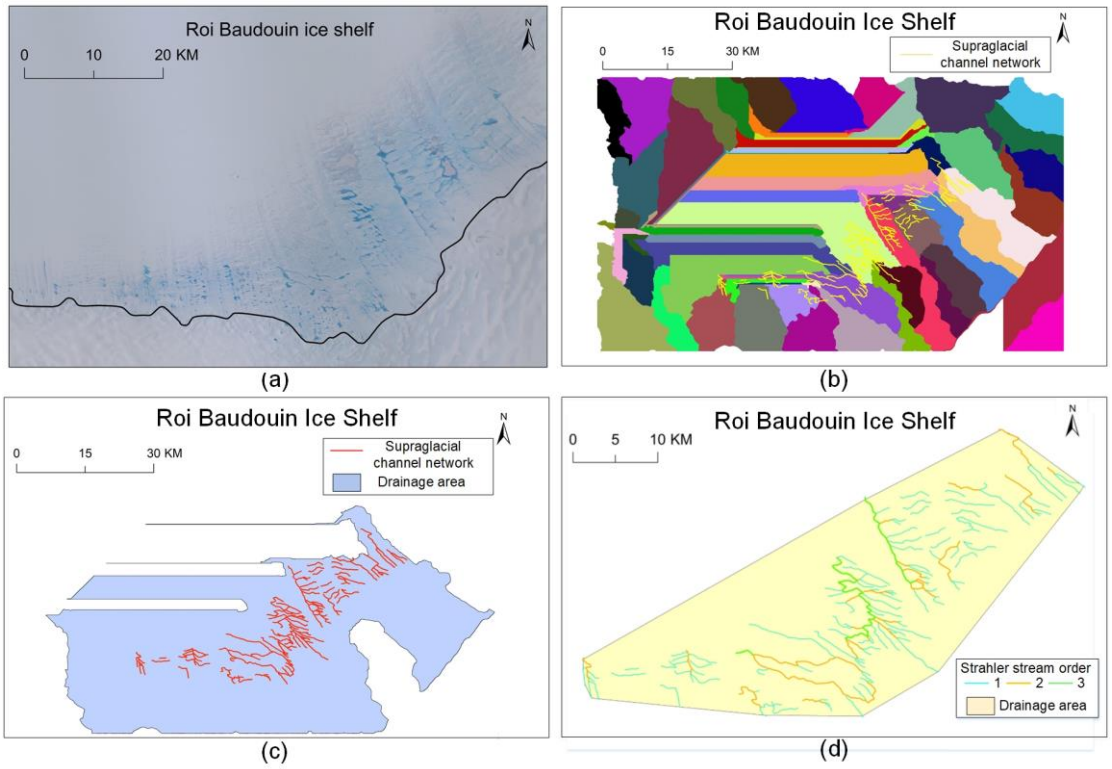

Figure 4.12 *Drainage basin extracted by different methods for Roi Baudouin Ice Shelf: (a)Landsat-8 OLI imagery in true-colour for the Roi Baudouin Ice Shelf; (b)drainage area derived from REMA DEM (solid-coloured patches), with supraglacial channel networks shown in yellow; (c) drainage basin of the supraglacial channel networks derived from DEM-based subbasins; (d) drainage basin generated from the Convex Hull method.*

5. Results

5.1 Distribution of supraglacial lakes and channels

Extensive surface water on Antarctic ice shelves was observed in the selected melt seasons in this study (Figure 5.1). The highest supraglacial meltwater extents were over the Bach (~147 km^2), Nivlisen (~111 km^2) and Riiser-Larsen (~100 km^2). Figure 5.1 provides the distribution of extracted supraglacial channel networks for the five selected Antarctic ice shelves. There are three types of meltwater features in supraglacial channel networks on the ice shelves: individual channels, individual lakes, and interconnected channel-lakes. Individual channels are the single channels which may flow into crevasses or moulins or are covered by the snow and thus not fully extracted from the imagery. As the individual channels are short and narrow and have few influences on the whole network, they were regarded as first-order channels (e.g., tributary without inflow) for further analysis. Individual lakes are those where no channel inflow is found. Some individual lakes can appear hollow because they are partially covered by ice and/or accumulated snow (typically an ice lid). In fact, there is the possibility that some individual lakes are fed by the channels. However, supraglacial channels less than 30 m wide cannot be identified due to the spatial limitations of the Landsat-8 imagery (30 m). Even the terminus (e.g., moulins, crevasses) of the individual channels are not included in the combined results. Interconnected channel-lakes refer to the channels flowing into a supraglacial lake. They consist of the whole supraglacial channel networks which deliver the meltwater across the ice shelves.

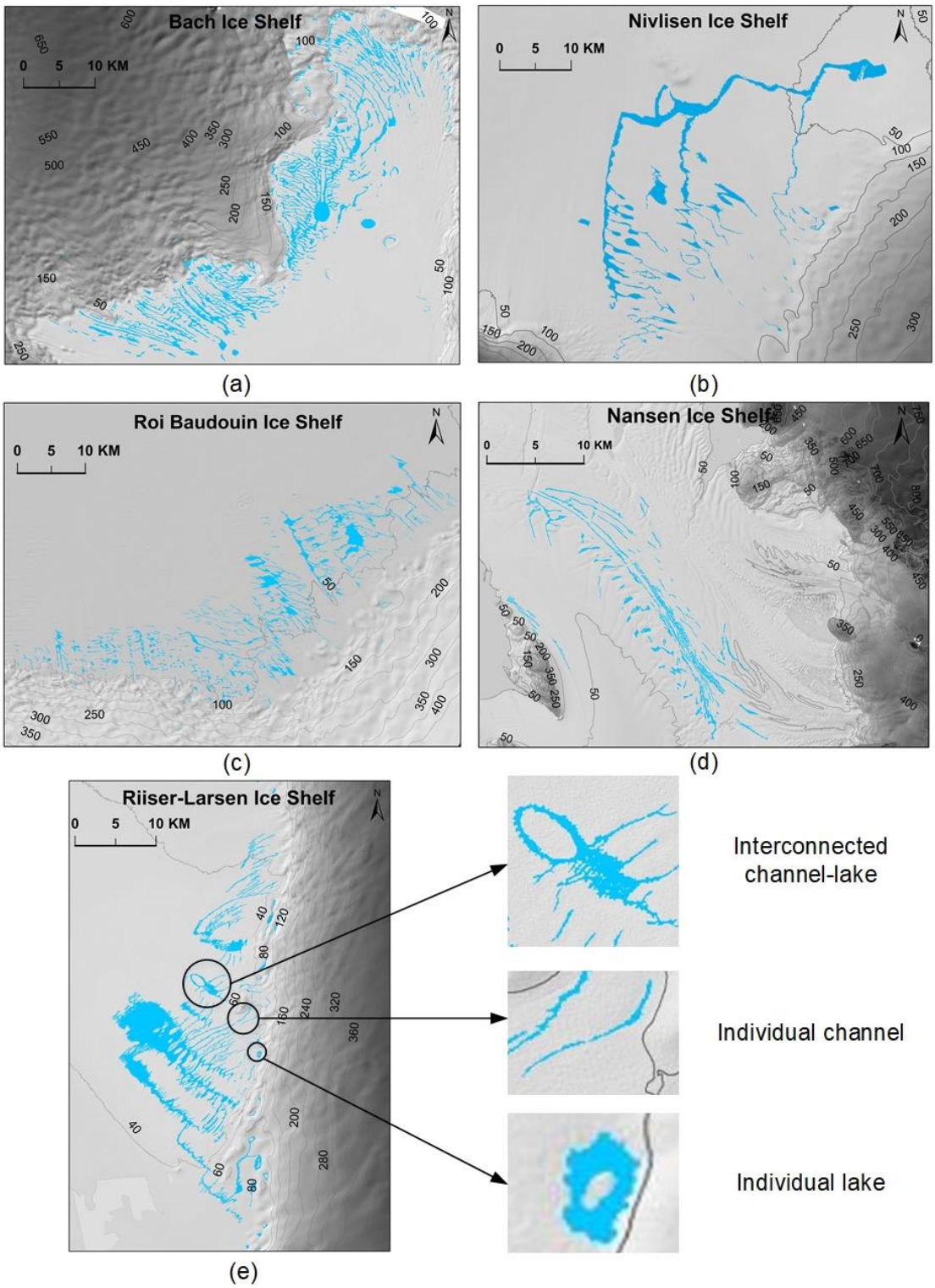

Figure 5.1 *Supraglacial channels and lakes extracted on each studied ice shelf. The blue polygons represent the surface water across the studied ice shelves. Underlying images are REMA DEM data (8 m spatial resolution). Elevation contours at 50 m intervals are depicted as well (dark grey lines with black numbers).*

The locations of supraglacial channels and lakes on Antarctic ice shelves are closely associated with the topography of the ice surface, with meltwater tending to accumulate in low surface depressions along the ice surface gradients. The active channels and lakes on the surface of the ice shelves are widely distributed in low elevations (less than 100 m) and near the grounding lines. REMA DEM data were used to observe ice surface topography, and the mean values and the range of elevation where supraglacial channels occur are shown in Table 5.1. Where the supraglacial channel networks exist, there is little variation in elevation, with a maximum range of 48 m (Riiser-Larsen Ice Shelf) and a minimum range of 9 m (Nansen Ice Shelf). Channels on the Nivlisen Ice Shelf reach the highest mean elevation of 62 m, and those on the Bach Ice Shelf are at the lowest mean elevation which is 23 m. It is worth noting from Figure 5.2 and Figure 5.3 that although most supraglacial channel networks on the five Antarctic ice shelves are found in topographic lows and flat areas, they span different ranges. Unlike the other four ice shelves, most meltwater on the Nivlisen Ice Shelf is stored on the relatively high elevation surfaces up-ice from the grounding line, which suggests there might be some factors to control its development.

Table 5.1 The elevation information of the catchment of supraglacial channel networks. Elevation refers to the entire ice shelf, whereas catchment elevation refers to the channel drainage area.

Ice shelf		**Bach**	**Nansen**	**Nivlisen**	**Riiser-Larsen**	**Roi Baudouin**
elevation (m)	Mean	171	300	81	122	120
catchment elevation (m)	Mean	23	35	62	35	48
	Range	10~40	20~54	40~85	26~74	42~58
	Std. deviation	4.17	4.80	7.06	7.20	2.80

The ice velocity data from Shen et.al (2020) was used in this study to examine the ice speed where hydrology features (i.e., supraglacial lakes and channels) occur. Figure 5.4 shows that surface lakes and channels are observed across a wide range of ice velocities on the studied Antarctic ice shelves. The red line in Figure 5.4 represents the mean annual ice velocity over the channelized area, which deviates from the ice shelf mean ice velocity by approximately +1.4% (Bach), +34.5% (Nansen), -9% (Nivlisen), -68% (Riiser-Larsen), -62.5% (Roi Baudouin), respectively. Notably, a large number of lakes and channels formed on slow-flowing ice surface. More than half of the hydrological features occurred on ice flowing <100 m yr^{-1} for the Bach, Nivlisen, Riiser-Larsen and Roi Baudouin ice shelves, while over half of the lakes and channels on the Nansen Ice Shelf surface existed in the areas at speeds of less than 150 m/yr.

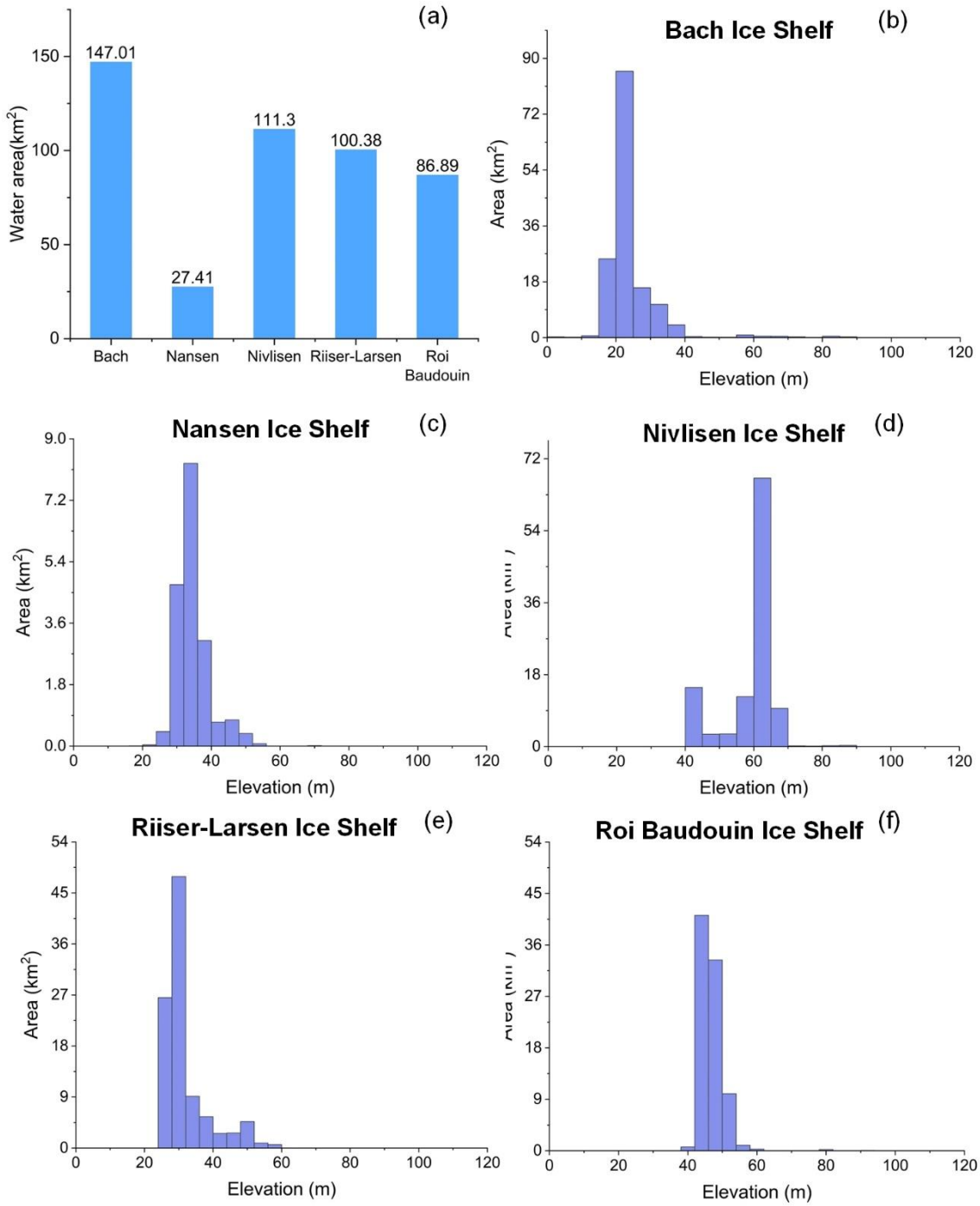

Figure 5.2 *Estimated surface area of supraglacial lakes and channels on studied ice shelves by elevation variables.*

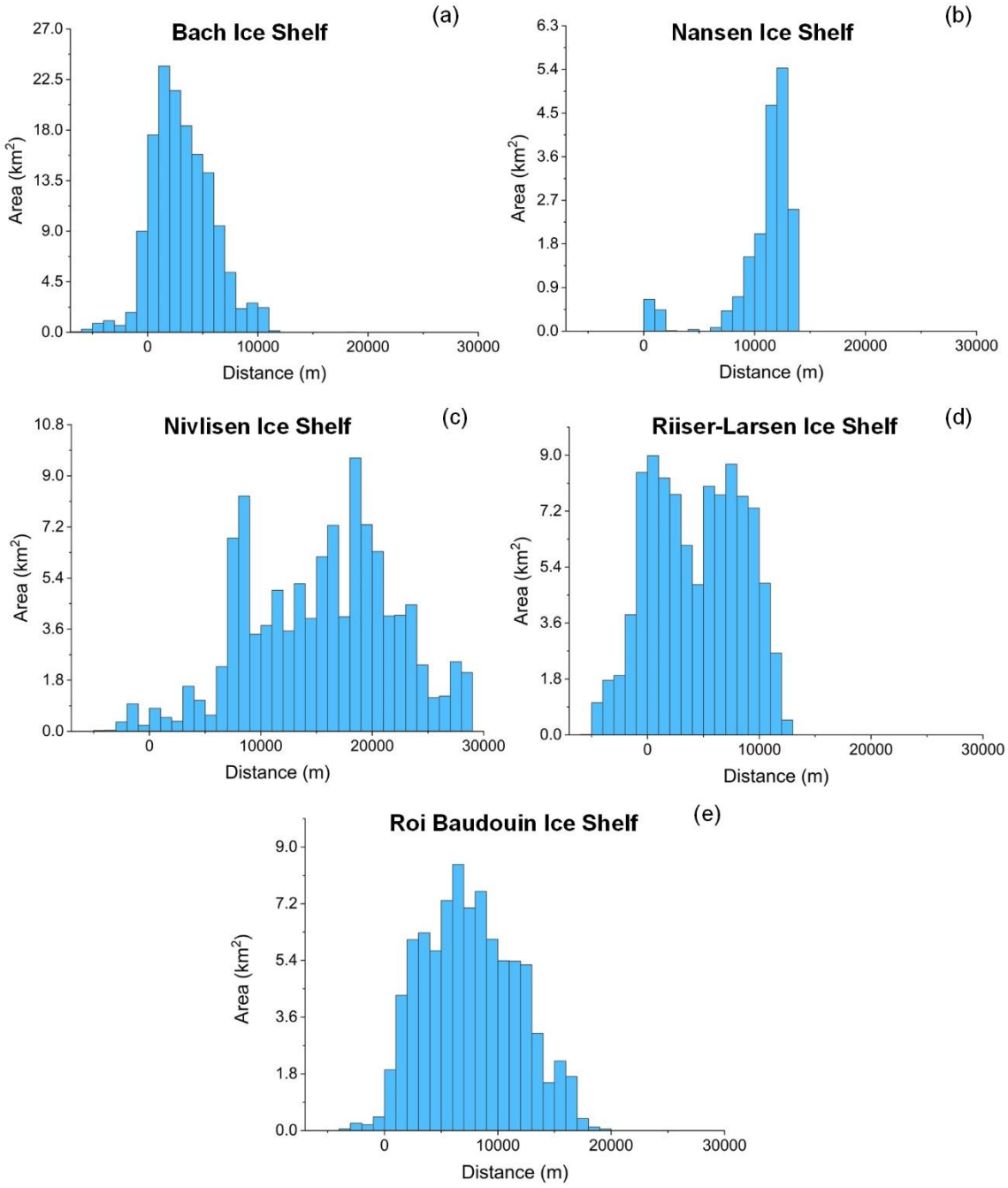

Figure 5.3 *Distance from supraglacial lakes and channels pixels to the grounding line (negative values indicate up-ice from the grounding line) of each studied ice shelf in Antarctica.*

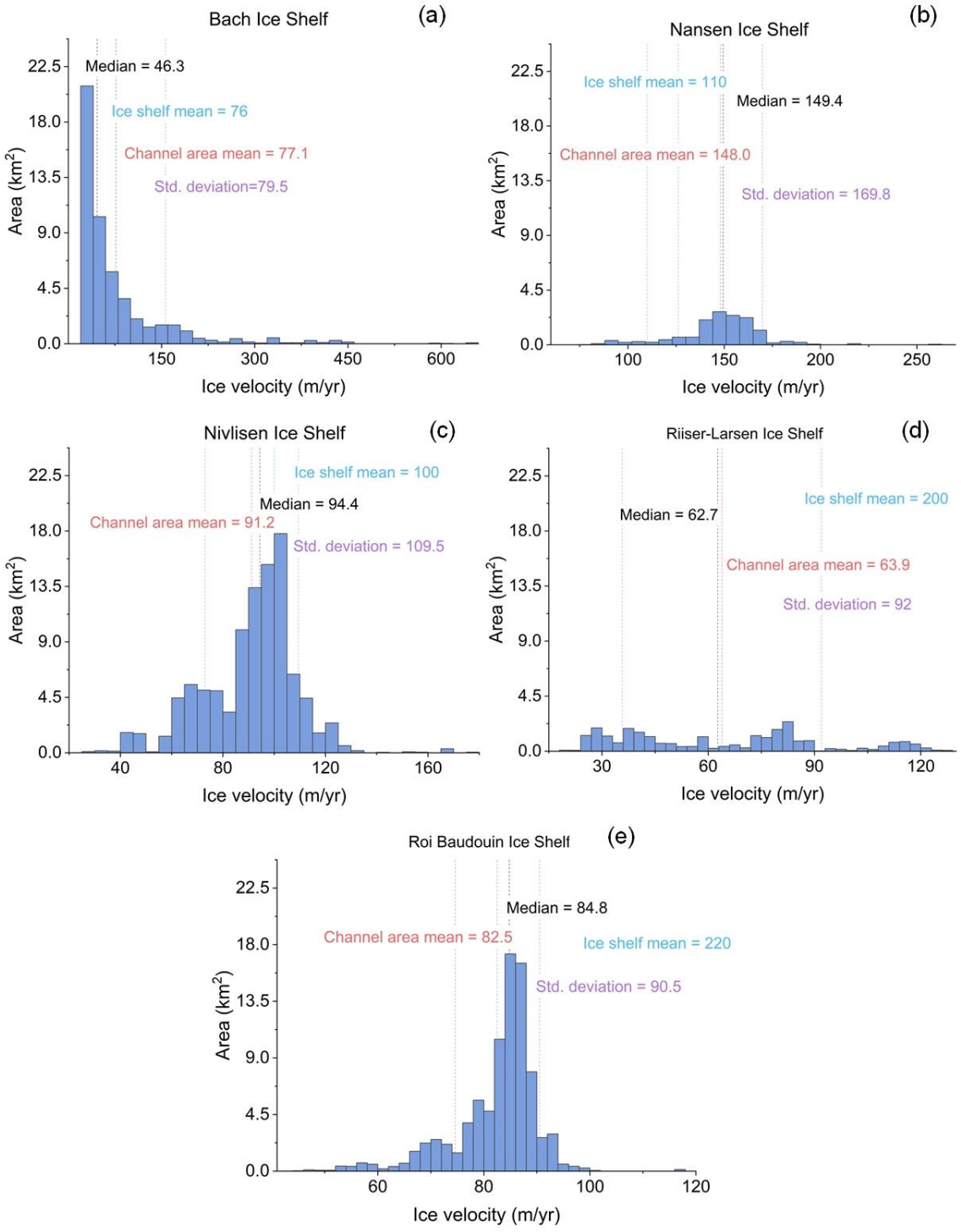

Figure 5.4 *Estimated surface area distribution of supraglacial lakes and channels related to ice velocity of each studied ice shelf.*

5.2 Supraglacial channel networks and drainage patterns

A total of 119 supraglacial channel networks were found on the five Antarctic ice shelves,

and the Strahler stream order of these supraglacial channel networks ranges from the first to the fourth. A channel network is defined as a network consisting of main channels and tributaries which connect to the main channel (Charlton, 2007). Figure 5.5 displays four different channel networks on the Bach Ice Shelf. Channels in the low-order network (i.e., the highest stream order is first- or second-order) are fewer in number and shorter in total length, which form a simple structure, while high-order channel networks including more longer channels (i.e., the highest stream order ≥ 3) exhibit complex drainage patterns (e.g., dendritic or parallel) and large length scales.

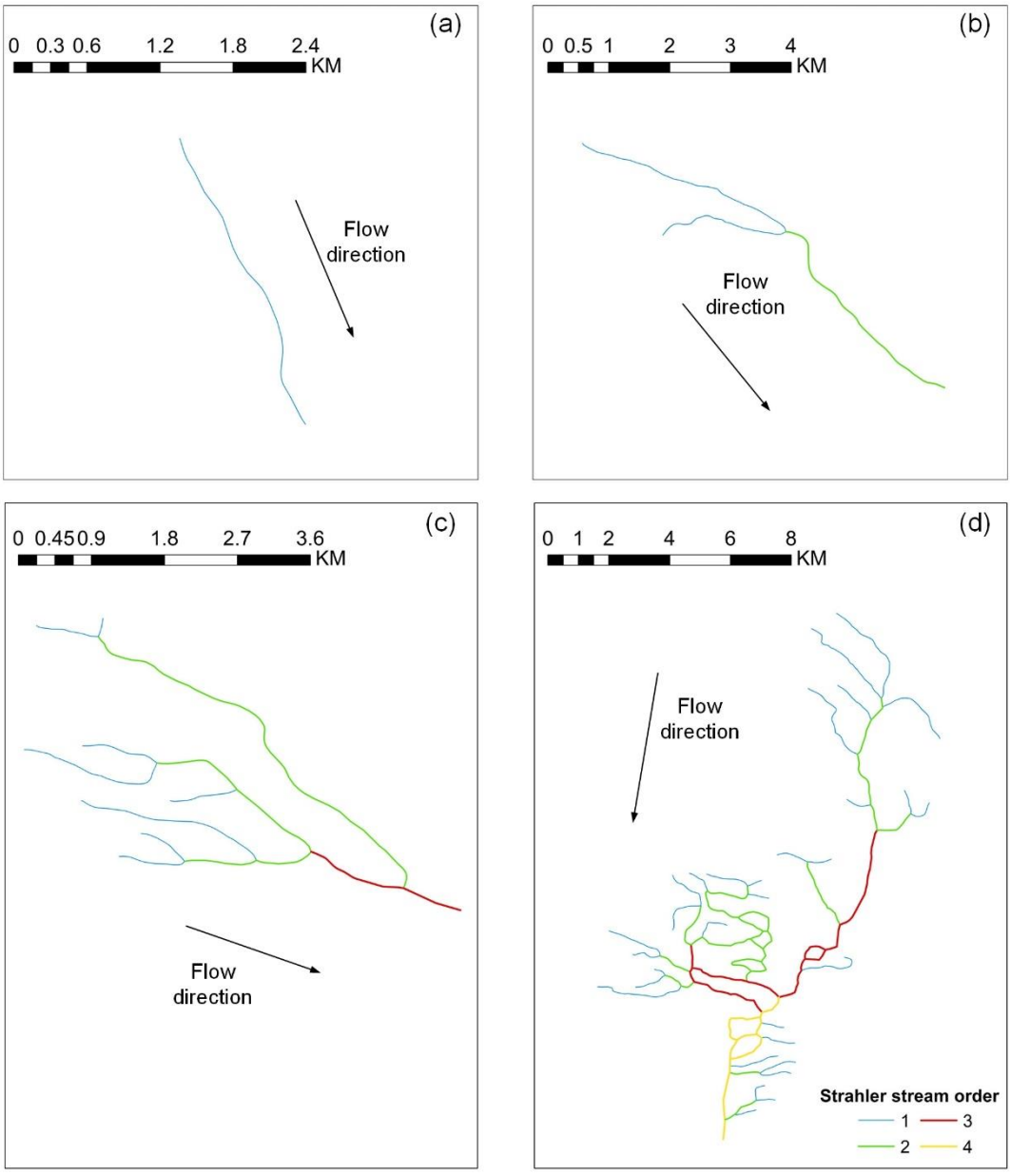

Figure 5.5 *Examples of supraglacial channel networks with different highest orders on*

the Bach Ice Shelf, ranging from first-order (Figure 5.5a) to fourth-order (Figure 5.5d). The black arrow means water flow direction. Lower-order networks (i.e., the highest order is first- or second-order) are shorter in length and have a simpler structure, while higher-order networks are longer and have multiple channels which make drainage patterns more complex.

Supraglacial channel networks quantified by the highest stream orders on each ice shelf are shown in Table 5.2. While Nansen Ice Shelf supports 61 channels in total, the 16 networks are fragmented and only contain channels of two low orders: first- and second-order. The channel networks on the other four ice shelves, i.e., Bach (45), Nivlisen (1), Riiser-Larsen (26) and Roi Baudouin (31), are found to be up to third- or fourth-order. There is the largest number of supraglacial channels (336 in total) on Bach ice shelf, and channels on its surface formed 45 networks containing first- to fourth-order drainage. For Nivlisen Ice Shelf, there was only one channel network composed of 47 channels with three stream orders. Although the stream orders of supraglacial channel networks of the five study sites are different, notable similarities can be observed. First-order channels are the most common channel configuration which account for more than 50% of the total number of channels for all five ice shelves. This result reveals that most supraglacial channel networks on the Antarctic ice shelves during the melt season are low-order (<3) channel networks despite the longer length of the high-order channel network.

Table 5.2 Summary number statistics of supraglacial channel networks

Ice Shelf	Highest stream order in a network	Number of channel networks	Number of channels				
			order 1	order 2	order 3	order 4	All
Bach	1	22	22	—	—	—	22
	2	16	62	33	—	—	95
	3	5	36	18	17	—	71

	4	2	56	43	22	27	148
	Total	**45**	**176**	**94**	**39**	**27**	**336**
Nansen	1	7	7	—	—	—	7
	2	9	30	24	—	—	54
	Total	**16**	**37**	**24**	—	—	**61**
Nivlisen	1	0	—	—	—	—	0
	2	0	—	—	—	—	0
	3	1	24	18	5	—	47
	Total	**1**	**24**	**18**	**5**	—	**47**
Riiser-Larsen	1	20	20	—	—	—	20
	2	3	8	5	—	—	13
	3	3	134	66	63	—	263
	Total	**26**	**162**	**71**	**63**	—	**296**
Roi Baudouin	1	19	19	—	—	—	19
	2	9	40	26	—	—	66
	3	3	65	34	25	—	124
	Total	**31**	**124**	**60**	**25**	—	**209**

The observed supraglacial channel networks are nearer the grounding zone and can be divided into two categories (Figure 5.6): dendritic and parallel drainage patterns. For example, the supraglacial channels on Bach, Nivlisen, Riiser-Larsen and Roi Baudouin ice shelves develop as dendritic drainage networks, suggesting that variations in elevation for these areas are not significant. In general, parallel drainage networks are usually found in areas with a pronounced slope or strong controls to the surface. The supraglacial channel networks on the Nansen ice shelf display a typical parallel drainage pattern where tributaries stretch out parallelly to the stem channel and then join it.

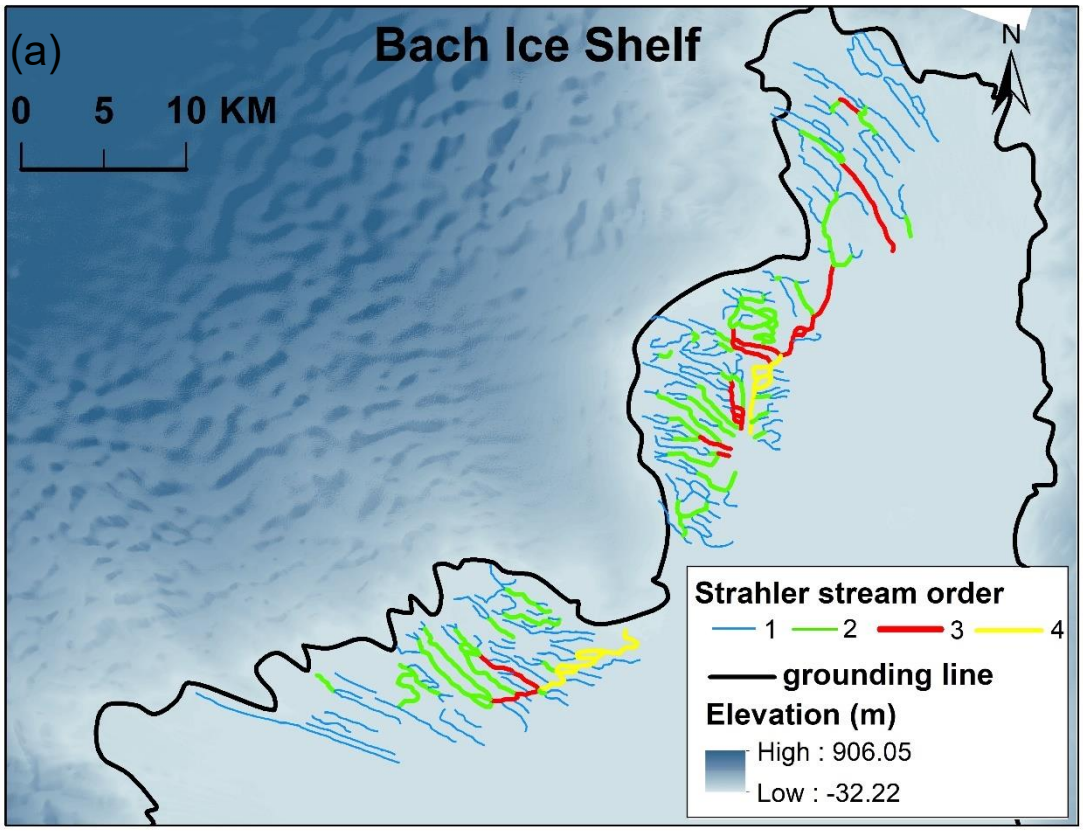
(a)
Bach Ice Shelf
0 5 10 KM
N
Strahler stream order
1 2 3 4
grounding line
Elevation (m)
High : 906.05
Low : -32.22

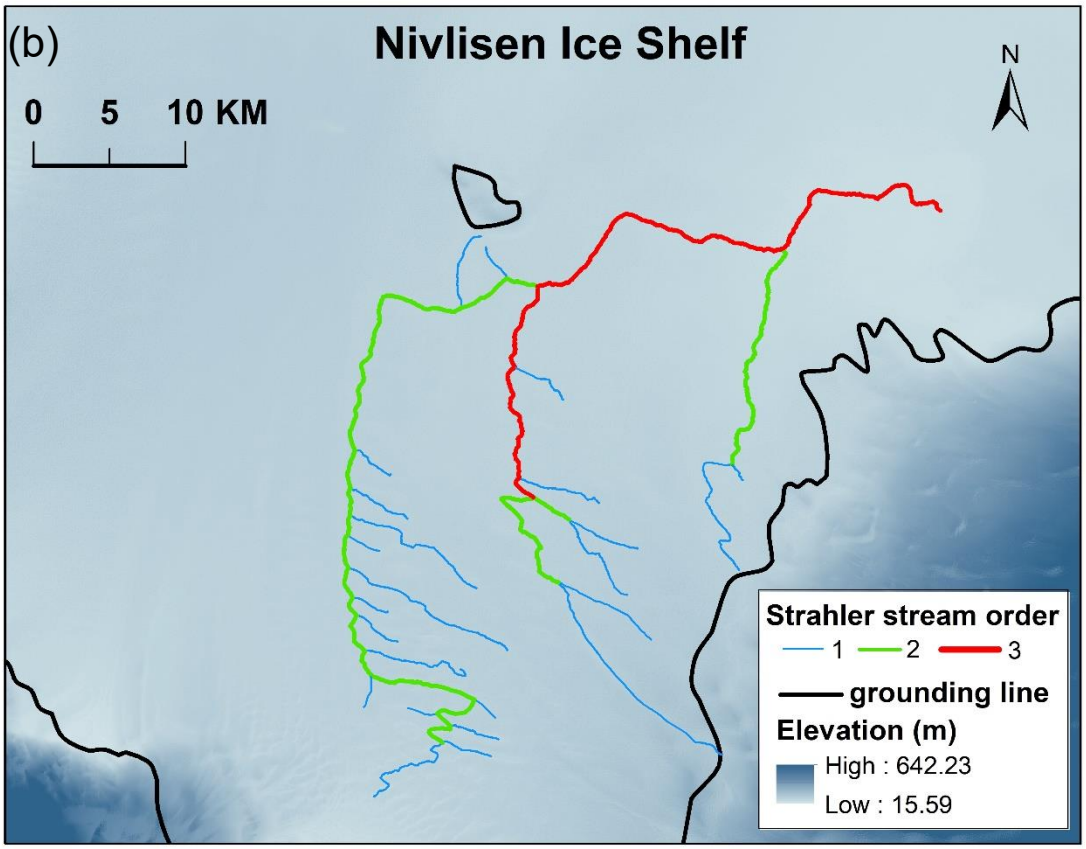
(b)
Nivlisen Ice Shelf
0 5 10 KM
N
Strahler stream order
1 2 3
grounding line
Elevation (m)
High : 642.23
Low : 15.59

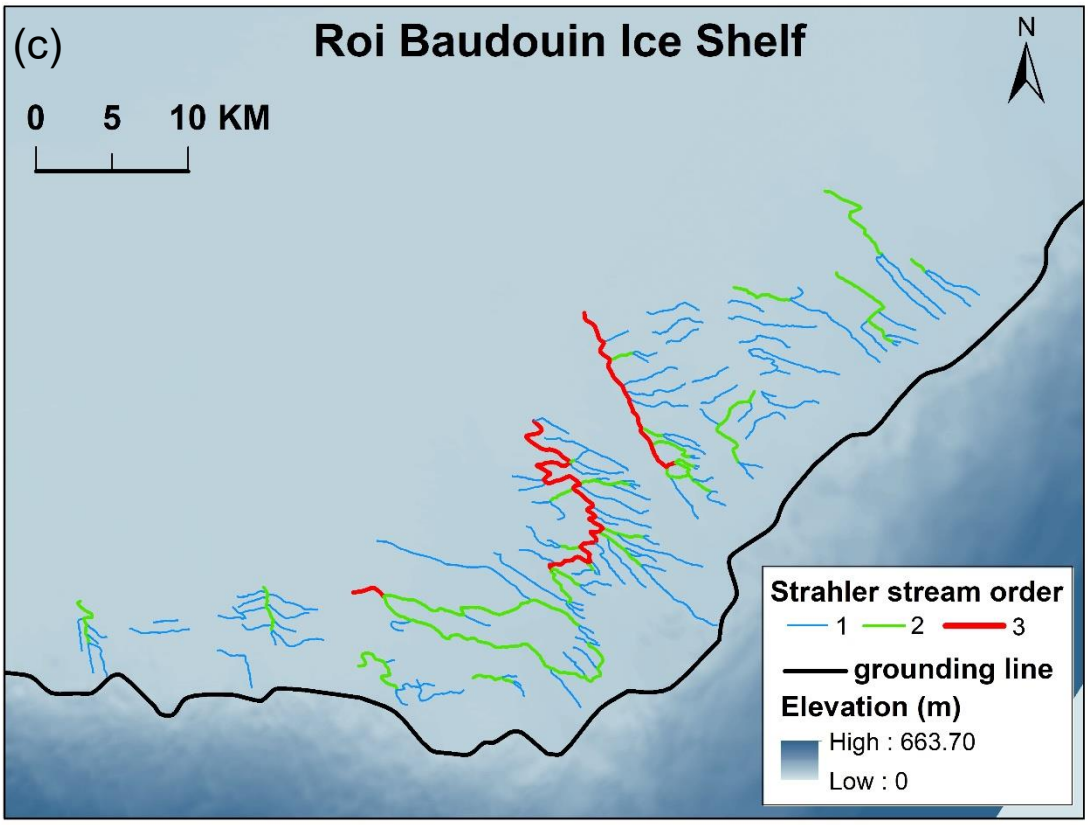
(c)
Roi Baudouin Ice Shelf
N
0 5 10 KM
Strahler stream order
1 2 3
grounding line
Elevation (m)
High : 663.70
Low : 0

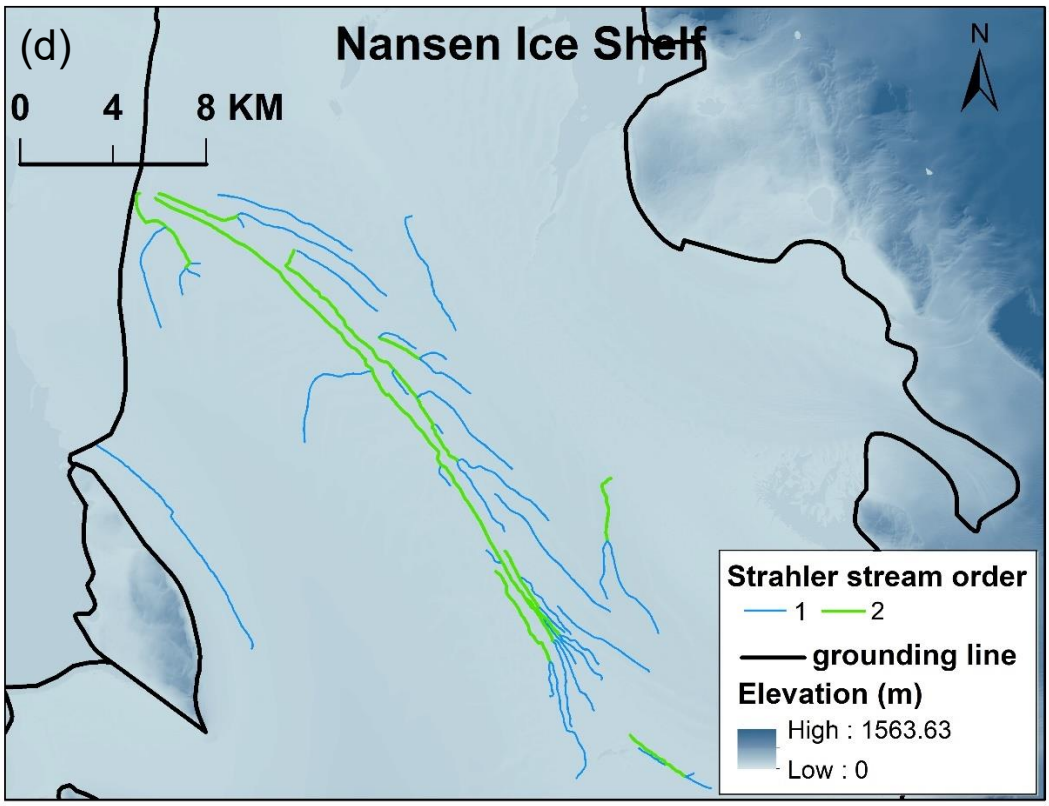
(d)
Nansen Ice Shelf
N
0 4 8 KM
Strahler stream order
1 2
grounding line
Elevation (m)
High : 1563.63
Low : 0

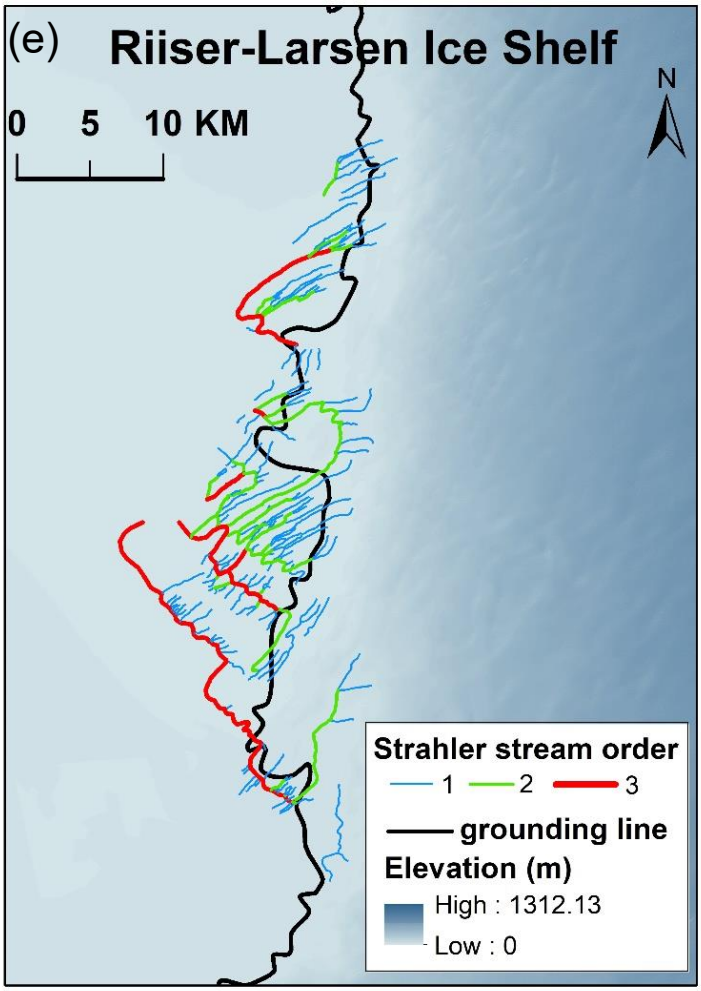

Figure 5.6 *The extracted supraglacial channel network for the studied ice shelves: (a) Bach, (b) Nivlisen, (c) Roi Baudouin, (d) Nansen, I Riiser-Larsen. Centrelines of different colours demonstrate corresponding Strahler stream order which ranges from the first to the fourth. Underlying images are REMA elevation data with grounding lines of Antarctic ice shelves. Low-order channels generally have short lengths and simple structures, whereas high-order channels are longer and more branching.*

5.3 Length, width, and depth of supraglacial channels

The length, width, and depth of supraglacial channels on the studied ice shelves are shown in Table 5.3. As presented in Figure 5.7, the length of each channel segment was calculated using the confluence points as the division points. The total length of the channel network on Bach Ice Shelf reaches a maximum of ~489 km, followed by the Roi Baudouin Ice Shelf (454 km), Riiser-Larsen ice shelf (421 km) and Nivlisen Ice Shelf (286 km). The supraglacial channels on the Nansen Ice Shelf were summed to ~190 km, which is the shortest of the five ice shelves. In terms of numbers, the Bach Ice Shelf has the highest number of channels, and the Nivlisen Ice Shelf has the lowest number.

Although there are more channels on Riiser-Larsen Ice Shelf than on Roi Baudouin Ice Shelf, its total channel length is smaller than that of the Roi Baudouin Ice Shelf. Similarly, the Nivlisen Ice Shelf has the least number of channels, but its total length is not the minimum. This suggests that there are more channels of shorter lengths on the Riiser-Larsen Ice Shelf, whereas the channels on the Nivlisen Ice Shelf are all longer.

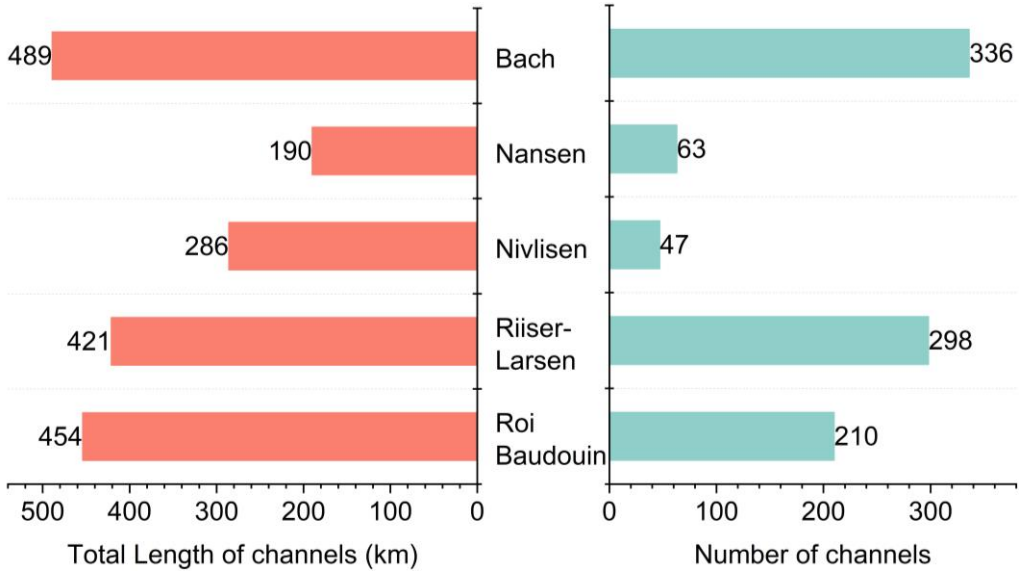

Figure 5.7 *Total numbers and length of supraglacial channels on Antarctic ice shelves.*

Table 5.3 Summary morphometry statistics of supraglacial channel networks

		Ice Shelf				
		Bach	Nansen	Nivlisen	Riiser-Larsen	Roi Baudouin
Mean channel length (m)	order 1	1793	3348	5918	1648	2439
	order 2	1192	2528	4958	1295	1822
	order 3	993	—	10899	963	1596
	order 4	846	—	—	—	—
Mean channel width (m)	order 1	136	112	110	85	95
	order 2	138	135	131	124	115
	order 3	165	—	184	282	171
	order 4	135	—	—	—	—

Mean channel depth (m)	order 1	1.5	0.8	1.3	1.1	1.3
	order 2	1.8	0.8	1.6	1.5	1.4
	order 3	1.9	—	2.0	1.8	2.0
	order 4	2.0	—	—	—	—

Figure 5.8 shows the total length of supraglacial channels by different stream orders. It is worth noting that the total length is the longest for the first-order channels on all five Antarctic ice shelves and is inversely proportional to stream order. In addition, it is observed that the mean length of supraglacial channels also decreases with stream orders, apart from on the Nansen Ice Shelf, which demonstrates that the third-order channels on Nansen ice shelf are long but few in number. The width and depth of supraglacial channels were sampled at 30 m intervals along each channel segment. The mean width ranges from 85 m to 171 m and the mean depth ranges from 0.8 m to 2.0 m. Overall, both mean channel width and depth increase from low to high stream order (Figure 5.9), but the variance in width is more pronounced than that of depth. As a result, supraglacial channels on Antarctic ice shelves tend to widen rather than deepen when the tributaries converge.

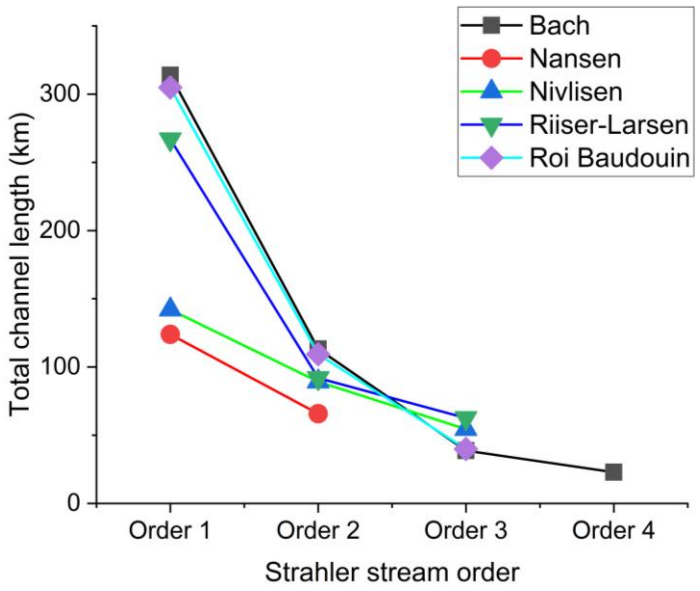

Figure 5.8 *The total length of supraglacial channels by different stream orders.*

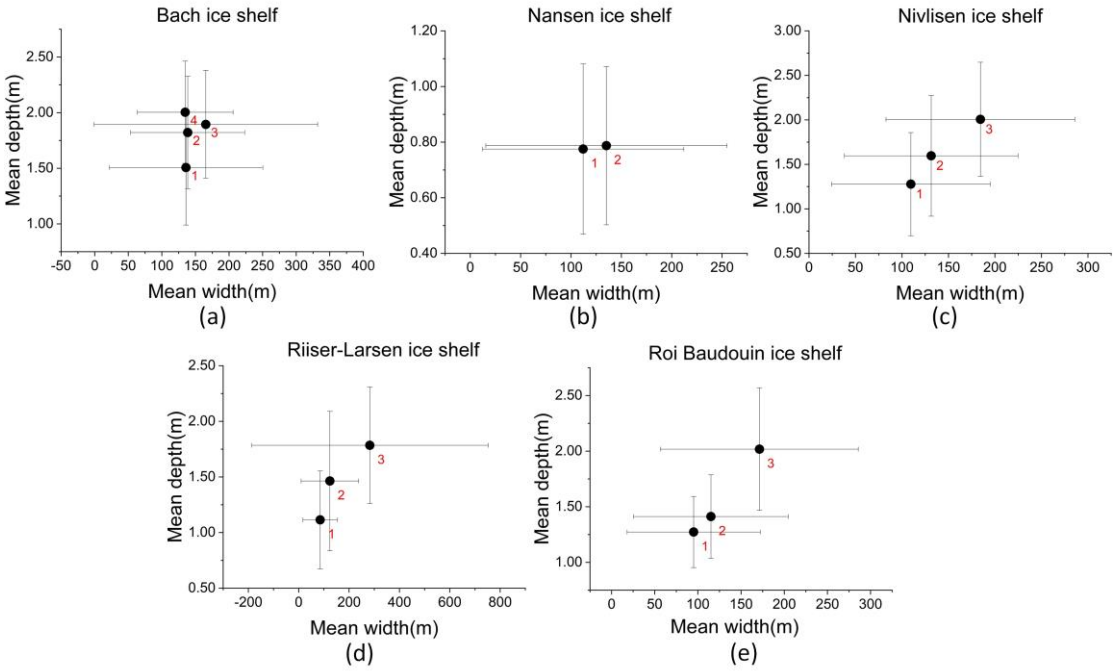

Figure 5.9 *Mean width and depth of supraglacial channel by stream orders (error bars indicate one standard deviation). Significant increase in mean channel width with increasing flow order, but only a small increase in depth.*

5.4 Sinuosity of supraglacial channels

The calculation of sinuosity was based on the length of the supraglacial channel segments which were divided by straight-line distances at 2000 m intervals. Table 5.4 displays the mean sinuosity values of different stream orders for all five studied ice shelves, which vary from 1 to 1.3 and are largely similar. There are some defined thresholds of sinuosity values in the literature to discriminate different types of channels. Brice et al. (1978) classified channels according to the degree of sinuosity, with values less than 1.05 referred to as straight, those between 1.05 and 1.25 are sinuous and those above 1.25 are meandering. It can be seen from the data in Figure 5.10 (a) that most supraglacial channels on the studied ice shelves are straight, followed by sinuous and meandering channels. Over the Nansen, Riiser-Larsen and Roi Baudouin ice shelves, the second- and third-order

channels are more likely to be meandering. But for the Bach and Nivlisen ice shelves, the majority of meandering channels are the first-order channels.

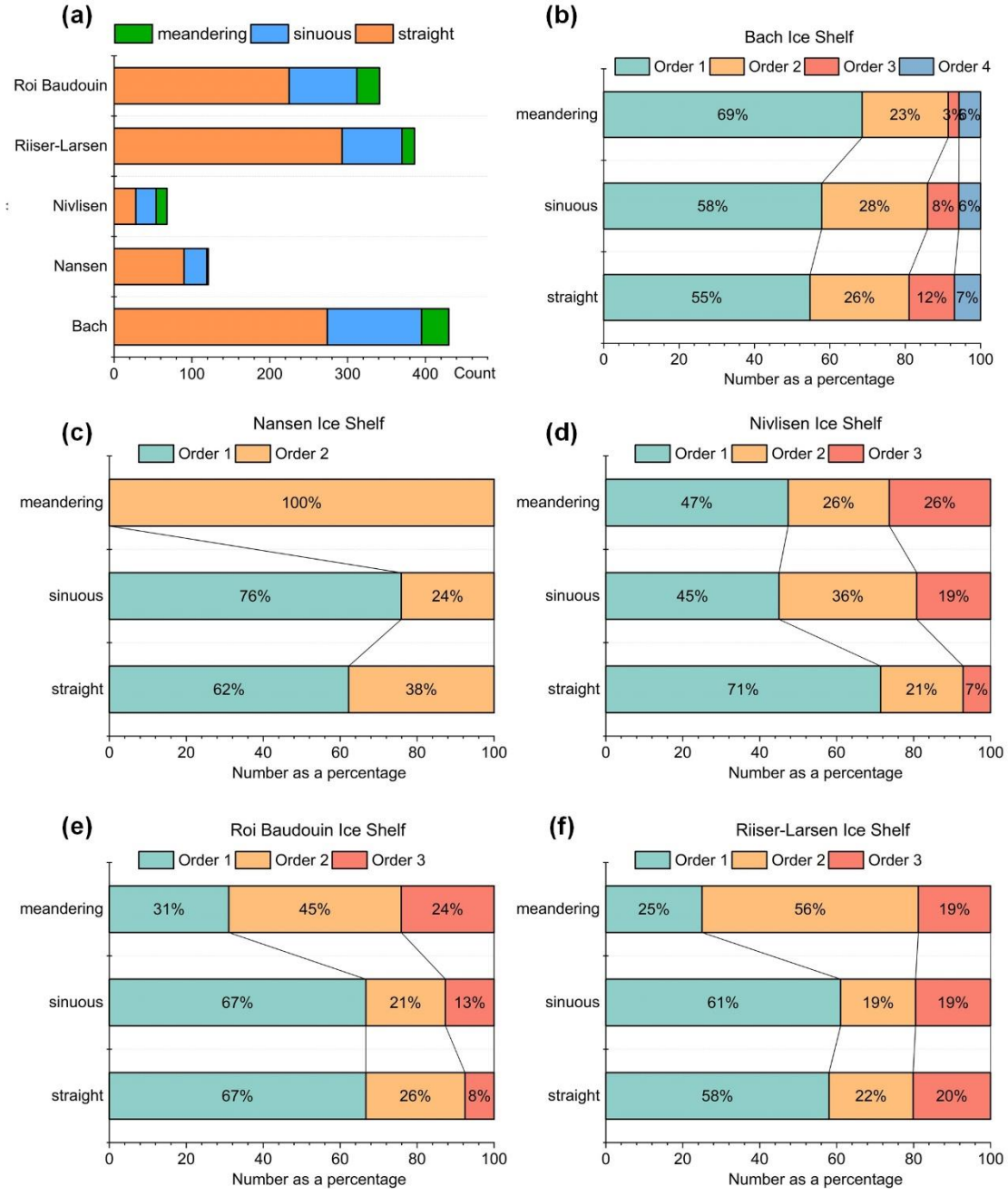

Figure 5.10 *Variation in the number of supraglacial channels with different degrees of curvature.*

Table 5.4 Sinuosity ratio (Si) of supraglacial channel networks

Ice Shelf	Bach	Nansen	Nivlisen	Riiser-Larsen	Roi Baudouin
stream order	Si	Si	Si	Si	Si
1	1.1	1.1	1.2	1.1	1.1
2	1.1	1.0	1.3	1.1	1.1
3	1.0	—	1.3	1.0	1.2
4	1.1	—	—	—	—

5.5 Bifurcation ratio of supraglacial channel networks

Bifurcation ratio (R_b) values were calculated for supraglacial channel networks containing at least two stream orders (51 in total). Most of the mapped supraglacial channels are braided networks. The numbers of channels of any order on each ice shelf are plotted against their corresponding stream order in Figure 5.11. The position of linking points on the lines indicates that the R_b is variable. Here, mean R_b and their standard deviations were calculated from second- to fourth-order channels to clarify this variability (Table 5.5). Generally, the Rb decreases in a downstream direction (i.e., high order) in terrestrial river networks. However, although the number of channels on the studied ice shelves decreases with increasing stream order, as seen in Figure 5.11 and shows a clear consistency, the bifurcation ratios corresponding to these channels do not show a regularity. The mean R_b values for second- and third-order channels range from 1.2 to 3.6 which is closer to the lower range of 2.0 to 4.0 for terrestrial rivers (Horton 1945). However, the mean R_b value for the fourth-order channels on Bach Ice Shelf is only 0.8 ±0.1, which indicates the number of third-order channels is less than that of fourth-order channels in the network, which might be because there are multiple channels at fourth-order.

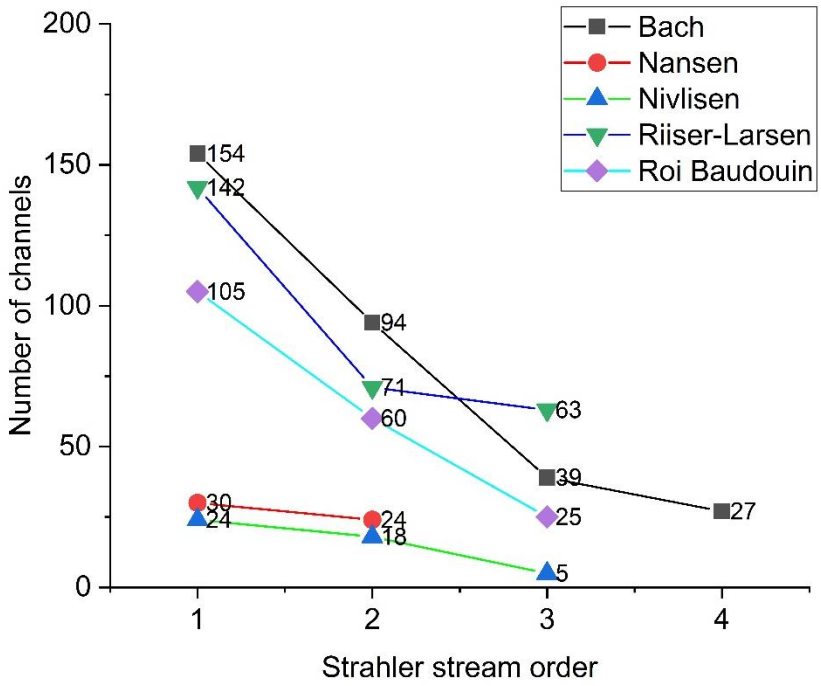

Figure 5.11 *The number of supraglacial channels by different stream orders for networks including at least two stream orders.*

Table 5.5 Mean bifurcation ratio (R_b) of supraglacial channel networks

Ice Shelf	**Bach**		**Nansen**		**Nivlisen**		**Riiser-Larsen**		**Roi Baudouin**	
R_b	Mean	Std	Mean	Std	Mean	Std	Mean	Std	Mean	Std
Rb_{12}	1.9	0.2	1.6	0.4	1.3	0	2.8	2.4	1.8	0.5
Rb_{23}	2.1	0.7			3.6	0	1.2	0.8	3.4	3.3
Rb_{34}	0.8	0.1								

5.6 Channel orientations

Figure 5.12 is a rose diagram showing channel orientation by Strahler stream order. Channel orientations on Bach Ice Shelf tend towards the southeast between 112.5 and 157.5 degrees. The orientation of the channels on Nivlisen Ice Shelf is lightly dispersed, with an obvious maximum to the northwest and some scattered orientations to the northeast. For Riiser-Larsen Ice Shelf, supraglacial channels are preferentially arranged

along the southwest and those on Roi Baudouin Ice Shelf flow in the northwest direction between 247.5 and 292.5 degrees. Channels on the Nansen ice terminate near the margin of ice, and the first-order channels flow in a southwest direction while the second-order channels trend to the northwest. Notably, the whole channel network has one preferential direction despite that there are some scattered stream orientations.

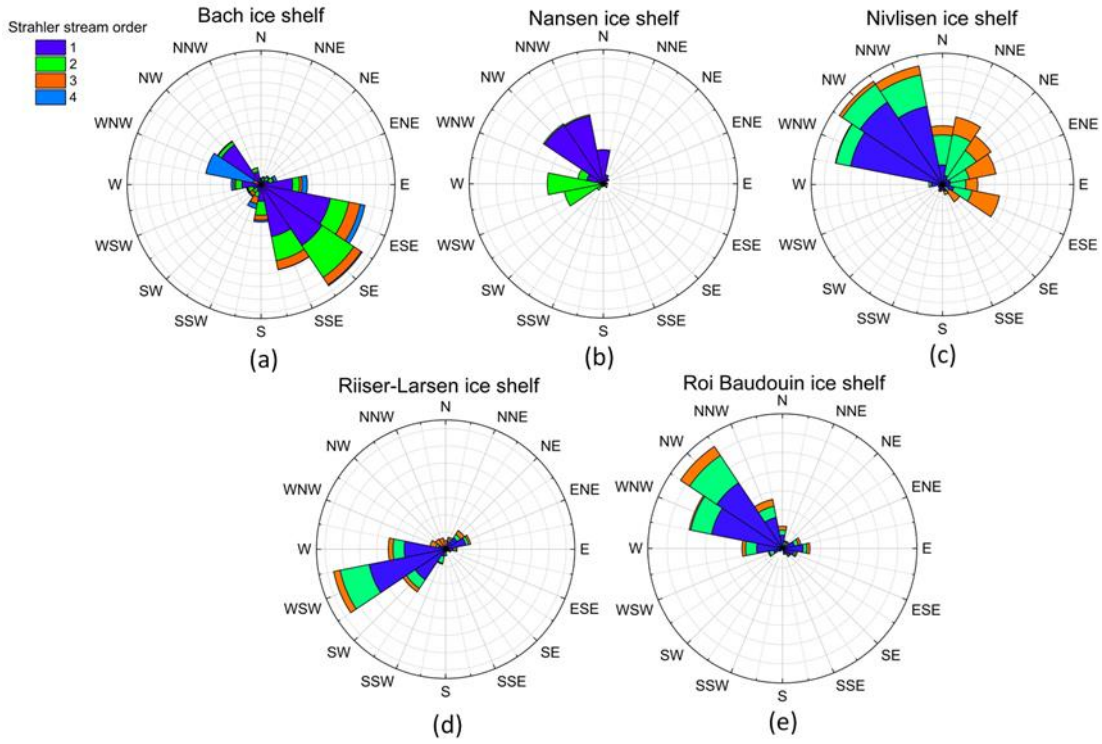

Figure 5.12 *Rose diagrams of supraglacial channels orientation for different ice shelves: (a) Bach, (b) Nansen, (c) Nivlisen, (d) Riiser-Larsen, I Roi Baudouin. Colours represent Strahler stream order. Each supraglacial channel network has a preferential orientation and sometimes all orders align, but sometimes they are at opposing angles*.

5.7 Surface and channel bed slopes

To explore the influence of surface topography on supraglacial channels, the water surface and bed slopes were computed by different stream orders. To obtain the elevation

difference between the up and downslope points from REMA DEM data, all the supraglacial channel segments were split into 100 m sections along the flowing orientation. Table 5.6 displays the surface slope of supraglacial channels by different stream orders, and Figure 5.13 presents the variations of water surface and bed slope of supraglacial channels on different ice shelves. The maximum surface slope of the first-order supraglacial channels on Nansen and Riiser-Larsen ice shelves reaches 0.0009, followed by Roi Baudouin, Nivlisen and Bach. For bed slopes, the Riiser-Larsen Ice Shelf has the lowest mean (0.0001) and the Roi Baudouin has the highest (0.0015). Notably, lower-order channels (i.e., first- and second-order) are generally steeper than high-order channels.

Table 5.6 The water surface and bed slope of supraglacial channels by different stream orders

Strahler stream order	**Mean slope (m/m)**	**Bach**	**Nansen**	**Nivlisen**	**Riiser-Larsen**	**Roi Baudouin**
Order 1	bed	0.0007	0.0009	0.0006	0.0008	0.0015
	surface	0.0005	0.0009	0.0004	0.0009	0.0006
Order 2	bed	0.0007	0.0001	0.0001	0.0006	0.0013
	surface	0.0005	0.0002	0.0003	0.0007	0.0005
Order 3	bed	0.0004		0.0004	0.0001	0.0002
	surface	0.0003		0.0004	0.0005	0.0002
Order 4	bed	0.0004				
	surface	0.0004				

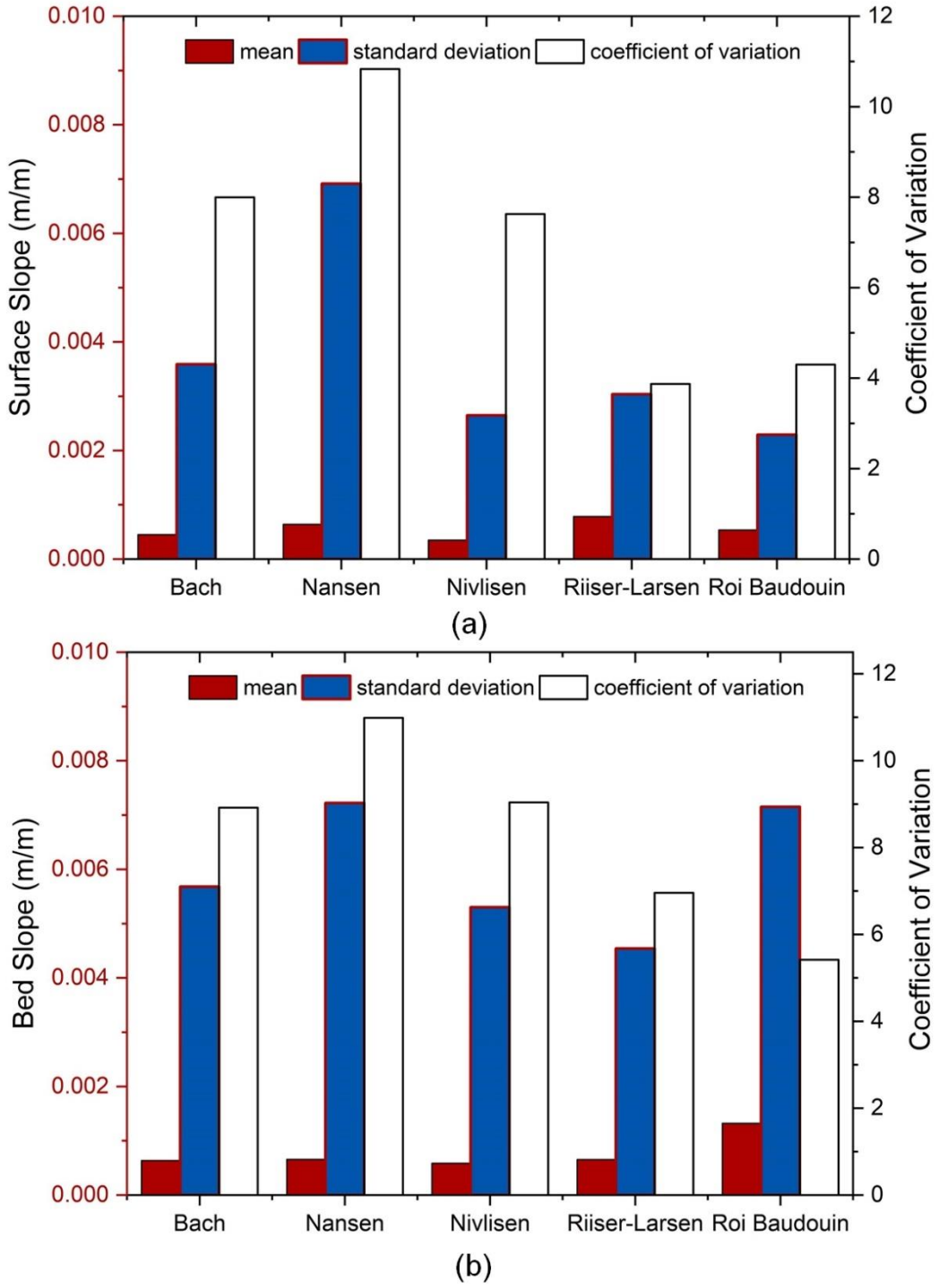

Figure 5.13 *Mean, standard deviation and coefficient of variation in surface and bed slope of supraglacial channels on Antarctic ice shelves.*

5.8 Drainage basin and drainage density

Drainage basins of the supraglacial channel networks for each ice shelf were estimated by the convex hull method (see Section 4.3.2.6). Figure 5.14 shows that the shape and size of drainage basins on ice shelves are different. The shape of the basin mainly depends on the size of the basin and the length of the stem channel of the basin. Drainage basins on the Bach, Nansen, Roi Baudouin and Riiser-Larsen Ice Shelf are elongated; such long, narrow basins have longer lag times when the meltwater drains from their outlet to the channels (Strahler, 1964; Pitcher and Smith, 2019; Das et al., 2022). In contrast, the drainage basin on the Nivlisen Ice Shelf is circular which is characterised by a shorter lag time and potentially higher peak discharge. Basin size also influences the lag time, and the details of drainage area are displayed in Table 5.7. The Nivlisen Ice Shelf has the largest basin area of 1,132 km^2, which is followed by Roi Baudouin (984 km^2), Bach (787 km^2), Riiser-Larsen (539 km^2) and Nansen (399 km^2). Generally, a large drainage basin indicates that water takes a longer time to flow through tributaries into the channel. The highest D_d values (0.78 km/km^2) of the supraglacial channel network on Riiser-Larsen Ice Shelf reveal fine drainage texture associated with faster routing (Yang et al., 2018), and the lowest D_d of 0.25 km/km^2 for Nivlisen Ice Shelf shows that channels are more widely spaced.

Table 5.7 The drainage area and drainage density (D_d) of supraglacial channel networks

Ice Shelf	Bach	Nansen	Nivlisen	Riiser-Larsen	Roi Baudouin
Drainage area (km^2)	787	399	1132	539	984
D_d **(km/km^2)**	0.62	0.47	0.25	0.78	0.46

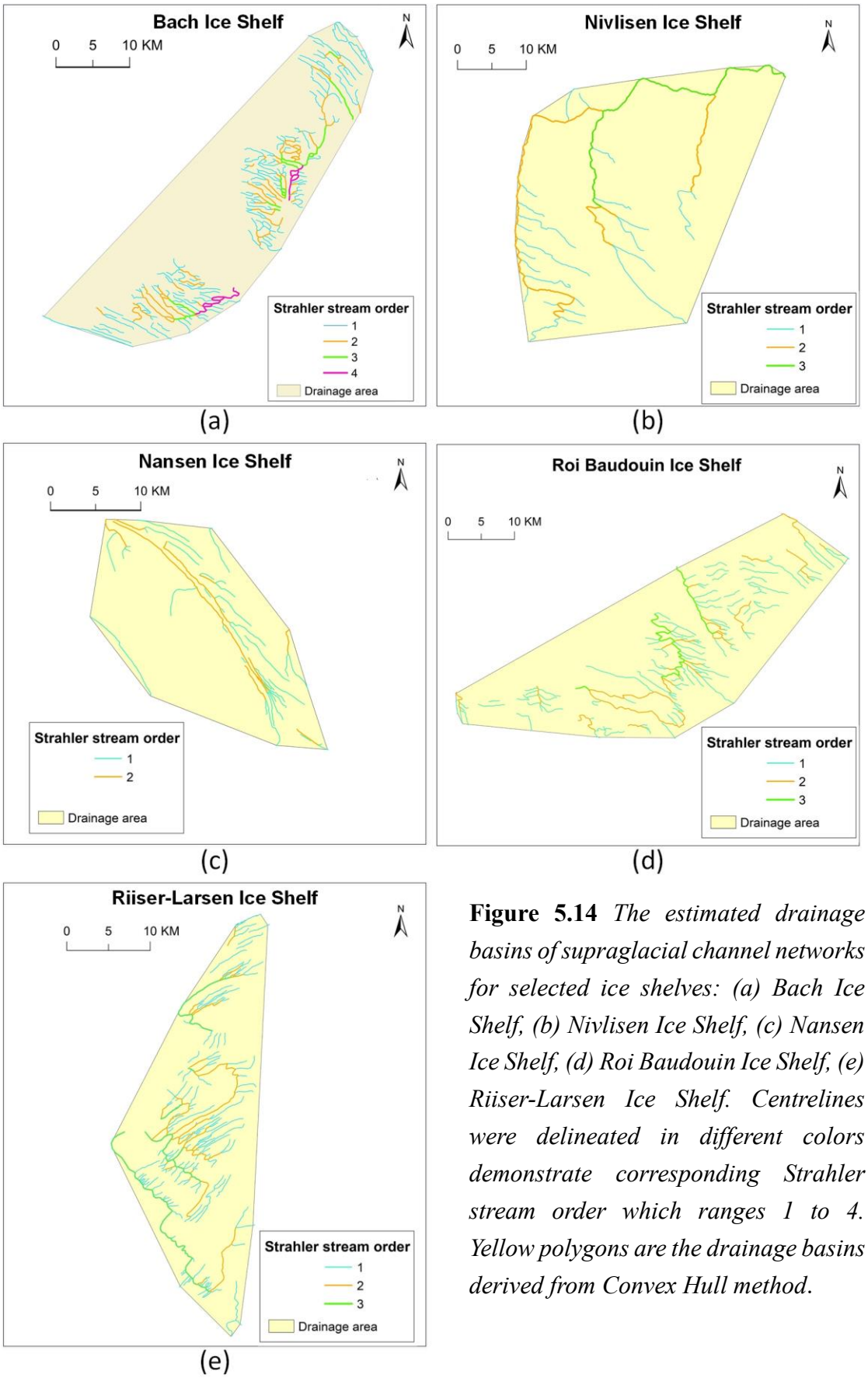

Figure 5.14 *The estimated drainage basins of supraglacial channel networks for selected ice shelves: (a) Bach Ice Shelf, (b) Nivlisen Ice Shelf, (c) Nansen Ice Shelf, (d) Roi Baudouin Ice Shelf, (e) Riiser-Larsen Ice Shelf. Centrelines were delineated in different colors demonstrate corresponding Strahler stream order which ranges 1 to 4. Yellow polygons are the drainage basins derived from Convex Hull method.*

6. Discussion

6.1 Characteristics and drainage patterns of supraglacial channel network on Antarctic ice shelves

This study presented three key questions in relation to supraglacial channels: (i) What do the channels on the surface of the Antarctic ice shelves look like? (ii) Are there any differences between supraglacial channels on different ice shelves? (iii) What factors control the development of the drainage patterns of the supraglacial channel networks on the Antarctic ice shelves? This section will discuss the first two questions primarily based on the results of this study, and the third question will be answered in Section 6.2.

In contrast to many previous studies on supraglacial hydrology on ice shelves, this study connects supraglacial lakes and channels as a well-integrated network through the Strahler stream order, rather than analysing them as independent features. Analysis of the topological relationships between supraglacial channels and lakes suggests that most lakes are interconnected with the channels. Some lakes are fed by the inflow channels, some are linked with outflow channels, and some are connected to both inflow and outflow channels (Figure 6.1). When supraglacial channels flow into a lake there are usually two scenarios: (1) discharge can be temporarily detained before flowing out from the outlet of the lake (Smith et al., 2015), (2) inflowing water penetrates the ice directly from a hydrofracturing moulin at the bottom of the lake (Das et al., 2008, Tedesco et al., 2013). Moreover, it is common to see the channels braid and form multichannel structures in the network. All these interconnected channel-lakes increase the complexity of supraglacial channel networks.

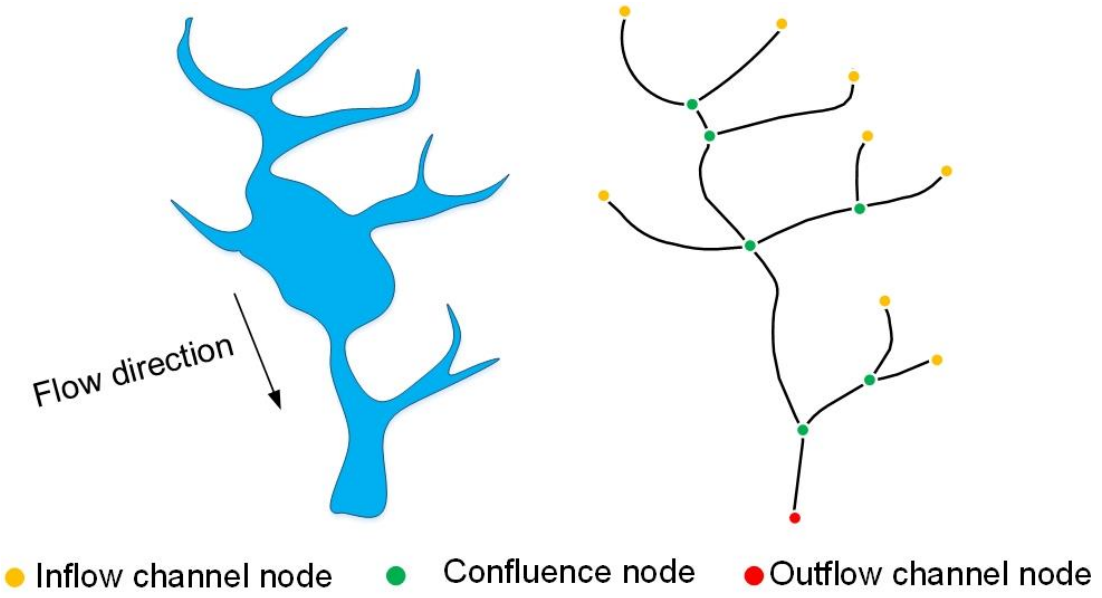

Figure 6.1 *Schematic diagram of interconnected channel-lakes. The left is part of supraglacial channel network which is common on the ice shelf, and the right is the centreline of the network, including the confluence nodes, inflow and outflow channel nodes*.

These connected channels and lakes form complete supraglacial drainage networks and exhibit various drainage patterns. Supraglacial channels on four ice shelves (e.g., Bach, Nivlisen, Riiser-Larsen and Roi Baudouin ice shelves) organize themselves into dendritic drainage networks (see Figure 5. 6a, b, c, e). The branching patterns have been argued to be an optimal state in the evolution of channel networks in the terrestrial environment (Kwang et al., 2021) such that in the absence of topographic, lithological and tectonic constraints, the most basic pattern of the drainage network should tend towards a dendritic form. This result also indicates that there are no significant external constraints acting to significantly perturb the elevation, slope or structure of the ice shelf, therefore allowing the supraglacial drainage system to form the optimal dendritic state. However, supraglacial channel networks on Nansen Ice Shelf display a parallel drainage pattern, which suggests there are topographic or structural controls on the formation of channel networks which force the drainage to follow particular routes. For terrestrial rivers, such patterns would, for example, be seen where the lithology or structure of rocks, or the

movement of tectonic faults, control topographic undulations and steer rivers (see Section 6.2).

Despite the different drainage patterns, supraglacial channel networks on Antarctic ice shelves are all found to exist close to the grounding line where the ice has the lower elevations, but where the ice shelves themselves do not collect significant depths of snow and firn. By examining the supraglacial channel networks on investigated ice shelves, it is concluded that a dendritic drainage pattern can be also recognised as the basic form in supraglacial environments, with deviations from local ice shelf topography or structure steer meltwater. Supraglacial channel networks on the investigated ice shelves in Antarctica show different drainage patterns but exhibit some similar fluvial characteristics to those of terrestrial rivers (Yang et al., 2016).

Figure 6.2 and Figure 6.3 present the results of the statistical correlation analysis between the number of channels, mean length and the stream orders. Firstly, supraglacial channels on all four ice shelves correlate significantly with numbers and stream orders. The numbers of channels decline exponentially as the stream order increases, and the R^2 values range from 0.74 to 0.98 which suggests compliance with Horton's laws. However, the mean lengths of supraglacial channels and stream orders show two different types of correlations despite the fact that they are all dendritic drainage patterns. Over the Bach, Riiser-Larsen and Roi Baudouin Ice Shelf, the mean length of channels shows an obviously exponential downward trend with increasing stream order. While the relationship between the mean length of channels and stream orders for Nivlisen Ice Shelf is negative. The reason for the inconsistent correlations with mean length and stream orders is that the supraglacial channel network on Nivlisen Ice Shelf was formed by long, continuous channels with a relatively small number of tributaries with low stream order (i.e., first- and second-order). However, channel networks on the remaining four ice shelves contained a large number of short, low-order tributaries that join into the stem channels, creating many confluence points and splitting the stem channels into segments

of the same stream order but shorter in length.

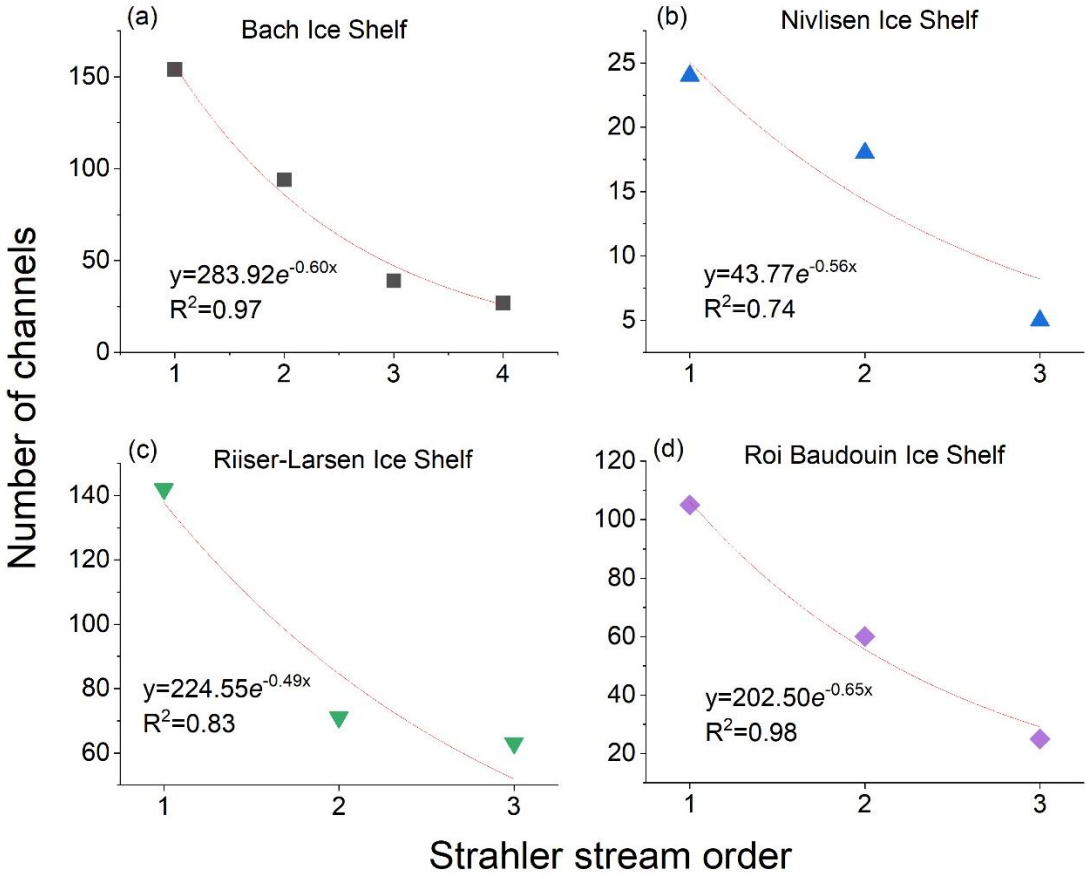

Figure 6.2 *Correlation between number and stream order of supraglacial channels.*

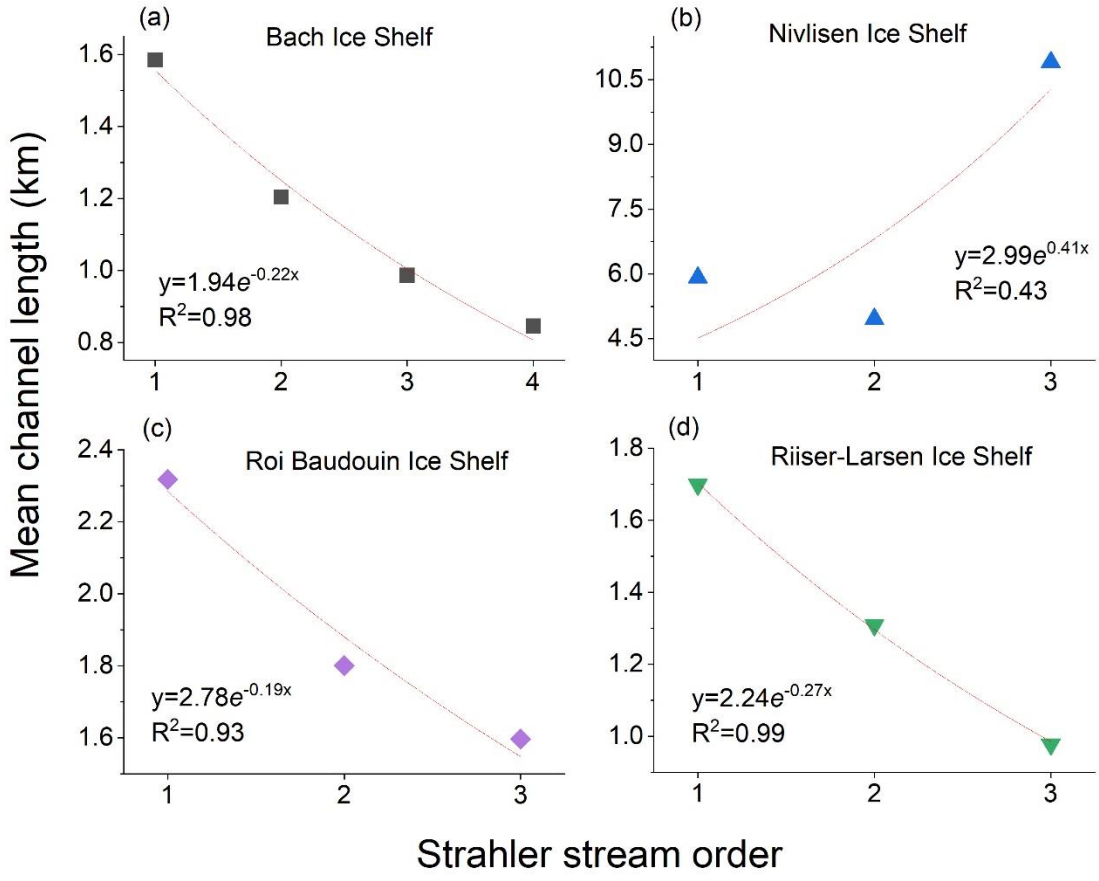

Figure 6.3 *Correlation between mean length and stream order of supraglacial channels.*

6.2 The effects of surface topography and structural glaciology

Satellite remote sensing over multiple years indicates that most supraglacial channel networks on ice shelves are persistent features year-to-year, generally forming from the end of December and keeping active to early January, corresponding with the austral summer months (Echelmeyer et al., 1991; Langley et al., 2016; Arthur et al., 2020b; Banwell et al., 2021; Dirscherl et al., 2021b). As observed in this study, supraglacial channel networks were generally located in the grounding zone that represents the transition area from grounded ice of the interior ice sheet to the floating shelf ice. It is characterised by the sudden change in slope or intense crevasses as seen from the satellite imagery.

In response to the question: 'what factors control the development of the drainage patterns of the supraglacial channel networks on Antarctic ice shelves?' this study investigated whether ice topography exerts control on drainage density by comparing the surface elevation and slope of supraglacial channel networks with *Dd*. A scatter diagram (Figure 6.4) and a correlation analysis were used to determine the relationship. This result indicates the linear regression (black line) coefficient of determination R^2 for *Dd* versus Mean elevation is 0.48, showing a pronounced negative correlation (i.e., when the surface elevation is higher, the channel distribution is sparser). This result is also supported by previous studies (Smith et al., 2015, Yang et al., 2016). Yang et al. (2016) mapped 523 supraglacial river networks on the southwest Greenland ice sheet, and Figure 6.5 (b) shows the relationship between drainage density and mean elevation of river networks from their study. The R^2 for drainage density and mean elevation is 0.29 ($p < 0.01$), suggesting drainage densities are lower at higher elevations. Furthermore, the correlation coefficient R^2 between drainage density and slope also reaches 0.47, suggesting that 47% of drainage density variance correlates with mean surface slope, which means the greater the slope, the more densely distributed the channels.

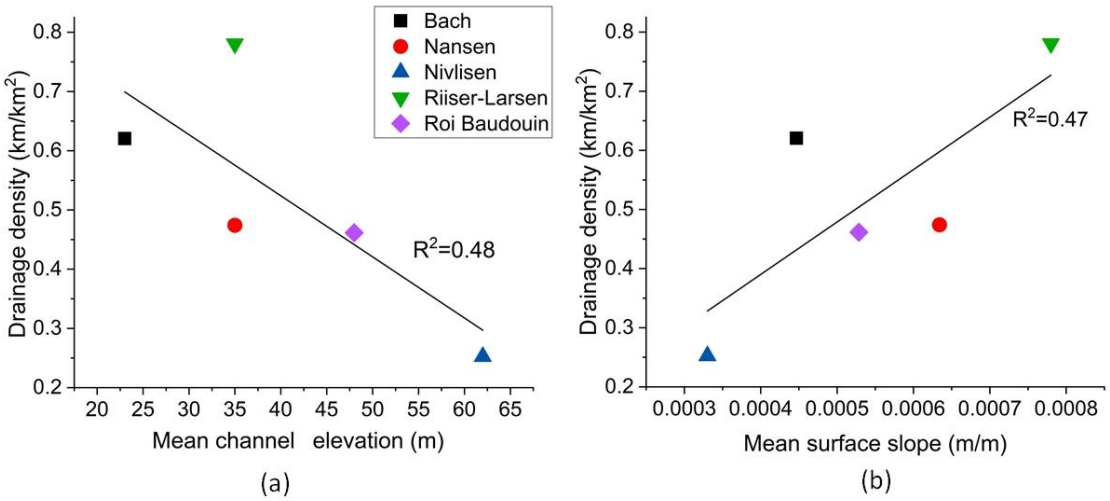

Figure 6.4 *Drainage density versus mean channel elevation and mean surface slope.*

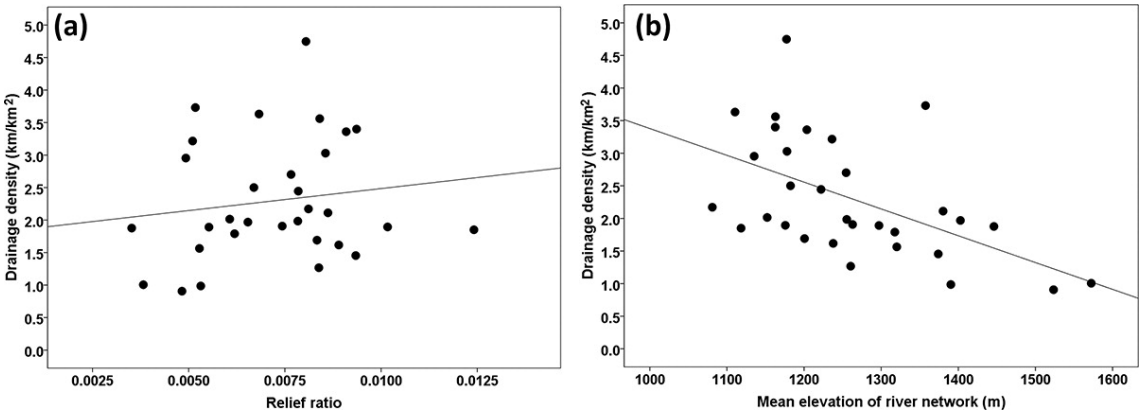

Figure 6.5 *Drainage density of the 40 longest supraglacial river networks in relation to (a) relief ratio; and (b) mean elevation. The black lines indicate the linear regression coefficient of determination* R^2. (Yang et al., 2015)

Additionally, it is found that all the supraglacial channel networks develop along a preferential direction (see Section 5.6). As seen in the images analysed from Landsat-8 OLI imagery (Figure 6.6 and Figure 6.7) for the five ice shelves on the Antarctic Ice Sheet, there are some longitudinal structures (also called "flow stripes", "flow bands"), crevasses and surface fractures existing aligned parallel to the principal ice-flow direction on the ice shelf (Holt et al., 2013; Kingslake et al., 2017). Given that these longitudinal surface features also have a clear directional orientation, they are likely to have a greater relationship with the flow direction of the supraglacial channels.

Take the Nansen Ice Shelf as an example, which has many obvious flow-stripes, fractures, rumples and nunataks marking its surface (Figure6.7a). Supraglacial channel networks on Nansen Ice Shelf close to the rumples and fractures become fragmented. Although there are some longitudinal structures, supraglacial lakes occur in 'branches' at various angles to those channels. This is possibly the result of the specific topography over which the ice flows before it crosses the grounding line. For example, according to Section 5.2, supraglacial lakes and channels were often found in low elevations and near the grounding line and in surface depressions generated by nunataks and longitudinal flow structures.

On the one hand, exposed rock (i.e., nunataks) may decrease the albedo and increase wind speeds to create more heavily scoured ice surfaces (Stokes et.al, 2019). On the other hand, grounded ice flow upstream can produce the downstream flow stripes and rumples, making it easier for meltwater to accumulate. Moreover, Dow et al. (2018) reported the calving event at Nansen Ice Shelf in 2016 was mainly driven by the basal channels underneath the shelf. They also pointed out that basal channels can lead to ice surface deformation, allowing supraglacial channels to divert into the transverse fractures, and this discovery suggests surface topography of the ice shelf can be influenced by the basal channel destabilization.

In summary, supraglacial channel networks prefer to occur in low elevations and flatter marginal areas of the ice shelves in Antarctica, their drainage patterns and density correlate with the local-scale surface topography. Where that surface topography is significantly disrupted by ice structures formed as ice flows over inland topography or around nunataks, the supraglacial channels will naturally follow those linear structures on the ice surface with little chance of escaping laterally unless they intercept a cross-cutting flow structure.

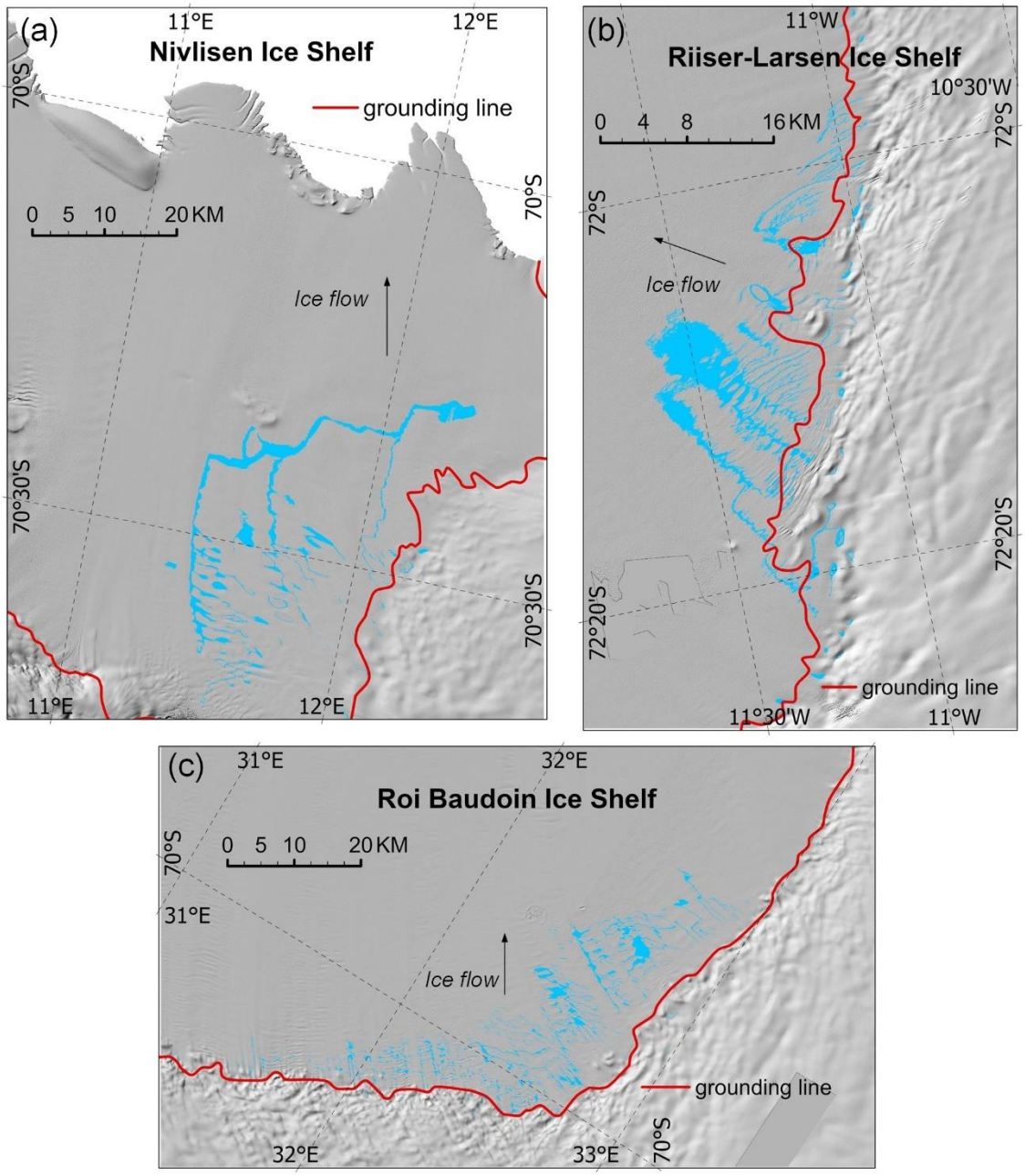

Figure 6.6 *Hillshade images from Landsat-8 OLI imagery for the studied ice shelves on the EAIS: (a)Nivlisen, (b)Riiser-Larsen, (c)Roi Baudouin. The blue polygons indicate extracted supraglacial channels and lakes in this study.*

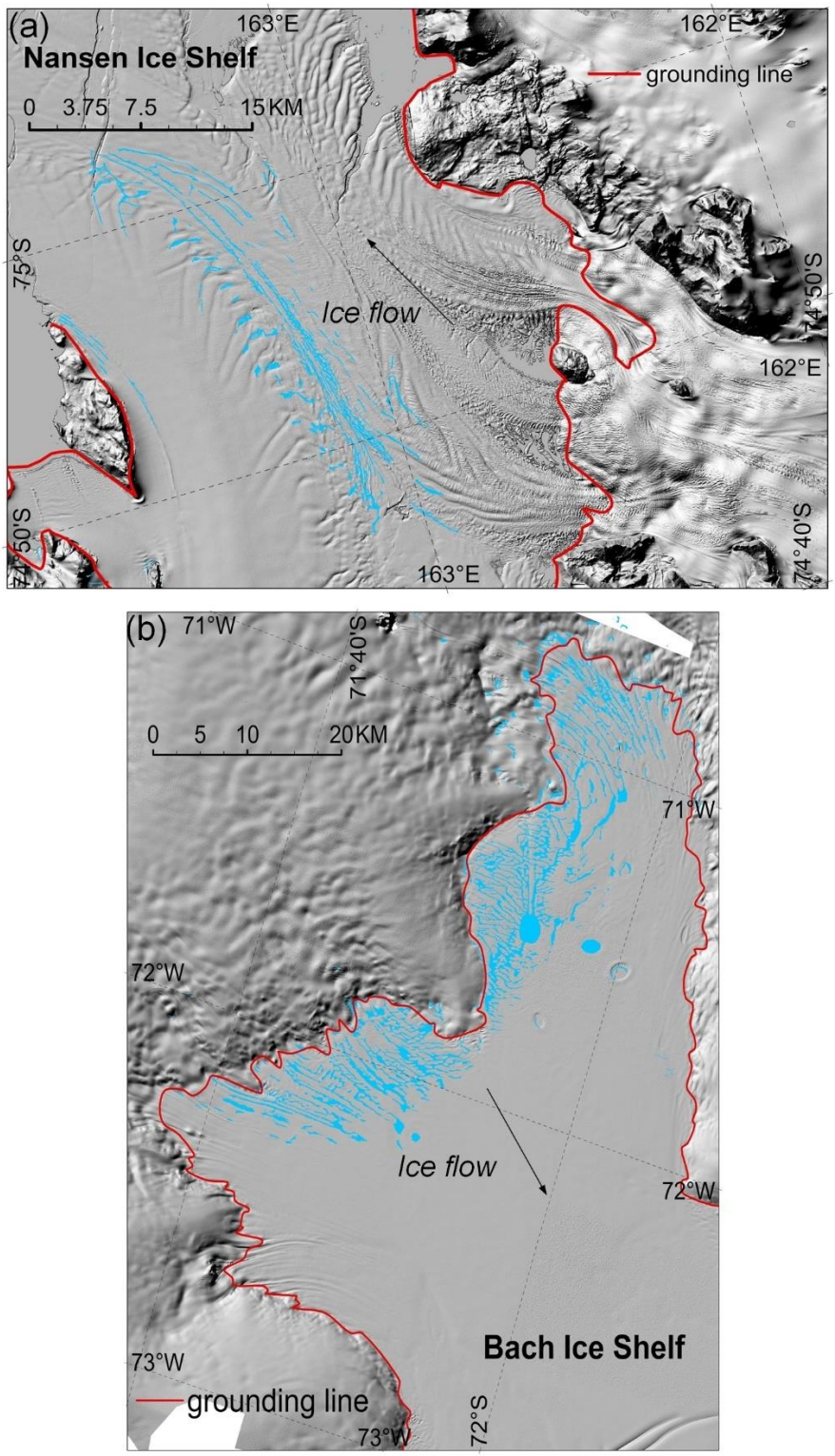

Figure 6.7 *Hillshade images from Landsat-8 OLI imagery for the studied ice shelves on the WAIS. a) Nansen, (b)Bach. The blue polygons indicate extracted supraglacial channels and lakes in this study*.

6.3 Limitations of the current study

Due to constraints on time, materials and methodology, the findings of this study have three major limitations that could be addressed in future research:

1.Firstly, Landsat-8 imagery with 30 m spatial resolution was used to map supraglacial channels and lakes, and delineation results from such moderate-resolution satellite imagery are enough to observe the well-developed channel networks on the ice surface and capture their drainage patterns (Lampkin and VanderBerg, 2014; Yang and Smith, 2016; Bell et al., 2017; Kingslake et al., 2017; Tuckett et al., 2021). However, some small and narrow channels which are less than 30 m wide have not been detected that may limit the scope of the analysis in this study. For example, some fluvial metrics (e.g., channel number, length and size) probably have been underestimated;

2.The second limitation concerns the evolution process of supraglacial channels. On the one hand, supraglacial channel networks on different ice shelves only have been extracted at the peak of the melt season when they reached their maximum extent. Therefore, the lack of long-term observations would limit the analysis of meltwater drainage variations (i.e., the time series of areal size, lengths, width, and depths). On the other hand, the terminations (i.e., moulins, crevasses) of the supraglacial channels were not identified in this study due to constraints in imagery resolution and time. Little is known about where the meltwater is eventually transported by the supraglacial channels and how differences in these terminations may affect the evolution of channel networks;

3. Thirdly, this study highlights the effects of surface topography and structural glaciology on supraglacial channels but lacks the analysis of other influencing factors such as surface melting, air temperatures and surface albedo. Local climatic controls would impact the melt events and further affect the evolution of supraglacial channels and lakes (Banwell et al., 2021; Arthur et al., 2020b; Tuckett et al., 2021). The meteorological data (e.g., near-

surface temperature) and regional climate models (e.g., the Regional Atmospheric Climate Model) would apply to investigate climatic controls on the formation of supraglacial channels.

6.4 Improvements for future work

Given the above limitations, although the goal and objectives of the study are considered to have been accomplished, some improvements could be done in future work to achieve better results:

1.Satellite imagery with high spatial resolutions (e.g., Sentinel-2 imagery with 10 m resolution) would be used to delineate the narrow channels (less than 30 m wide) for more accurate observations of supraglacial drainage system;

2.Identify the terminations of supraglacial channels (i.e., quantify the number of channels that flow off the ice versus into lakes versus into the ice) and analyse the drainage of surface meltwater;

3.Observe the morphology and evolution process of supraglacial channels concerning possible controlling factors such as ice surface slope, structural glaciology and modelled ice surface properties (i.e., snowfall, firn thickness, runoff) from publicly available regional climate models (e.g., the Regional Atmospheric Climate Model).

7. Conclusions

In this study, supraglacial channel networks on five Antarctic ice shelves: Bach (2020), Nansen (2022), Nivlisen(2020), Riiser-Larsen(2020) and Roi Baudouin (2022) were mapped from the Landsat-8 satellite imagery during the melt season in 2020 and 2022. Quantification of the supraglacial channel networks was explored by calculating various fluvial morphology metrics (e.g., length, width, depth, sinuosity, bifurcation ratio, orientations, slopes, and drainage density). These results were analysed, together with previous related studies, leading to the following key conclusions:

1.Widespread supraglacial lakes and channels were observed on all five Antarctic ice shelves in the melt seasons of 2020 and 2022, and most of them were interconnected to form channel networks at various scales (containing channels from first- to fourth-order).

During the melt season, extensive lakes and channels were found on the ice surface, and the majority of these were interconnected, with only a few existing independently. Key fluvial metrics (i.e., number, length, width, depth, Si, Rb, orientation, slopes and *Dd*) were measured for 119 channel networks. The results show that supraglacial channel networks generally occurred in flat areas (bed slope < 0.001) with low elevations (<100 m) and near the grounding lines, and the mean widths (85 ~ 282 m) and mean depths (0.8 ~ 2.0 m) of supraglacial channels both increase from low to high Strahler stream order, while the mean lengths (846 ~ 10,899 m) decrease. Additionally, more than half of the channels were straight and a few channels at higher stream order (stream order ≥ 2) showed sinuosity.

2.Supraglacial channel networks have configurations that are unique to each ice shelf.

Two drainage patterns were found on the surface of the studied ice shelves. Supraglacial channel networks on Bach, Nivlisen, Riiser-Larsen and Roi Baudouin Ice Shelf developed as dendritic drainage pattern which is also the most common and basic pattern for terrestrial channel networks, but a more parallel drainage pattern was observed on Nansen Ice Shelf. Moreover, only the channel networks on Nansen Ice Shelf were directly flowing off the ice shelf and into the sea, while the channel networks on the remaining four ice shelves all flowed into the supraglacial lakes or other terminations (likely percolating into the snow/firn layer but possibly into crevasses or cryoconites) near the grounding lines. There was only one large supraglacial channel network (total length reaches 286 km) on Nivlisen Ice Shelf, while many channel networks of different scales (including channels from first- to fourth stream order) were found on the other four ice shelves.

3.The structure of supraglacial channel networks is significantly affected by surface topography and structural glaciology of ice shelves.

The results indicate supraglacial channel networks have a strongly preferred direction which was broadly consistent with the ice flow direction and ice surface slope. Secondly, supraglacial lakes and channels were often found in the surface depressions that generated longitudinal surface flow structures (i.e., flow stripes and rumples). Thirdly, the drainage density (D_d) shows obvious correlations with mean elevation and mean surface slope (i.e., when the surface elevation is higher, the channel distribution is sparser; and when the surface is steeper, the channel distribution is denser).

8. References

Abrahamsen, E. P. (2012). *Oceanographic conditions beneath Fimbul Ice Shelf, Antarctica.* University of Southampton.

Acharya, T. D., Subedi, A. and Lee, D. H. (2019). Evaluation of machine learning algorithms for surface water extraction in a Landsat 8 scene of Nepal. *Sensors,* 19**,** 2769.

Agosta, C., Amory, C., Kittel, C., Orsi, A., Favier, V., Gallée, H., Van Den Broeke, M. R., Lenaerts, J., Van Wessem, J. M. and Van De Berg, W. J. (2019). Estimation of the Antarctic surface mass balance using the regional climate model MAR (1979–2015) and identification of dominant processes. *The Cryosphere,* 13**,** 281-296.

Alley, K. E., Wild, C. T., Luckman, A., Scambos, T. A., Truffer, M., Pettit, E. C., Muto, A., Wallin, B., Klinger, M. and Sutterley, T. (2021). Two decades of dynamic change and progressive destabilization on the Thwaites Eastern Ice Shelf. *The Cryosphere,* 15**,** 5187-5203.

Arthur, J. F., Stokes, C., Jamieson, S. S., Carr, J. R. and Leeson, A. A. (2020a). Recent understanding of Antarctic supraglacial lakes using satellite remote sensing. *Progress in Physical Geography: Earth and Environment,* 44**,** 837-869.

Arthur, J. F., Stokes, C. R., Jamieson, S. S., Carr, J. R. and Leeson, A. A. (2020b). Distribution and seasonal evolution of supraglacial lakes on Shackleton Ice Shelf, East Antarctica. *The Cryosphere,* 14**,** 4103-4120.

Arthur, J. F., Stokes, C. R., Jamieson, S. S., Rachel Carr, J., Leeson, A. A. and Verjans, V. (2022). Large interannual variability in supraglacial lakes around East Antarctica.

Nature communications, 13**,** 1-12.

Bajjali, W. (2017). *ArcGIS for environmental and water issues*, Springer.

Banwell, A. F., Arnold, N. S., Willis, I. C., Tedesco, M. and Ahlstrøm, A. P. (2012). Modeling supraglacial water routing and lake filling on the Greenland Ice Sheet. *Journal of Geophysical Research: Earth Surface*, 117(F4).

Banwell, A. F., Caballero, M., Arnold, N. S., Glasser, N. F., Mac Cathles, L. and Macayeal, D. R. (2014). Supraglacial lakes on the Larsen B ice shelf, Antarctica, and at Paakitsoq, West Greenland: a comparative study. *Annals of Glaciology,* 55**,** 1-8.

Banwell, A. F., Datta, R. T., Dell, R. L., Moussavi, M., Brucker, L., Picard, G., Shuman, C. A. and Stevens, L. A. (2021). The 32-year record-high surface melt in 2019/2020 on the northern George VI Ice Shelf, Antarctic Peninsula. *The Cryosphere,* 15**,** 909-925.

Banwell, A. F., Macayeal, D. R. and Sergienko, O. V. (2013). Breakup of the Larsen B Ice Shelf triggered by chain reaction drainage of supraglacial lakes. *Geophysical Research Letters,* 40**,** 5872-5876.

Banwell, A. F., Willis, I. C., Macdonald, G. J., Goodsell, B. and Macayeal, D. R. (2019). Direct measurements of ice-shelf flexure caused by surface meltwater ponding and drainage. *Nature communications,* 10**,** 1-10.

Bell, R. E., Banwell, A. F., Trusel, L. D. and Kingslake, J. (2018). Antarctic surface hydrology and impacts on ice-sheet mass balance. *Nature Climate Change,* 8**,** 1044-1052.

Bell, R. E., Chu, W., Kingslake, J., Das, I., Tedesco, M., Tinto, K. J., Zappa, C. J., Frezzotti, M., Boghosian, A. and Lee, W. S. (2017). Antarctic ice shelf potentially stabilized by export of meltwater in surface river. *Nature,* 544**,** 344-348.

Benn, D. I., Thompson, S., Gulley, J., Mertes, J., Luckman, A. and Nicholson, L. (2017). Structure and evolution of the drainage system of a Himalayan debris-covered glacier, and its relationship with patterns of mass loss. *The Cryosphere,* 11**,** 2247-2264.

Bevan, S. L., Luckman, A., Hubbard, B., Kulessa, B., Ashmore, D., Kuipers Munneke, P., O'leary, M., Booth, A., Sevestre, H. and Mcgrath, D. (2017). Centuries of intense surface melt on Larsen C Ice Shelf. *The Cryosphere,* 11**,** 2743-2753.

Brice, J. and Blodgett, J. (1978). Countermeasures for Hydraulic Problems at Bridges, Volume 1- Analysis and Assessment.

Budd, W. F. (1970). Ice flow over bedrock perturbations *Journal of Glaciology*, 9(55), 29-48.

Budd, W. F., & Carter, D. B. (1971). An analysis of the relation between the surface and bedrock profiles of ice caps. *Journal of Glaciology*, 10(59), 197-209.

Burton-Johnson, A., Black, M., Fretwell, P. T. and Kaluza-Gilbert, J. (2016). An automated methodology for differentiating rock from snow, clouds and sea in Antarctica from Landsat 8 imagery: a new rock outcrop map and area estimation for the entire Antarctic continent. *The Cryosphere,* 10**,** 1665-1677.

Campbell, I. B. and Claridge, G. G. C. (1987). *Antarctica: soils, weathering processes and environment*, Elsevier.

Charlton, R. (2007). *Fundamentals of fluvial geomorphology*, Routledge.

Clason, C., Mair, D. W., Burgess, D. O. and Nienow, P. W. (2012). Modelling the delivery of supraglacial meltwater to the ice/bed interface: application to southwest Devon Ice Cap, Nunavut, Canada. *Journal of Glaciology,* 58**,** 361-374.

Clason, C. C., Mair, D., Nienow, P., Bartholomew, I., Sole, A., Palmer, S. and Schwanghart, W. (2015). Modelling the transfer of supraglacial meltwater to the bed of Leverett Glacier, Southwest Greenland. *The Cryosphere,* 9**,** 123-138.

Cook, A. J. and Vaughan, D. G. (2010). Overview of areal changes of the ice shelves on the Antarctic Peninsula over the past 50 years. *The cryosphere,* 4**,** 77-98.

Cooley, S. W., Smith, L. C., Stepan, L. and Mascaro, J. (2017). Tracking dynamic northern surface water changes with high-frequency planet CubeSat imagery. *Remote Sensing,* 9**,** 1306.

Corr, D., Leeson, A., Mcmillan, M., Zhang, C. and Barnes, T. (2022). An inventory of supraglacial lakes and channels across the West Antarctic Ice Sheet. *Earth System Science Data,* 14**,** 209-228.

Council, N. R. (2011). *Future science opportunities in Antarctica and the Southern Ocean*, National Academies Press.

Crozier, J., Karlstrom, L. and Yang, K. (2018). Basal control of supraglacial meltwater catchments on the Greenland Ice Sheet. *The Cryosphere,* 12**,** 3383-3407.

Cuffey, K. M. and Paterson, W. S. B. (2010). *The physics of glaciers*, Academic Press.

Das, B. C., Islam, A. and Sarkar, B. (2022). Drainage Basin Shape Indices to Understanding Channel Hydraulics. *Water Resources Management***,** 1-25.

Das, S. B., Joughin, I., Behn, M. D., Howat, I. M., King, M. A., Lizarralde, D. and Bhatia, M. P. (2008). Fracture propagation to the base of the Greenland Ice Sheet during supraglacial lake drainage. *Science,* 320**,** 778-781.

Deconto, R. M. and Pollard, D. (2016). Contribution of Antarctica to past and future sea-level rise. *Nature,* 531**,** 591-597.

Dell, R., Arnold, N., Willis, I., Banwell, A., Williamson, A., Pritchard, H. and Orr, A. (2020). Lateral meltwater transfer across an Antarctic ice shelf. *The Cryosphere,* 14**,** 2313-2330.

Dell, R. L., Banwell, A. F., Willis, I. C., Arnold, N. S., Halberstadt, A. R. W., Chudley, T. R. and Pritchard, H. D. (2022). Supervised classification of slush and ponded water on Antarctic ice shelves using Landsat 8 imagery. *Journal of Glaciology,* 68**,** 401-414.

Dirscherl, M., Dietz, A. J., Kneisel, C. and Kuenzer, C. (2020). Automated mapping of Antarctic supraglacial lakes using a machine learning approach. *Remote Sensing,* 12**,** 1203.

Dirscherl, M., Dietz, A. J., Kneisel, C. and Kuenzer, C. (2021a). A novel method for automated supraglacial lake mapping in Antarctica using Sentinel-1 SAR imagery and deep learning. *Remote Sensing,* 13**,** 197.

Dirscherl, M. C., Dietz, A. J. and Kuenzer, C. (2021b). Seasonal evolution of Antarctic

supraglacial lakes in 2015–2021 and links to environmental controls. *The Cryosphere,* 15**,** 5205-5226.

Dong, Y., Zhao, J., Floricioiu, D., Krieger, L., Fritz, T. and Eineder, M. (2021). High-resolution topography of the Antarctic Peninsula combining the TanDEM-X DEM and Reference Elevation Model of Antarctica (REMA) mosaic. *The Cryosphere,* 15**,** 4421-4443.

Dunmire, D., Lenaerts, J., Banwell, A., Wever, N., Shragge, J., Lhermitte, S., Drews, R., Pattyn, F., Hansen, J. and Willis, I. (2020). Observations of buried lake drainage on the Antarctic Ice Sheet. *Geophysical research letters,* 47**,** e2020GL087970.

Echelmeyer, K., Clarke, T. and Harrison, W. D. (1991). Surficial glaciology of Jakobshavns Isbræ, West Greenland: Part I. Surface morphology. *Journal of Glaciology*, 37, 368-382.

Eisermann, H., Eagles, G., Ruppel, A. S., Läufer, A. and Jokat, W. (2021). Bathymetric control on Borchgrevink and Roi Baudouin ice shelves in East Antarctica. *Journal of Geophysical Research: Earth Surface,* 126**,** e2021JF006342.

Ewing, K. J. (1972). Supraglacial streams of the Kaskawulsh Glacier.

Feng, D., Gleason, C. J., Yang, X. and Pavelsky, T. M. (2019). Comparing discharge estimates made via the BAM algorithm in high-order Arctic rivers derived solely from optical CubeSat, Landsat, and Sentinel-2 data. *Water Resources Research,* 55**,** 7753-7771.

Fernández, R. and Parker, G. (2021). Laboratory observations on meltwater meandering rivulets on ice. *Earth Surface Dynamics,* 9**,** 253-269.

Frasson, R. P. D. M., Pavelsky, T. M., Fonstad, M. A., Durand, M. T., Allen, G. H., Schumann, G., Lion, C., Beighley, R. E. and Yang, X. (2019). Global relationships between river width, slope, catchment area, meander wavelength, sinuosity, and discharge. *Geophysical Research Letters,* 46**,** 3252-3262.

Fretwell, P., Pritchard, H. D., Vaughan, D. G., Bamber, J. L., Barrand, N. E., Bell, R., Bianchi, C., Bingham, R., Blankenship, D. D. and Casassa, G. (2013). Bedmap2: improved ice bed, surface and thickness datasets for Antarctica. *The Cryosphere,* 7**,** 375-393.

Germain, S. S. and Moorman, B. (2016). The development of a pulsating supraglacial stream. *Annals of Glaciology,* 57**,** 31-38.

Gioia, D., Schiattarella, M. and Giano, S. I. (2018). Right-angle pattern of minor fluvial networks from the Ionian terraced belt, southern Italy: Passive structural control or foreland bending? *Geosciences,* 8**,** 331.

Gleason, C. J., Yang, K., Feng, D., Smith, L. C., Liu, K., Pitcher, L. H., Chu, V. W., Cooper, M. G., Overstreet, B. T. and Rennermalm, A. K. (2021). Hourly surface meltwater routing for a Greenlandic supraglacial catchment across hillslopes and through a dense topological channel network. *The Cryosphere,* 15**,** 2315-2331.

Gleyzer, A., Denisyuk, M., Rimmer, A. and Salingar, Y. (2004). A fast recursive gis algorithm for computing strahler stream order in braided and nonbraided networks 1. *JAWRA Journal of the American Water Resources Association,* 40**,** 937-946.

Gordon, N. D., McMahon, T. A., and Finlayson, B. L. (1992). Stream hydrology : an introduction for ecologists. *Wiley*.

Gudmundsson, G. H. (2003). Transmission of basal variability to a glacier surface. *Journal of Geophysical Research: Solid Earth*, 108(B5).

Hill, T. and Dow, C. F. (2021). Modeling the dynamics of supraglacial rivers and distributed meltwater flow with the Subaerial Drainage System (SaDS) model. *Journal of Geophysical Research: Earth Surface,* 126**,** e2021JF006309.

Holt, T., Glasser, N. and Quincey, D. (2013). The structural glaciology of southwest Antarctic Peninsula Ice Shelves (ca. 2010). *Journal of Maps,* 9**,** 523-531.

Horton, R. E. (1945). Erosional development of streams and their drainage basins; hydrophysical approach to quantitative morphology. *Geological society of America bulletin,* 56**,** 275-370.

Howat, I. M., Porter, C., Smith, B. E., Noh, M.-J. and Morin, P. (2019). The reference elevation model of Antarctica. *The Cryosphere,* 13**,** 665-674.

Jarosch, A. and Gudmundsson, M. (2012). A numerical model for meltwater channel evolution in glaciers. *The Cryosphere,* 6**,** 493-503.

Karlstrom, L., Gajjar, P. and Manga, M. (2013). Meander formation in supraglacial streams. *Journal of Geophysical Research: Earth Surface,* 118**,** 1897-1907.

Karlstrom, L. and Yang, K. (2016). Fluvial supraglacial landscape evolution on the Greenland Ice Sheet. *Geophysical Research Letters,* 43**,** 2683-2692.

Khazendar, A., Rignot, E., Schroeder, D. M., Seroussi, H., Schodlok, M. P., Scheuchl, B., Mouginot, J., Sutterley, T. C. and Velicogna, I. (2016). Rapid submarine ice

melting in the grounding zones of ice shelves in West Antarctica. *Nature communications,* 7**,** 1-8.

King, L., Hassan, M. A., Yang, K. and Flowers, G. (2016). Flow routing for delineating supraglacial meltwater channel networks. *Remote Sensing,* 8**,** 988.

Kingslake, J., Ely, J. C., Das, I. and Bell, R. E. (2017). Widespread movement of meltwater onto and across Antarctic ice shelves. *Nature,* 544**,** 349-352.

Kingslake, J., Ng, F. and Sole, A. (2015). Modelling channelized surface drainage of supraglacial lakes. *Journal of Glaciology,* 61**,** 185-199.

Knighton, A. (1985). Channel form adjustment in supraglacial streams, Austre Okstindbreen, Norway. *Arctic and Alpine Research,* 17**,** 451-466.

Kostrzewski, A. and Zwolinski, Z. (1995). Hydraulic geometry of a supraglacial stream, Ragnarbreen, Spitsbergen. *Quaestiones Geographicae. Zeszyt Specjalny,* 4.

Koziol, C., Arnold, N., Pope, A. and Colgan, W. (2017). Quantifying supraglacial meltwater pathways in the Paakitsoq region, West Greenland. *Journal of Glaciology,* 63**,** 464-476.

Kwang, J. S., Langston, A. L. and Parker, G. (2021). The role of lateral erosion in the evolution of nondendritic drainage networks to dendricity and the persistence of dynamic networks. *Proceedings of the National Academy of Sciences,* 118**,** e2015770118.

Lampkin, D. J., and VanderBerg, J. (2011). A preliminary investigation of the influence of basal and surface topography on supraglacial lake distribution near Jakobshavn

Isbrae, western Greenland. *Hydrological Processes*, 25(21), 3347-3355.

Lampkin, D. J., and VanderBerg, J. (2014). Supraglacial melt channel networks in the Jakobshavn Isbræ region during the 2007 melt season. *Hydrological Processes*, 28(25), 6038-6053.

Langley, E. S., Leeson, A. A., Stokes, C. R. and Jamieson, S. S. (2016). Seasonal evolution of supraglacial lakes on an East Antarctic outlet glacier. *Geophysical Research Letters*, 43(16), 8563-8571.

Leeson, A., Forster, E., Rice, A., Gourmelen, N. and Van Wessem, J. (2020). Evolution of supraglacial lakes on the Larsen B ice shelf in the decades before it collapsed. *Geophysical Research Letters,* 47**,** e2019GL085591.

Legleiter, C. J., Roberts, D. A. and Lawrence, R. L. (2009). Spectrally based remote sensing of river bathymetry. *Earth Surface Processes and Landforms,* 34**,** 1039-1059.

Lenaerts, J., Lhermitte, S., Drews, R., Ligtenberg, S., Berger, S., Helm, V., Smeets, C., Van Den Broeke, M., Van De Berg, W. J. and Van Meijgaard, E. (2017). Meltwater produced by wind–albedo interaction stored in an East Antarctic ice shelf. *Nature climate change,* 7, 58-62.

Leopold, L.B., Wolman, M.G., and Miller, J.P. (1964).Fluvial processes in geomorphology: San Francisco, W.H. Freeman, 522 p.

Liggett, D., Storey, B. and Cook, Y. (2015). Exploring the Last Continent. *Exploring the Last Continent.* Springer.

Lindsay, J. B. and Creed, I. F. (2006). Distinguishing actual and artefact depressions in digital elevation data. *Computers & Geosciences,* 32**,** 1192-1204.

Lu, X., Yang, K., Lu, Y., Gleason, C. J., Smith, L. C. and Li, M. (2020a). Small Arctic rivers mapped from Sentinel-2 satellite imagery and ArcticDEM. *Journal of Hydrology,* 584**,** 124689.

Lu, Y., Yang, K., Lu, X., Li, Y., Gao, S., Mao, W. and Li, M. (2021). Response of supraglacial rivers and lakes to ice flow and surface melt on the northeast Greenland ice sheet during the 2017 melt season. *Journal of Hydrology,* 602**,** 126750.

Lu, Y., Yang, K., Lu, X., Smith, L. C., Sole, A. J., Livingstone, S. J., Fettweis, X. and Li, M. (2020b). Diverse supraglacial drainage patterns on the Devon ice Cap, Arctic Canada. *Journal of Maps,* 16**,** 834-846.

MacAYEAL, D. R., Sergienko, O. V. and Banwell, A. F. (2015). A model of viscoelastic ice-shelf flexure. *Journal of Glaciology,* 61**,** 635-645.

Magesh, N., Jitheshlal, K., Chandrasekar, N. and Jini, K. (2012). GIS based morphometric evaluation of Chimmini and Mupily watersheds, parts of Western Ghats, Thrissur District, Kerala, India. *Earth Science Informatics*, 5, 111-121.

Maidment, D. R. and Morehouse, S. (2002). *Arc Hydro: GIS for water resources*, ESRI, Inc.

Marston, R. A. (1983). Supraglacial stream dynamics on the Juneau Icefield. *Annals of the Association of American Geographers,* 73**,** 597-608.

Mcfeeters, S. K. (1996). The use of the Normalized Difference Water Index (NDWI) in the delineation of open water features. *International journal of remote sensing,* 17**,** 1425-1432.

Mcgrath, D., Steffen, K., Rajaram, H., Scambos, T., Abdalati, W. and Rignot, E. (2012). Basal crevasses on the Larsen C Ice Shelf, Antarctica: Implications for meltwater ponding and hydrofracture. *Geophysical research letters,* 39.

Moussavi, M., Pope, A., Halberstadt, A. R. W., Trusel, L. D., Cioffi, L. and Abdalati, W. (2020). Antarctic supraglacial lake detection using Landsat 8 and Sentinel-2 imagery: Towards continental generation of lake volumes. *Remote Sensing,* 12**,** 134.

Moussavi, M. S., Abdalati, W., Pope, A., Scambos, T., Tedesco, M., Macferrin, M. and Grigsby, S. (2016). Derivation and validation of supraglacial lake volumes on the Greenland Ice Sheet from high-resolution satellite imagery. *Remote sensing of environment,* 183**,** 294-303.

Nicolas, J. P., Vogelmann, A. M., Scott, R. C., Wilson, A. B., Cadeddu, M. P., Bromwich, D. H., Verlinde, J., Lubin, D., Russell, L. M. and Jenkinson, C. (2017). January 2016 extensive summer melt in West Antarctica favoured by strong El Niño. *Nature communications,* 8**,** 1-10.

Omran, A., Dietrich, S., Abouelmagd, A., Michael, M. and Geosciences (2016). New ArcGIS tools developed for stream network extraction and basin delineations using Python and java script. *Computers,* 94**,** 140-149.

Ortega, J. A., Gómez-Heras, M., Perez-López, R. and Wohl, E. (2014). Multiscale structural and lithologic controls in the development of stream potholes on granite

bedrock rivers. *Geomorphology,* 204**,** 588-598.

Parker, G. (1975). Meandering of supraglacial melt streams. *Water Resources Research,* 11**,** 551-552.

Pitcher, L. H. and Smith, L. C. (2019). Supraglacial streams and rivers. *Annual Review of Earth and Planetary Sciences,* 47**,** 421-452.

Poinar, K., Joughin, I., Das, S. B., Behn, M. D., Lenaerts, J. T. and Van Den Broeke, M. R. (2015). Limits to future expansion of surface-melt-enhanced ice flow into the interior of western Greenland. *Geophysical Research Letters,* 42**,** 1800-1807.

Pope, A., Scambos, T. A., Moussavi, M., Tedesco, M., Willis, M., Shean, D. and Grigsby, S. (2016). Estimating supraglacial lake depth in West Greenland using Landsat 8 and comparison with other multispectral methods. *The Cryosphere,* 10**,** 15-27.

Pratap, B., Dey, R., Matsuoka, K., Moholdt, G., Lindbäck, K., Goel, V., Laluraj, C. and Thamban, M. (2022). Three-decade spatial patterns in surface mass balance of the Nivlisen Ice Shelf, central Dronning Maud Land, East Antarctica. *Journal of Glaciology,* 68**,** 174-186.

Resmi, M., Babeesh, C. and Achyuthan, H. (2019). Quantitative analysis of the drainage and morphometric characteristics of the Palar River basin, Southern Peninsular India; using bAd calculator (bearing azimuth and drainage) and GIS. *Geology, ecology, landscapes,* 3.

Rignot, E., Jacobs, S., Mouginot, J. and Scheuchl, B. (2013). Ice-shelf melting around Antarctica. *Science,* 341**,** 266-270.

Rignot, E., Mouginot, J. and Scheuchl, B. (2011). Ice flow of the Antarctic ice sheet. *Science,* 333**,** 1427-1430.

Rintoul, S. R., Chown, S. L., Deconto, R. M., England, M. H., Fricker, H. A., Masson-Delmotte, V., Naish, T. R., Siegert, M. J. and Xavier, J. C. (2018). Choosing the future of Antarctica. *Nature,* 558**,** 233-241.

Rippin, D. M., Pomfret, A. and King, N. (2015). High resolution mapping of supra-glacial drainage pathways reveals link between micro-channel drainage density, surface roughness and surface reflectance. *Earth Surface Processes and Landforms,* 40**,** 1279-1290.

Roux, C., Alber, A., Bertrand, M., Vaudor, L. and Piégay, H. (2015). "FluvialCorridor": A new ArcGIS toolbox package for multiscale riverscape exploration. *Geomorphology,* 242**,** 29-37.

Scott, D., Hood, E. and Nassry, M. (2010). In-stream uptake and retention of C, N and P in a supraglacial stream. *Annals of Glaciology,* 51**,** 80-86.

Schwenk, J. and Hariharan, J. (2021). RivGraph: Automatic extraction and analysis of river and delta channel network topology. *Journal of Open Source Software,* 6.

Shepherd, A., Ivins, E., Rignot, E., Smith, B., Van Den Broeke, M., Velicogna, I., Whitehouse, P., Briggs, K., Joughin, I. and Krinner, G. (2018). Mass balance of the Antarctic Ice Sheet from 1992 to 2017. *Nature,* 558**,** 219-222.

Shen, Q., Wang, H., Shum, C.K., Jiang, L (2020). Antarctic-Wide Annual Ice Flow Maps from Landsat 8 Imagery between 2013 and 2019. *PANGAEA*.

Smith, L. C., Chu, V. W., Yang, K., Gleason, C. J., Pitcher, L. H., Rennermalm, A. K., Legleiter, C. J., Behar, A. E., Overstreet, B. T. and Moustafa, S. E. (2015). Efficient meltwater drainage through supraglacial streams and rivers on the southwest Greenland ice sheet. *Proceedings of the National Academy of Sciences,* 112**,** 1001-1006.

Sneed, W. A. and Hamilton, G. S. (2011). Validation of a method for determining the depth of glacial melt ponds using satellite imagery. *Annals of Glaciology,* 52**,** 15-22.

Song, X., Xu, G., Bai, Y. and Xu, D. (2016). Experiments on the short-term development of sine-generated meandering rivers. *Journal of Hydro-environment Research*, 11, 42-58.

Spergel, J. J., Kingslake, J., Creyts, T., Van Wessem, M. and Fricker, H. A. (2021). Surface meltwater drainage and ponding on Amery Ice Shelf, East Antarctica, 1973–2019. *Journal of Glaciology***,** 1-14.

St Germain, S. L. and Moorman, B. J. J. J. O. G. (2019). Long-term observations of supraglacial streams on an Arctic glacier. 65**,** 900-911.

Stokes, C. R., Sanderson, J. E., Miles, B. W., Jamieson, S. S. and Leeson, A. A. (2019). Widespread distribution of supraglacial lakes around the margin of the East Antarctic Ice Sheet. *Scientific reports,* 9**,** 1-14.

Strahler, A. N. (1957). Quantitative analysis of watershed geomorphology. *Eos, Transactions American Geophysical Union,* 38**,** 913-920.

Strahler, A. N. (1964). Quantitative geomorphology of drainage basin and channel

networks. *Handbook of applied hydrology*.

Stumpf, R. P., Holderied, K. and Sinclair, M. (2003). Determination of water depth with high-resolution satellite imagery over variable bottom types. *Limnology and Oceanography,* 48**,** 547-556.

Sukristiyanti, S., Maria, R. and Lestiana, H. (Year) Published. Watershed-based morphometric analysis: a review. IOP conference series: earth and environmental science, 2018. IOP Publishing, 012028.

Tay, L. T., Sagar, B. D. and Chuah, H. T. (2006). Allometric relationships between traveltime channel networks, convex hulls, and convexity measures. *Water resources research,* 42.

Tedesco, M., Willis, I. C., Hoffman, M. J., Banwell, A. F., Alexander, P. and Arnold, N. S. (2013). Ice dynamic response to two modes of surface lake drainage on the Greenland ice sheet. *Environmental Research Letters,* 8**,** 034007.

Tuckett, P. A., Ely, J. C., Sole, A. J., Livingstone, S. J., Davison, B. J., Melchior Van Wessem, J. and Howard, J. (2019). Rapid accelerations of Antarctic Peninsula outlet glaciers driven by surface melt. *Nature Communications,* 10**,** 4311.

Tuckett, P. A., Ely, J. C., Sole, A. J., Lea, J. M., Livingstone, S. J., Jones, J. M. and Van Wessem, J. M. (2021). Automated mapping of the seasonal evolution of surface meltwater and its links to climate on the Amery Ice Shelf, Antarctica. *The Cryosphere*, 15, 5785-5804Turcotte, D. L., Pelletier, J. D. and Newman, W. I. (1998). Networks with side branching in biology. *Journal of Theoretical Biology,* 193**,** 577-592.

Vieli, A., Payne, A. J., Shepherd, A. and Du, Z. (2007). Causes of pre-collapse changes of the Larsen B ice shelf: Numerical modelling and assimilation of satellite observations. *Earth Planetary Science Letters,* 259**,** 297-306.

Weertman, J. (1973). Can a water-filled crevasse reach the bottom surface of a glacier. *IASH publ,* 95**,** 139-145.

Whipple, K. X., Snyder, N. P. and Dollenmayer, K. (2000). Rates and processes of bedrock incision by the Upper Ukak River since the 1912 Novarupta ash flow in the Valley of Ten Thousand Smokes, Alaska. *Geology,* 28**,** 835-838.

Williamson, A. G., Arnold, N. S., Banwell, A. F. and Willis, I. C. (2017). A Fully Automated Supraglacial lake area and volume Tracking ("FAST") algorithm: Development and application using MODIS imagery of West Greenland. *Remote Sensing of Environment,* 196**,** 113-133.

Willis, I. C., Arnold, N. S. and Brock, B. W. (2002). Effect of snowpack removal on energy balance, melt and runoff in a small supraglacial catchment. *Hydrological Processes,* 16**,** 2721-2749.

Xing, Z., Chi, Z., Yang, Y., Chen, S., Huang, H., Cheng, X. and Hui, F. (2020). Accuracy Evaluation of Four Greenland Digital Elevation Models (DEMs) and Assessment of River Network Extraction. *Remote Sensing,* 12**,** 3429.

Yang, K., Li, M., Liu, Y., Cheng, L., Huang, Q. and Chen, Y. (2015a). River detection in remotely sensed imagery using Gabor filtering and path opening. *Remote Sensing,* 7**,** 8779-8802.

Yang, K. and Smith, L. C. (2012). Supraglacial streams on the Greenland Ice Sheet

delineated from combined spectral–shape information in high-resolution satellite imagery. *IEEE Geoscience Remote Sensing Letters,* 10**,** 801-805.

Yang, K. and Smith, L. C. (2016). Internally drained catchments dominate supraglacial hydrology of the southwest Greenland Ice Sheet. *Journal of Geophysical Research: Earth Surface,* 121**,** 1891-1910.

Yang, K., Smith, L. C., Chu, V. W., Gleason, C. J. and Li, M. (2015b). A caution on the use of surface digital elevation models to simulate supraglacial hydrology of the Greenland ice sheet. *IEEE Journal of Selected Topics in Applied Earth Observations,* 8**,** 5212-5224.

Yang, K., Smith, L. C., Chu, V. W., Pitcher, L. H., Gleason, C. J., Rennermalm, A. K. and Li, M. (2016). Fluvial morphometry of supraglacial river networks on the southwest Greenland Ice Sheet. *GIScience & Remote Sensing,* 53**,** 459-482.

Yang, K., Smith, L. C., Cooper, M. G., Pitcher, L. H., Van As, D., Lu, Y., Lu, X. and Li, M. (2021). Seasonal evolution of supraglacial lakes and rivers on the southwest Greenland Ice Sheet. *Journal of Glaciology,* 67**,** 592-602.

Yang, K., Smith, L. C., Fettweis, X., Gleason, C. J., Lu, Y. and Li, M. J. R. S. O. E. (2019a). Surface meltwater runoff on the Greenland ice sheet estimated from remotely sensed supraglacial lake infilling rate. 234**,** 111459.

Yang, K., Smith, L. C., Karlstrom, L., Cooper, M. G., Tedesco, M., Van As, D., Cheng, X., Chen, Z. and Li, M. (2018). A new surface meltwater routing model for use on the Greenland Ice Sheet surface. *The Cryosphere,* 12**,** 3791-3811.

Yang, K., Smith, L. C., Sole, A., Livingstone, S. J., Cheng, X., Chen, Z. and Li, M.

(2019b). Supraglacial rivers on the northwest Greenland Ice Sheet, Devon Ice Cap, and Barnes Ice Cap mapped using Sentinel-2 imagery. *International Journal of Applied Earth Observation and Geoinformation,* 78**,** 1-13.

Yuan, J., Chi, Z., Cheng, X., Zhang, T., Li, T. and Chen, Z. (2020). Automatic extraction of supraglacial lakes in southwest greenland during the 2014–2018 melt seasons based on convolutional neural network. *Water,* 12**,** 891.

Zatko, M. C. and Warren, S. G. (2015). East Antarctic sea ice in spring: spectral albedo of snow, nilas, frost flowers and slush, and light-absorbing impurities in snow. *Annals of Glaciology,* 56**,** 53-64.

Zeng, C., Bird, S., Luce, J. J. and Wang, J. (2015). A natural-rule-based-connection (NRBC) method for river network extraction from high-resolution imagery. *Remote Sensing,* 7**,** 14055-14078.